CLIMATE DIAGNOSTICS BULLETIN

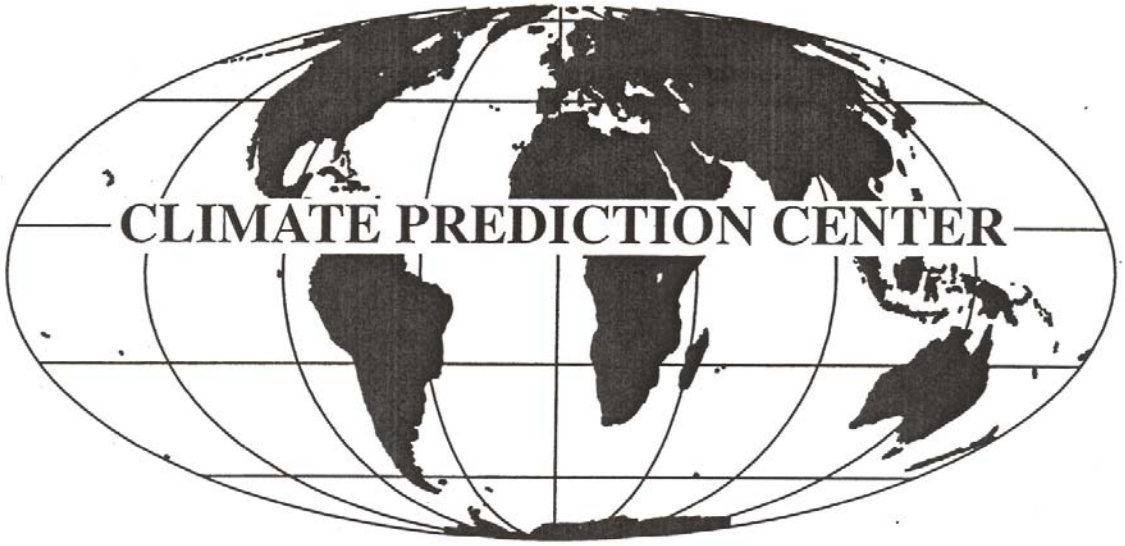

JANUARY 2018

NEAR REAL-TIME OCEAN / ATMOSPHERE

Monitoring, Assessments, and Prediction

U.S. DEPARTMENT OF COMMERCE
National Oceanic and Atmospheric Administration
National Weather Service

National Centers for Environmental Prediction

CLIMATE DIAGNOSTICS BULLETIN

CLIMATE PREDICTION CENTER
Attn: Climate Diagnostics Bulletin
W/NP52, Room 605, WWBG
Camp Springs, MD 20746-4304

Chief Editor: Gerald D. Bell
Editors: Wei Shi, Michelle L'Heureux, and Michael Halpert
Bulletin Production: Wei Shi

ExternalCollaborators:

Center for Ocean-Atmospheric Prediction Studies (COAPS)
Cooperative Institute for Research in the Atmosphere (CIRA)
Earth & Space Research
International Research Institute for Climate and Society (IRI)
Joint Institute for the Study of the Atmosphere and Ocean (JISAO)
Lamont-Doherty Earth Observatory (LDEO)
NOAA-CIRES, Climate Diagnostics Center
NOAA-AOML, Atlantic Oceanographic and Meteorological Laboratory
NOAA-NESDIS-STAR, Center for Satellite Applications and Research
NOAA-NDBC, National Data Buoy Center
Scripps Institution of Oceanography

Software: Most of the bulletin figures generated at CPC are created using the Grid Analysis and Display System (GrADS).

- Climate Diagnostics Bulletin available on the World Wide Web

The CDB is available on the World Wide Web. The address of the online version of the CDB is:

http://www.cpc.ncep.noaa.gov/products/CDB

If you have any problems accessing the bulletin, contact Dr. Wei Shi by E-mail:

Wei.Shi@noaa.gov

Table of Contents

FIGURE

Tropical Highlights - December 2017

Sea surface temperatures (SSTs) during December 2017 were below-average across the central and eastern equatorial Pacific (Fig. T18, Table T2). The latest monthly Niño indices were -0.3°C for the Niño 4 region, -0.8°C for the Niño 3.4 region, and -1.5°C for the Niño 1+2 region (Table T2, Fig. T5). The depth of the oceanic thermocline (measured by the depth of the 20°C isotherm) was below-average over much of the eastern equatorial Pacific (Figs. T15, T16), and the corresponding sub-surface temperatures were 1-4°C below average (Fig. T17).

Also during December, the lower-level trade winds were above-average over the western equatorial Pacific while the upper-level westerly winds were near-average over much of the equatorial Pacific (Table T1, Figs. T20, T21). Meanwhile, convection was enhanced over western equatorial Pacific and suppressed over the central equatorial Pacific (Figs. T25, E3). Collectively, these oceanic and atmospheric anomalies reflect La Niña conditions.

For the latest status of the ENSO cycle see the ENSO Diagnostic Discussion at:
http://www.cpc.ncep.noaa.gov/products/analysis_monitoring/enso_advisory/index.html

Month	SLP Anomalies		Tahiti minus Darwin SOI	850-hPa Zonal Wind Index			200-hPa Wind Index	OLR Index
	Tahiti	Darwin		5N-5S 135E-180	5N-5S 175W-140W	5N-5S 135W-120W	5N-5S 165W-110W	5N-5S 160E-160W
JAN 18	0.1	-1.9	1.1	1.4	0.8	0.1	0.9	1.8
DEC 17	-0.3	-0.1	-0.1	0.5	0.4	-0.1	0.3	0.9
NOV 17	0.2	-1.5	0.9	0.8	0.9	0.2	1.0	1.1
OCT 17	0.3	-1.4	0.9	0.6	0.3	-0.4	1.0	0.7
SEP 17	1.2	0.1	0.6	1.2	0.2	0.0	-0.3	0.8
AUG 17	0.6	-0.4	0.5	0.8	0.0	-0.4	-0.3	0.3
JUL 17	1.2	-0.2	0.8	0.9	0.3	-0.7	-0.2	-0.4
JUN 17	-0.3	0.6	-0.4	0.4	-0.4	-0.8	-0.4	0.6
MAY 17	0.7	0.2	0.3	1.0	0.0	-0.6	-0.3	0.1
APR 17	-0.5	-0.2	-0.2	0.3	-0.1	-0.5	-0.4	0.4
MAR 17	0.7	-0.9	0.9	1.5	0.9	0.0	0.8	1.1
FEB 17	0.1	0.3	-0.1	0.6	0.4	-1.4	-0.2	1.4
JAN 17	-0.3	-0.7	0.2	0.7	0.2	-0.6	0.5	1.1

TABLE T1 - Atmospheric index values for the most recent 12 months. Indices are standardized by the mean annual standard deviation, except for the Tahiti and Darwin SLP anomalies which are in units of hPa. Positive (negative) values of 200-hPa zonal wind index imply westerly (easterly) anomalies. Positive (negative) values of 850-hPa zonal wind indices imply easterly (westerly) anomalies. Anomalies are departures from the 1981-2010 base period means.

Month	PACIFIC SST								ATLANTIC SST				GLOBAL	
	Niño 1+2 0-10S 90W-80W		Niño 3 5N-5S 150W-90W		Niño 3.4 5N-5S 170W-120W		Niño 4 5N-5S 160E-150W		N.ATL 5N-20N 60W-30W		S. ATL 0-20S 30W-10E		TROPICS 10N-10S 0-360	
JAN 18	-0.8	23.7	-1.1	24.5	-0.8	25.8	-0.3	28.0	0.3	26.3	-0.1	25.6	-0.1	27.5
DEC 17	-1.5	21.3	-1.1	24.0	-0.8	25.8	-0.3	28.2	0.6	27.4	-0.3	24.4	-0.1	27.6
NOV 17	-1.2	20.4	-1.0	23.9	-0.9	25.8	-0.2	28.5	0.2	27.9	0.0	24.0	0.1	27.7
OCT 17	-1.3	19.5	-0.6	24.3	-0.5	26.2	-0.1	28.6	0.2	28.3	0.2	23.6	0.1	27.5
SEP 17	-0.7	19.7	-0.7	24.2	-0.4	26.3	0.0	28.7	0.4	28.5	0.1	23.2	0.1	27.4
AUG 17	-0.5	20.2	-0.2	24.8	-0.2	26.7	0.2	28.9	0.5	28.3	0.3	23.4	0.3	27.4
JUL 17	-0.1	21.5	0.2	25.9	0.4	27.6	0.4	29.2	0.6	27.8	0.1	23.9	0.3	27.8
JUN 17	0.1	23.0	0.3	26.8	0.6	28.2	0.6	29.4	0.5	27.3	0.5	25.5	0.3	28.3
MAY 17	0.8	25.1	0.5	27.6	0.5	28.3	0.3	29.1	0.5	26.9	0.2	26.4	0.3	28.8
APR 17	0.9	26.5	0.6	28.1	0.3	28.1	0.2	28.6	0.3	26.2	0.2	27.2	0.3	28.9
MAR 17	2.0	28.6	0.5	27.7	0.1	27.3	-0.1	28.1	0.1	25.7	0.1	27.2	0.3	28.6
FEB 17	1.6	27.7	0.6	27.0	0.1	26.9	-0.1	28.0	0.3	25.9	0.0	26.6	0.3	28.1
JAN 17	1.2	25.8	-0.0	25.6	-0.3	26.3	-0.1	28.2	0.4	26.4	0.4	26.0	0.2	27.9

TABLE T2. Mean and anomalous sea surface temperature (°C) for the most recent 12 months. Anomalies are departures from the 1981–2010 adjusted OI climatology (Smith and Reynolds 1998, *J. Climate*, **11**, 3320-3323).

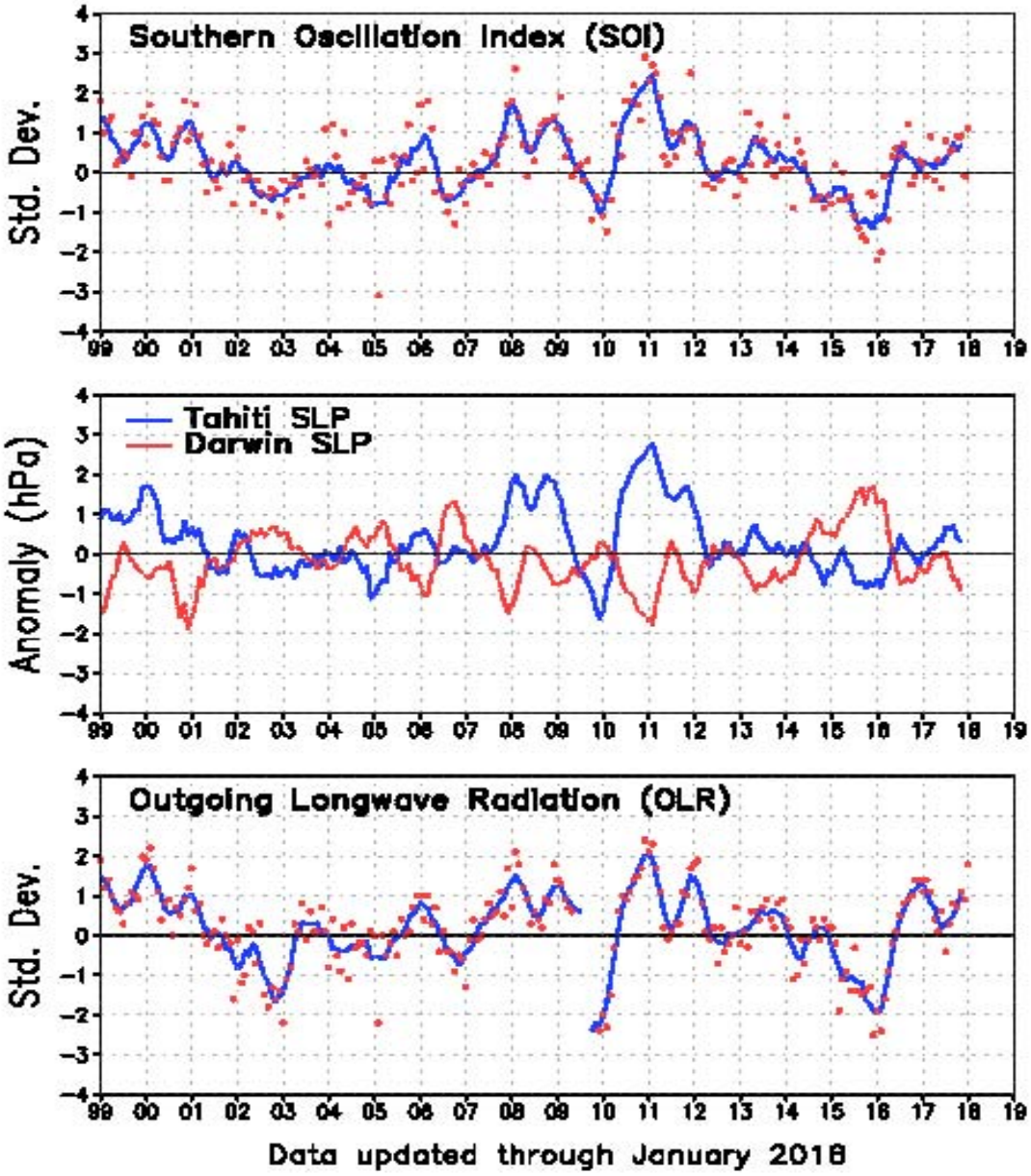

FIGURE T1. Five-month running mean of the Southern Oscillation Index (SOI) (top), sea-level pressure anomaly (hPa) at Darwin and Tahiti (middle), and outgoing longwave radiation anomaly (OLR) averaged over the area 5N-5S, 160E-160W (bottom). Anomalies in the top and middle panels are departures from the 1981-2010 base period means and are normalized by the mean annual standard deviation. Anomalies in the bottom panel are departures from the 1981-2010 base period means. Individual monthly values are indicated by "x"s in the top and bottom panels. The x-axis labels are centered on July.

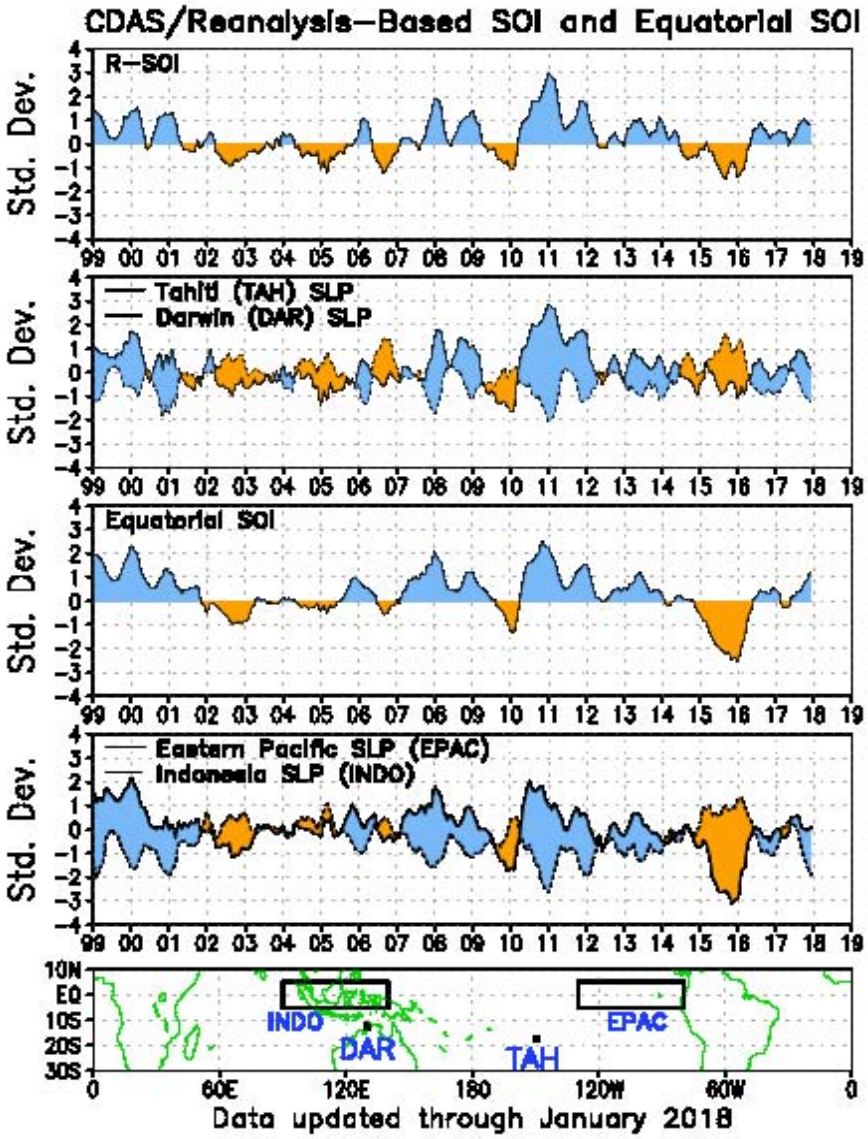

FIGURE T2. Three-month running mean of a CDAS/Reanalysis-derived (a) Southern Oscillation Index (RSOI), (b) standardized pressure anomalies near Tahiti (solid) and Darwin (dashed), (c) an equatorial SOI ([EPAC] - [INDO]), and (d) standardized equatorial pressure anomalies for (EPAC) (solid) and (INDO) (dashed). Anomalies are departures from the 1981-2010 base period means and are normalized by the mean annual standard deviation. The equatorial SOI is calculated as the normalized difference between the standardized anomalies averaged between 5°N–5°S, 80°W–130°W (EPAC) and 5°N–5°S, 90°E–140°E (INDO).

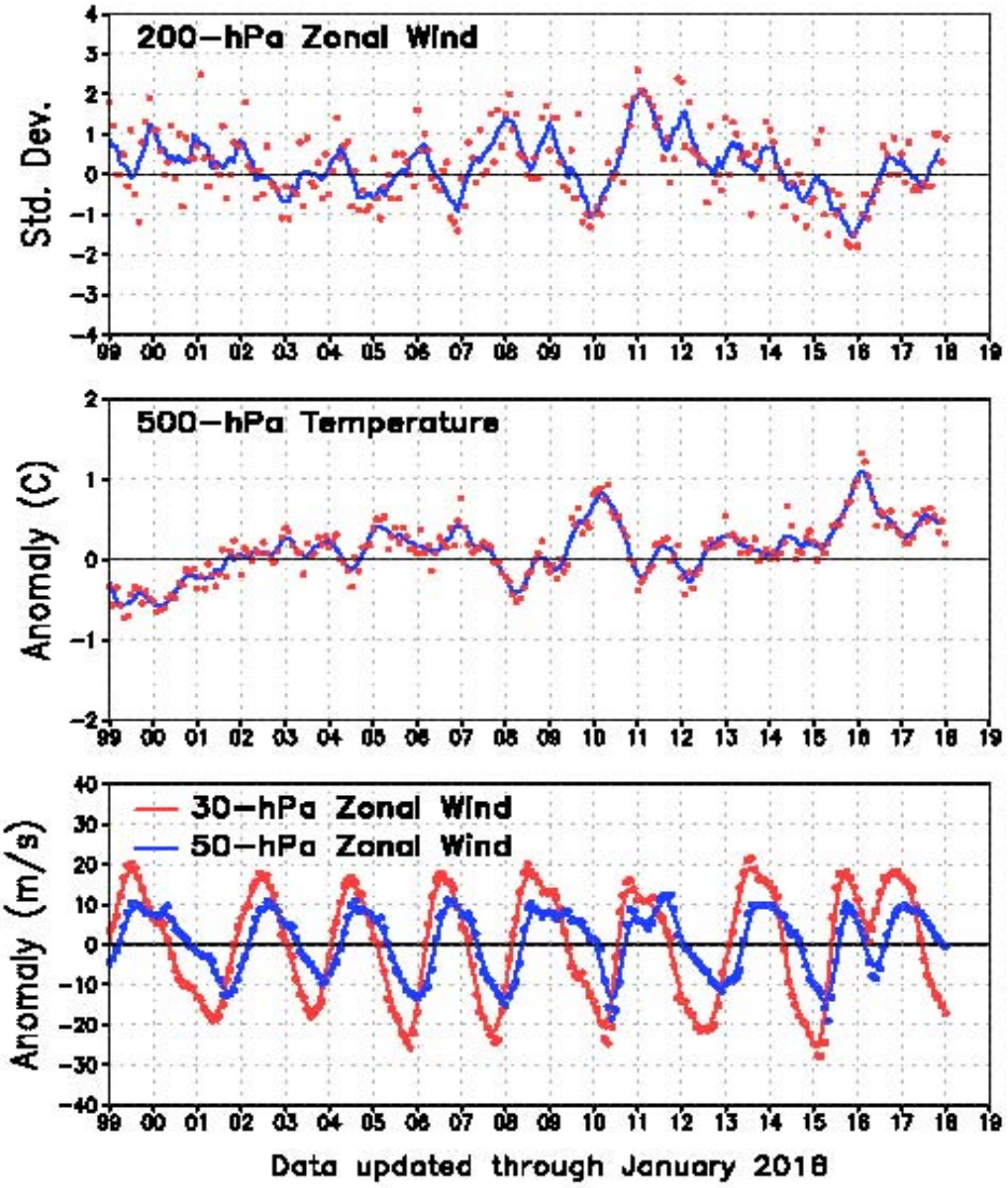

FIGURE T3. Five-month running mean (solid lines) and individual monthly mean (dots) of the 200-hPa zonal wind anomalies averaged over the area 5N-5S, 165W-110W (top), the 500-hPa virtual temperature anomalies averaged over the latitude band 20N-20S (middle), and the equatorial zonally-averaged zonal wind anomalies at 30-hPa (red) and 50-hPa (blue) (bottom). In the top panel, anomalies are normalized by the mean annual standard deviation. Anomalies are departures from the 1981-2010 base period means. The x-axis labels are centered on January.

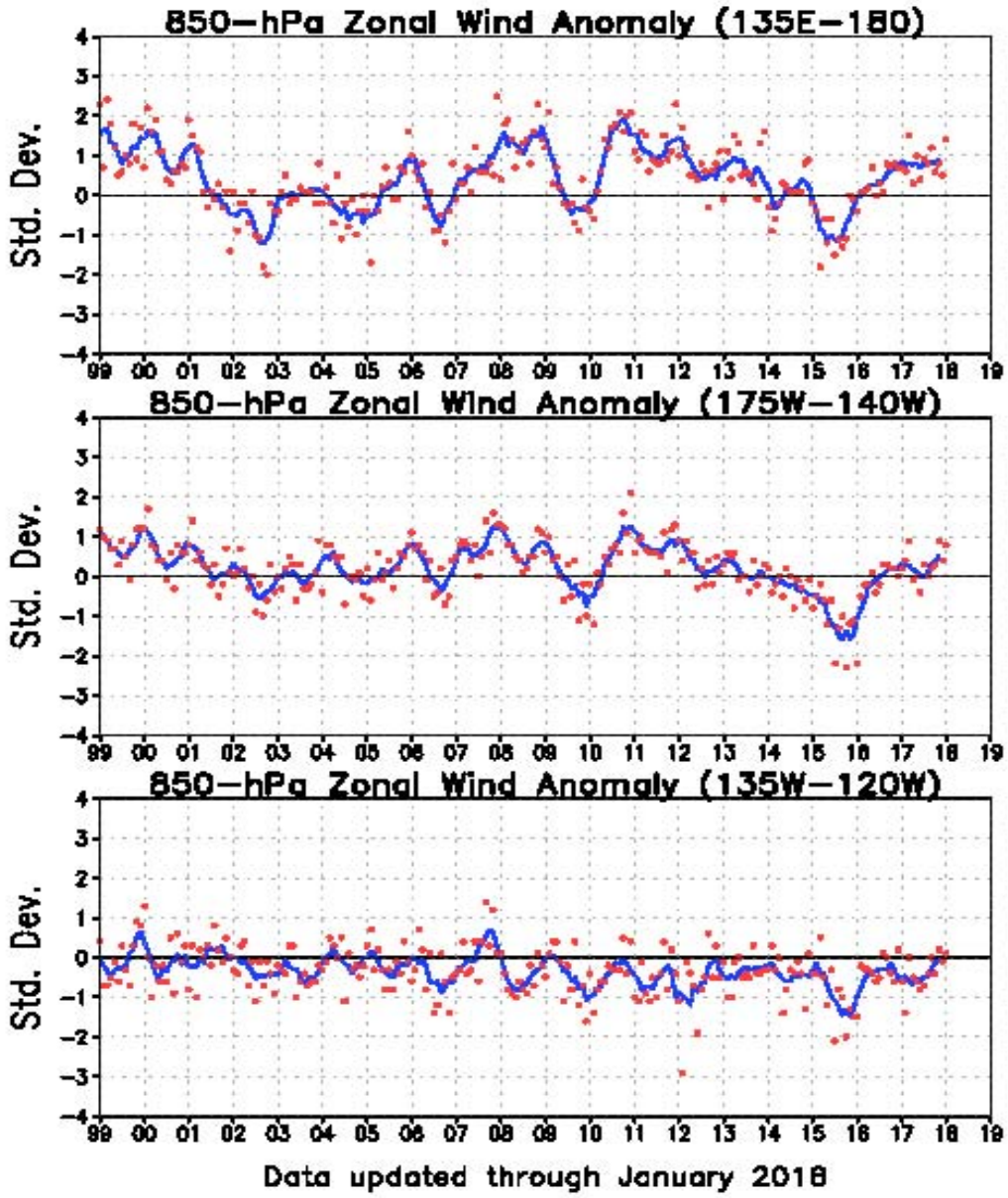

FIGURE T4. Five-month running mean (solid line) and individual monthly mean (dots) of the standardized 850-hPa zonal wind anomaly index in the latitude belt 5N-5S for 135E-180 (top), 175W-140W (middle) and 135W-120W (bottom). Anomalies are departures from the 1981-2010 base period means and are normalized by the mean annual standard deviation.The x-axis labels are centered on January. Positive (negative) values indicate easterly (westerly) anomalies.

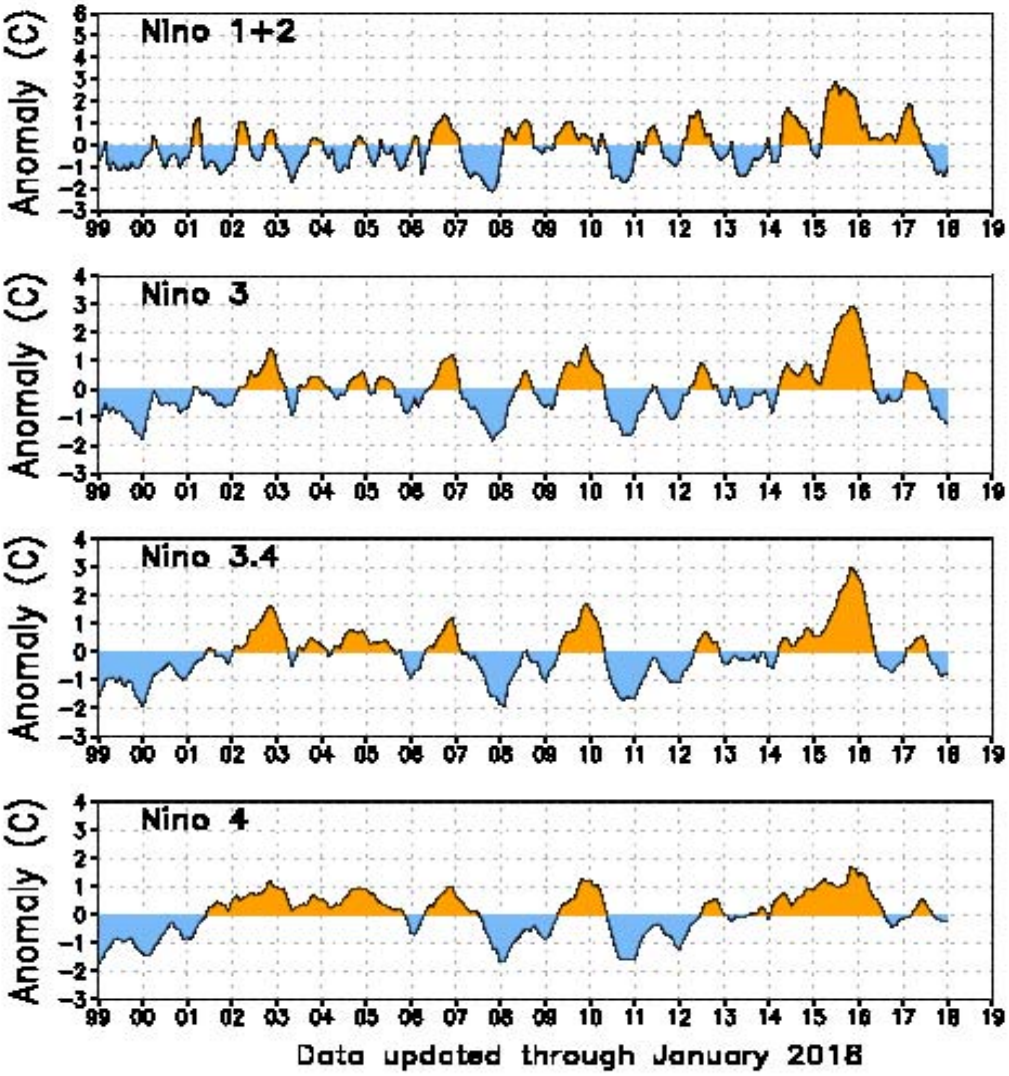

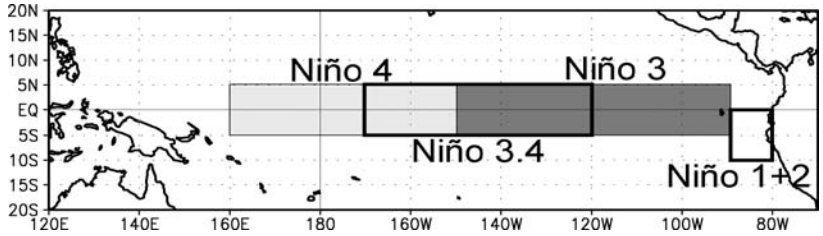

FIGURE T5. Nino region indices, calculated as the area-averaged sea surface temperature anomalies (C) for the specified region. The Nino 1+2 region (top) covers the extreme eastern equatorial Pacific between 0-10S, 90W-80W. The Nino-3 region (2nd from top) spans the eastern equatorial Pacific between 5N-5S, 150W-90W. The Nino 3.4 region 3rd from top) spans the east-central equatorial Pacific between 5N-5S, 170W-120W. The Nino 4 region (bottom) spans the date line and covers the area 5N-5S, 160E-150W. Anomalies are departures from the 1981-2010 base period monthly means *(Smith and Reynolds 1998, J. Climate, 11, 3320-3323)*. Monthly values of each index are also displayed in Table 2.

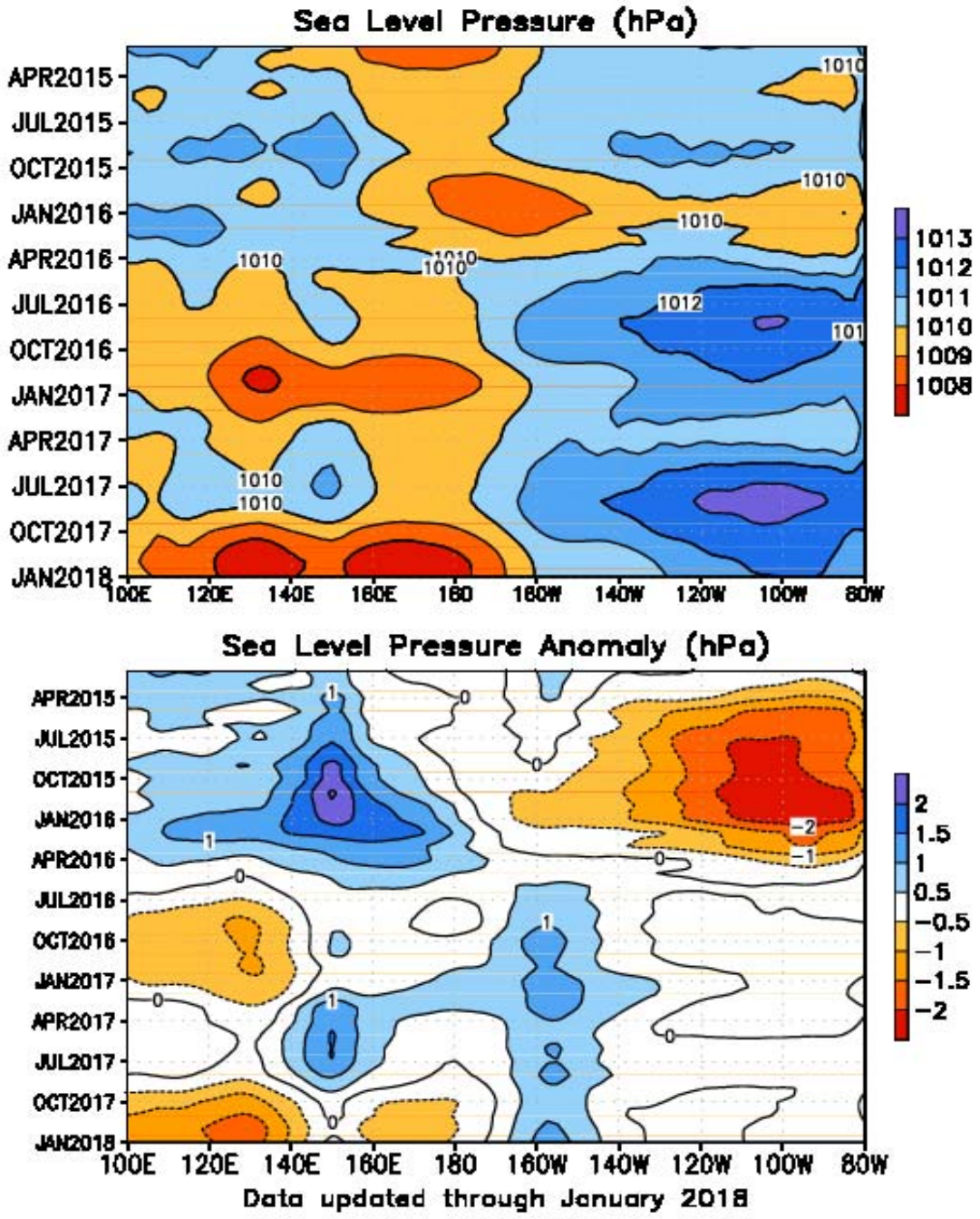

FIGURE T6. Time-longitude section of mean (top) and anomalous (bottom) sea level pressure (SLP) averaged between 5N-5S (CDAS/Reanalysis). Contour interval is 1.0 hPa (top) and 0.5 hPa (bottom). Dashed contours in bottom panel indicate negative anomalies. Anomalies are departures from the 1981-2010 base period monthly means. The data are smoothed temporally using a 3-month running average.

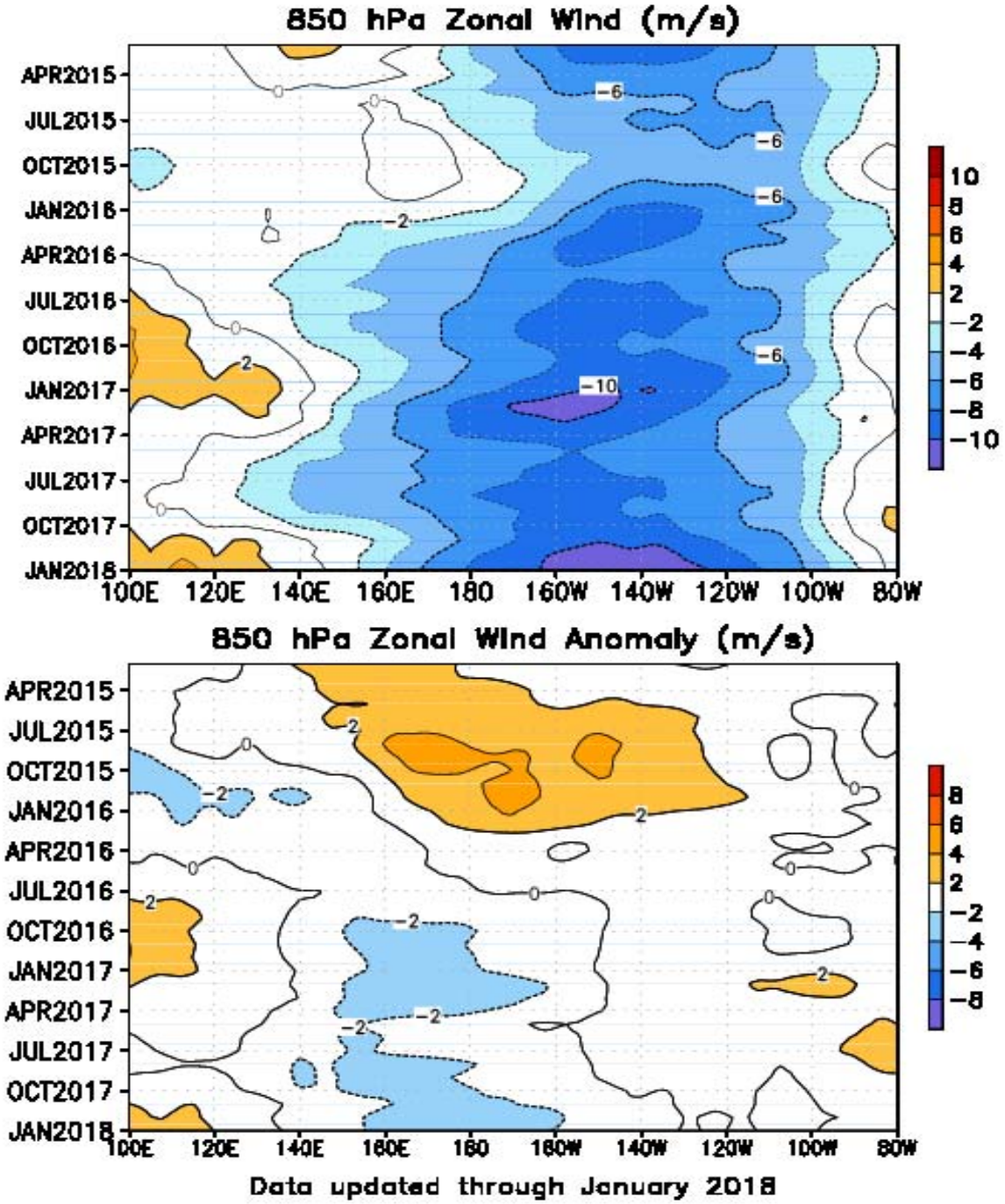

FIGURE T7. Time-longitude section of mean (top) and anomalous (bottom) 850-hPa zonal wind averaged between 5N-5S (CDAS/Reanalysis). Contour interval is 2 ms^{-1}. Blue shading and dashed contours indicate easterlies (top) and easterly anomalies (bottom). Anomalies are departures from the 1981-2010 base period monthly means. The data are smoothed temporally using a 3-month running average.

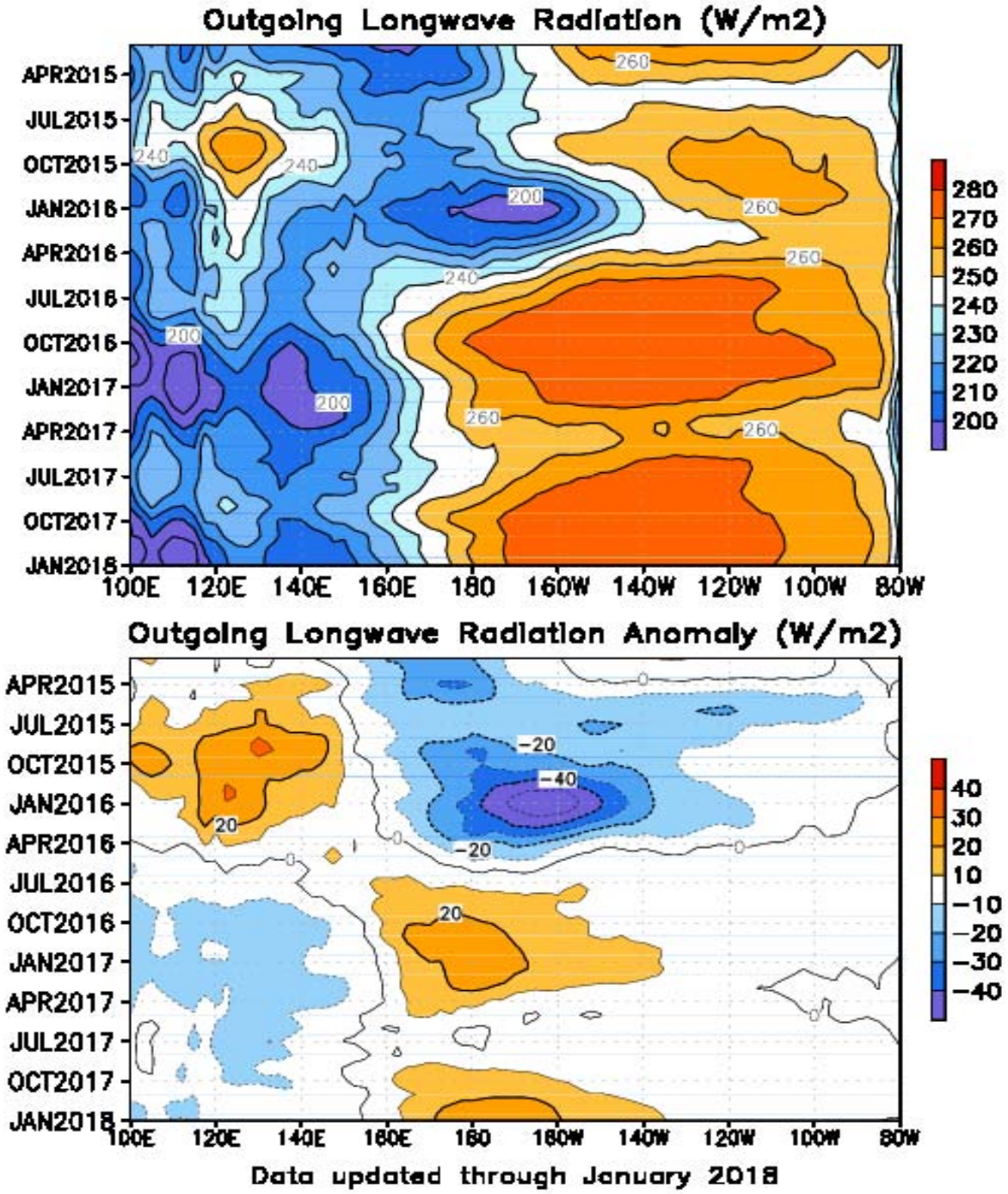

FIGURE T8. Time-longitude section of mean (top) and anomalous (bottom) outgoing longwave radiation (OLR) averaged between 5N-5S. Contour interval is 10 Wm^{-2}. Dashed contours in bottom panel indicate negative OLR anomalies. Anomalies are departures from the 1981-2010 base period monthly means. The data are smoothed temporally using a 3-month running average.

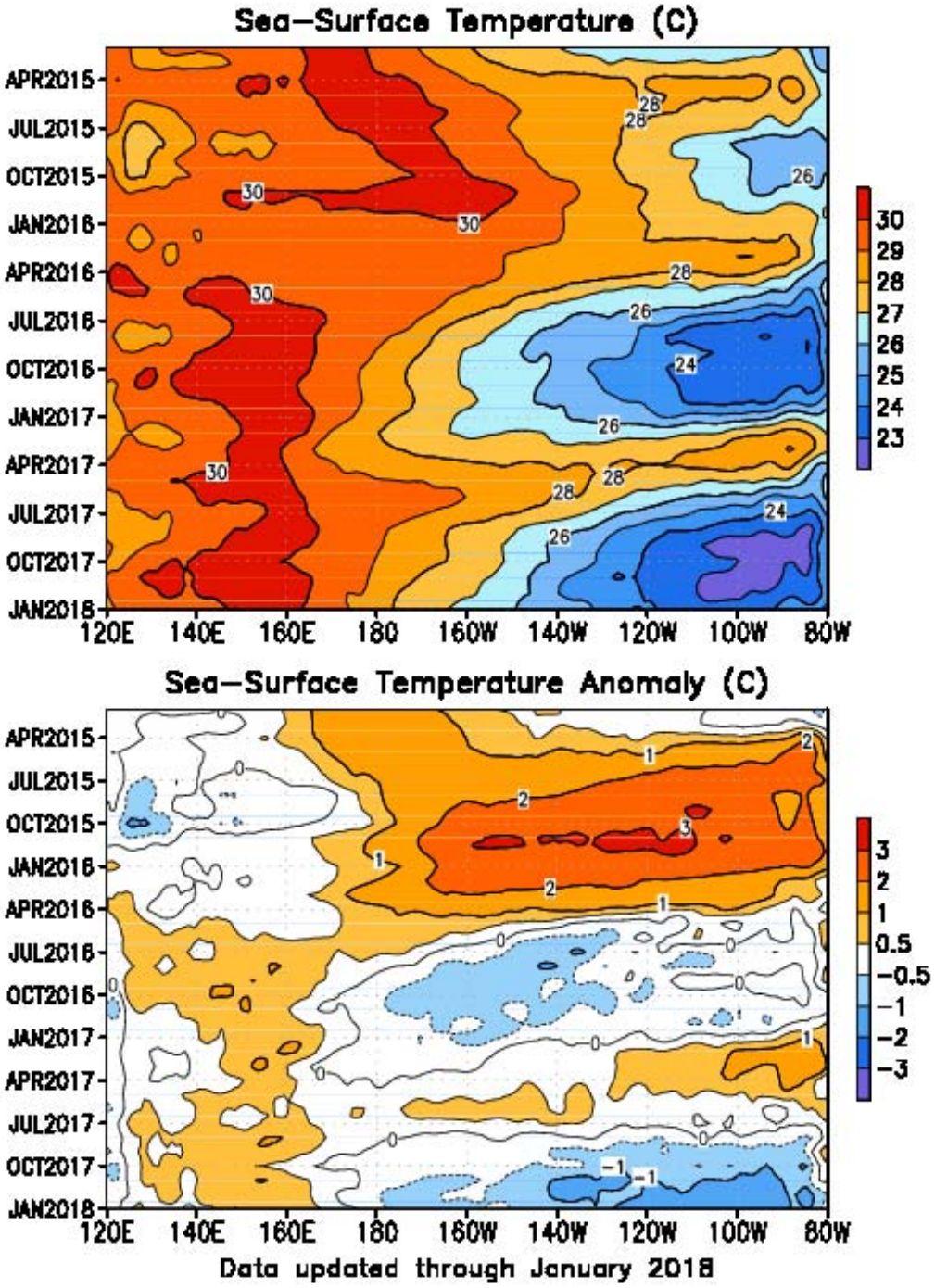

FIGURE T9. Time-longitude section of monthly mean (top) and anomalous (bottom) sea surface temperature (SST) averaged between 5N-5S. Contour interval is 1C (top) and 0.5C (bottom). Dashed contours in bottom panel indicate negative anomalies. Anomalies are departures from the 1981-2010 base period means (Smith and Reynolds 1998, *J. Climate*, **11**, 3320-3323).

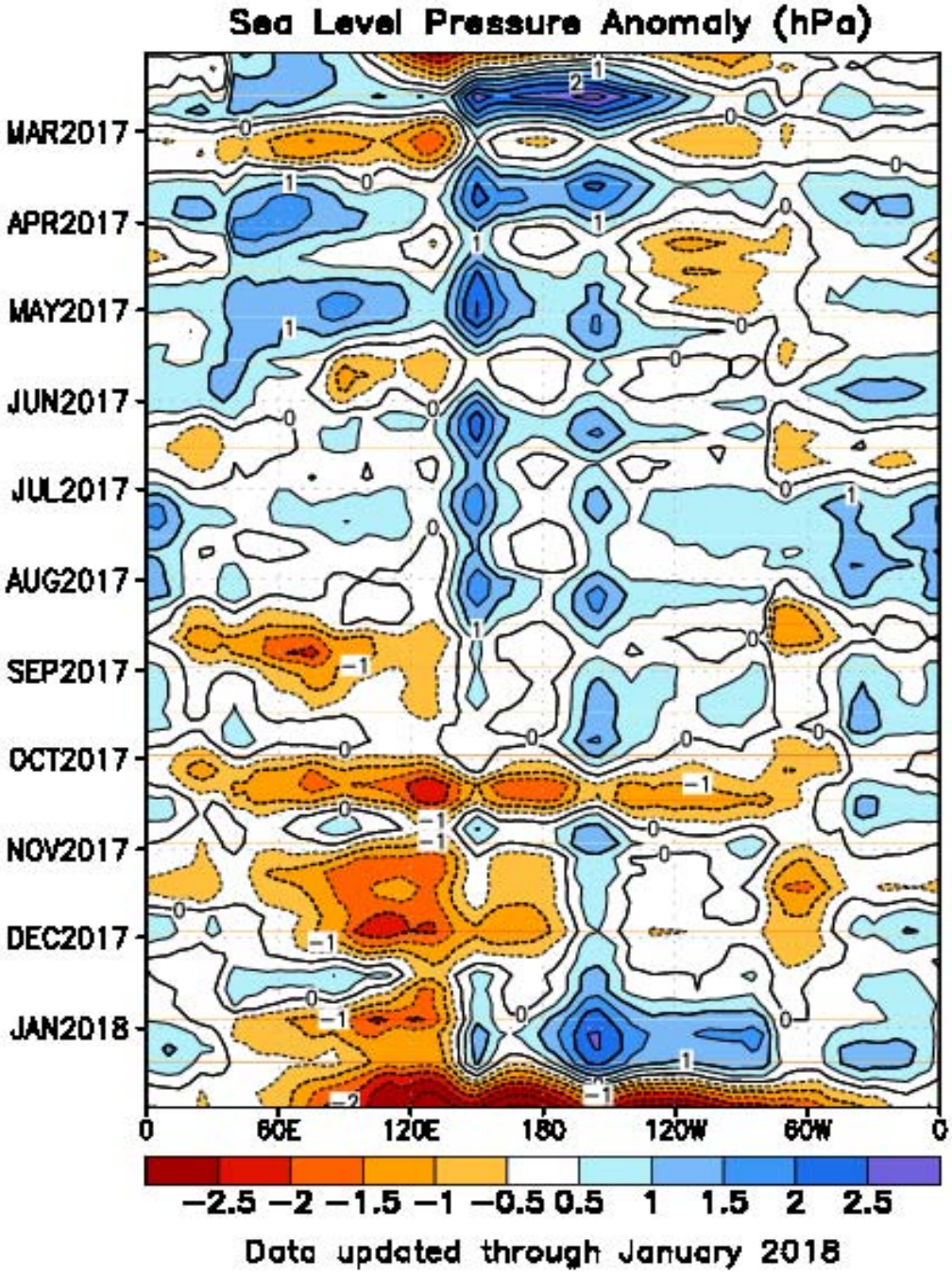

FIGURE T10. Time-longitude section of anomalous sea level pressure (hPa) averaged between 5N-5S (CDAS/Reanaysis). Contour interval is 1 hPa. Dashed contours indicate negative anomalies. Anomalies are departures from the 1981-2010 base period pentad means. The data are smoothed temporally using a 3-point running average.

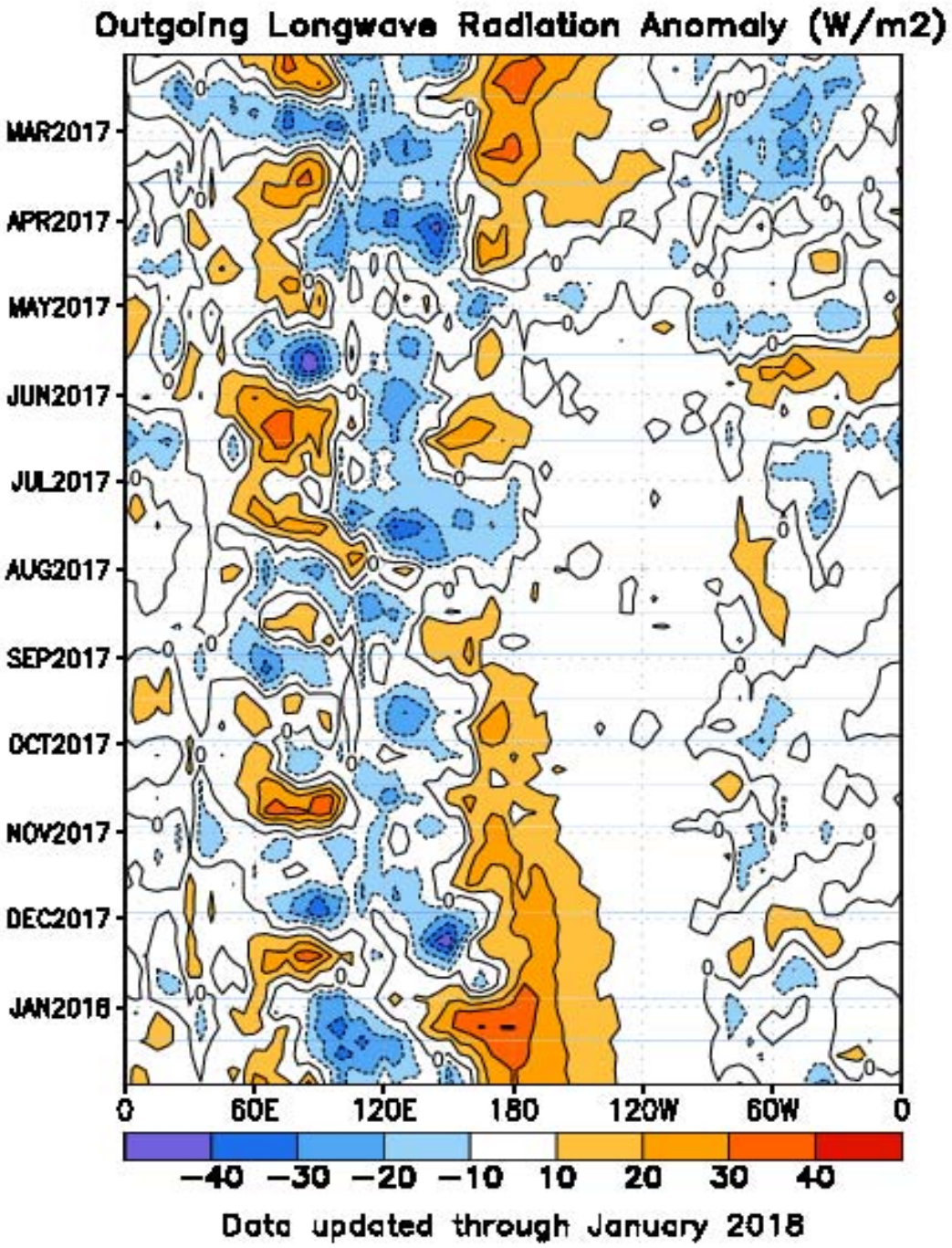

FIGURE T11. Time-longitude section of anomalous outgoing longwave radiation averaged between 5N-5S. Contour interval is 15 Wm^{-2}. Dashed contours indicate negative anomalies. Anomalies are departures from the 1981-2010 base period pentad means. The data are smoothed temporally using a 3-point running average.

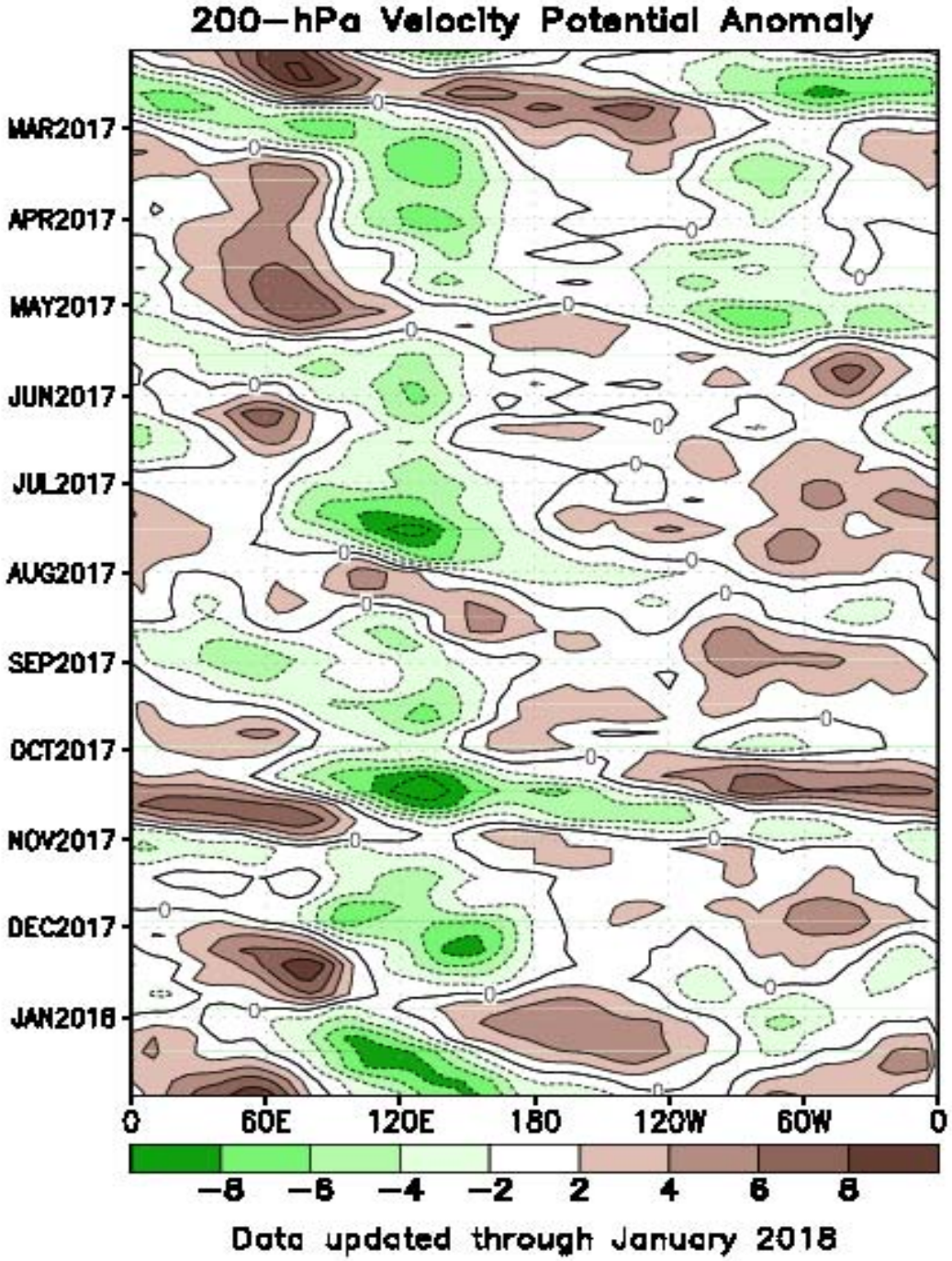

FIGURE T12. Time-longitude section of anomalous 200-hPa velocity potential averaged between 5N-5S (CDAS/Reanalysis). Contour interval is 3 x 10^6 m^2s^{-1}. Dashed contours indicate negative anomalies. Anomalies are departures from the 1981-2010 base period pentad means. The data are smoothed temporally using a 3-point running average.

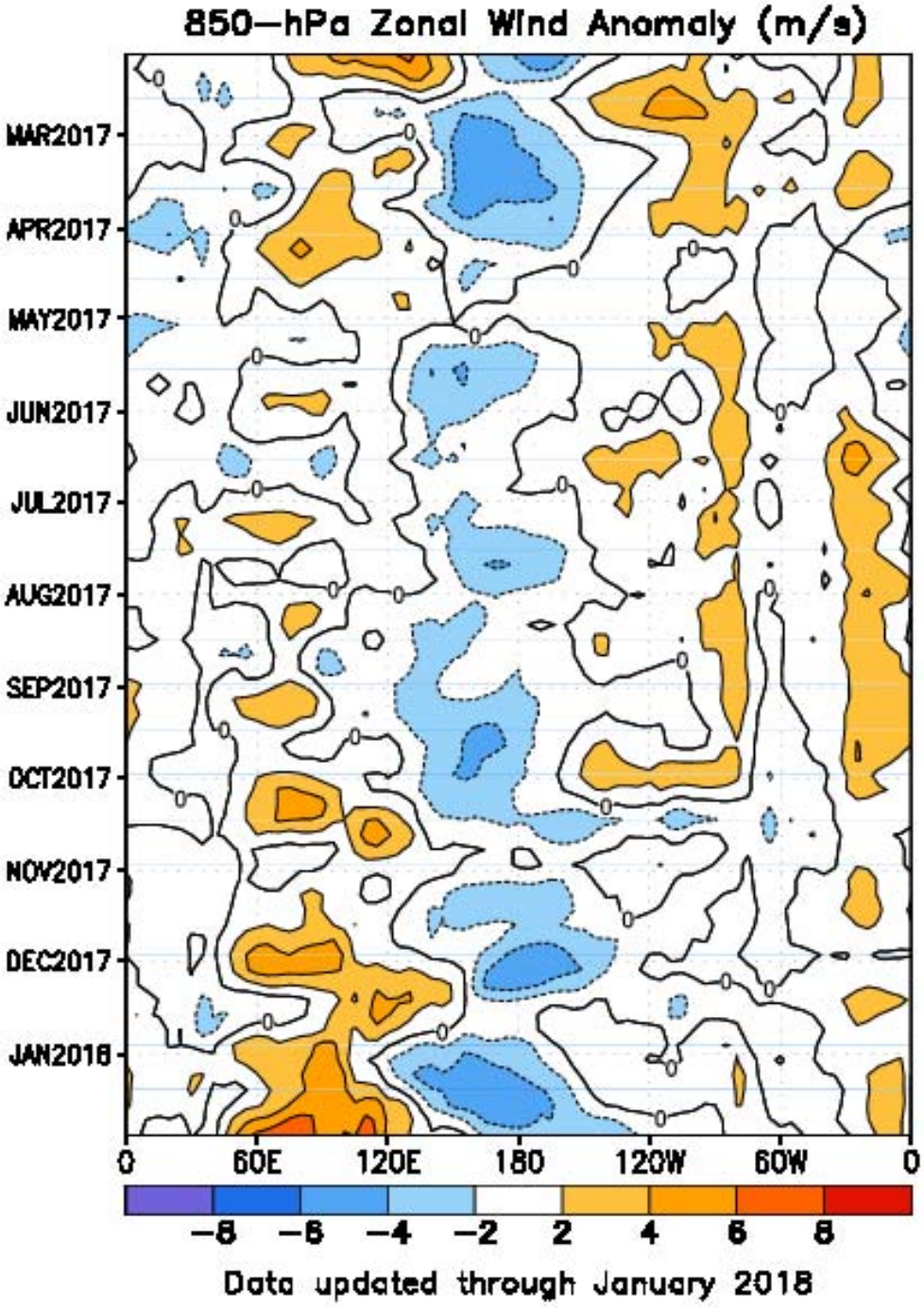

FIGURE T13. Time-longitude section of anomalous 850-hPa zonal wind averaged between 5N-5S (CDAS/Reanalysis). Contour interval is 2 ms^{-1}. Dashed contours indicate negative anomalies. Anomalies are departures from the 1981-2010 base period pentad means. The data are smoothed temporally by using a 3-point running average.

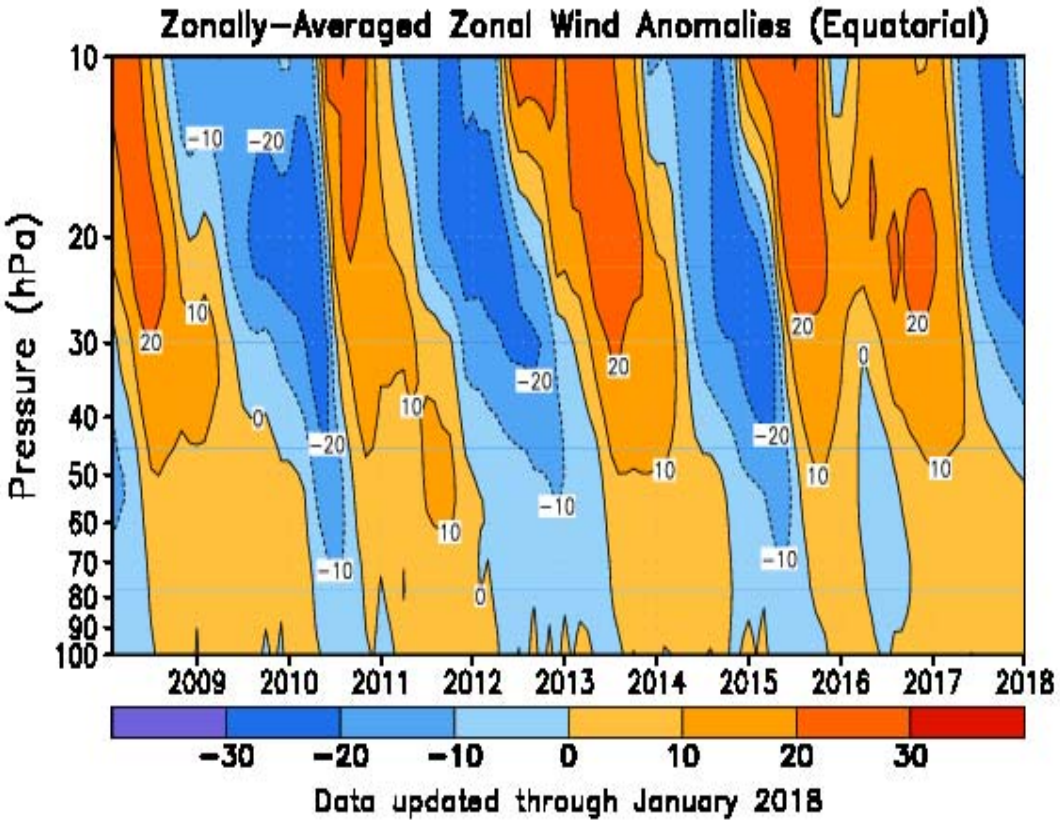

FIGURE T14. Equatorial time-height section of anomalous zonally-averaged zonal wind (m s^{-1}) (CDAS/Reanalysis). Contour interval is 10 ms^{-1}. Anomalies are departures from the 1981-2010 base period monthly means.

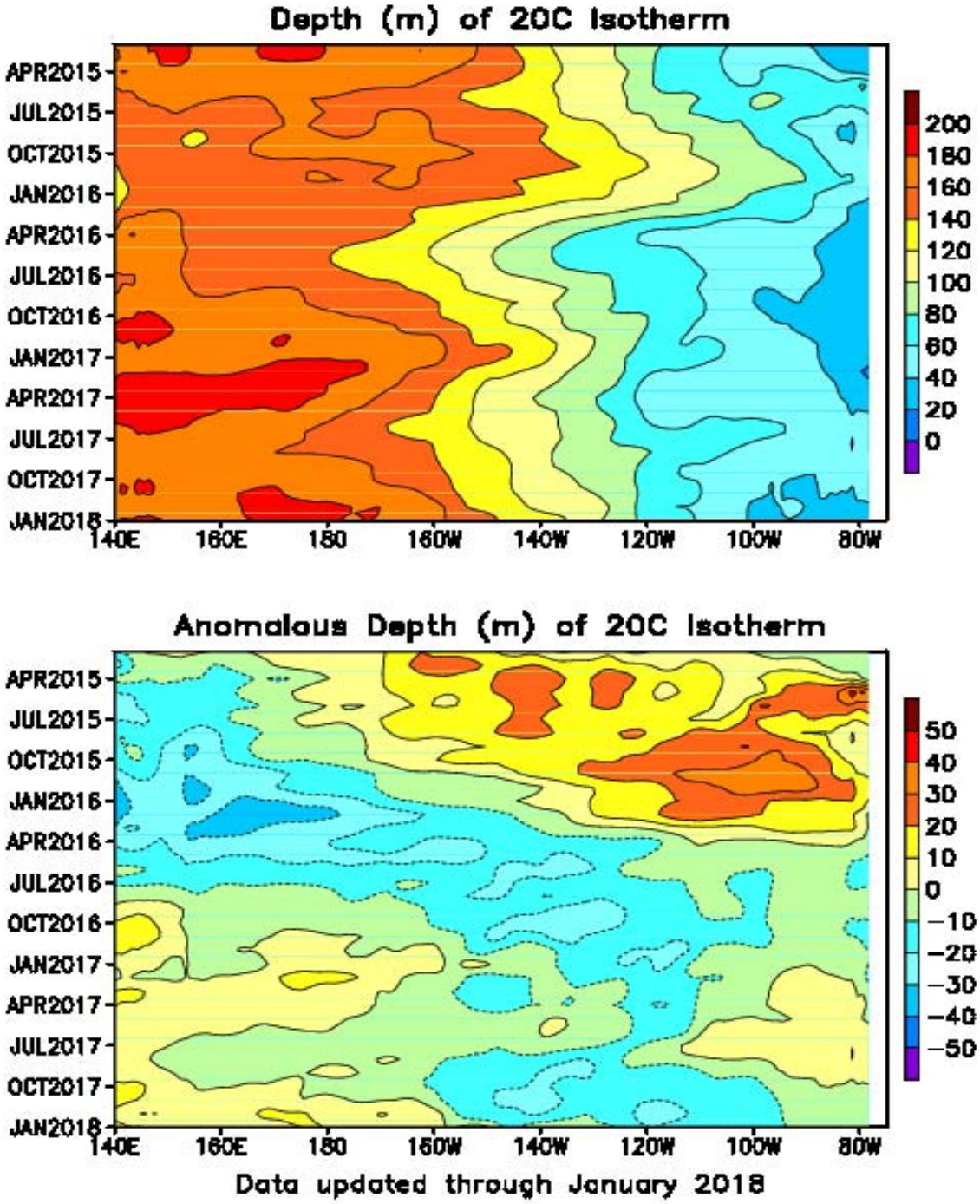

FIGURE T15. Mean (top) and anomalous (bottom) depth of the 20C isotherm averaged between 5N-5S in the Pacific Ocean. Data are derived from the NCEP's global ocean data assimilation system which assimilates oceanic observations into an oceanic GCM (Behringer, D. W., and Y. Xue, 2004: Evaluation of the global ocean data assimilation system at NCEP: The Pacific Ocean. AMS 84th Annual Meeting, Seattle, Washington, 11-15). The contour interval is 10 m. Dashed contours in bottom panel indicate negative anomalies. Anomalies are departures from the 1981-2010 base period means.

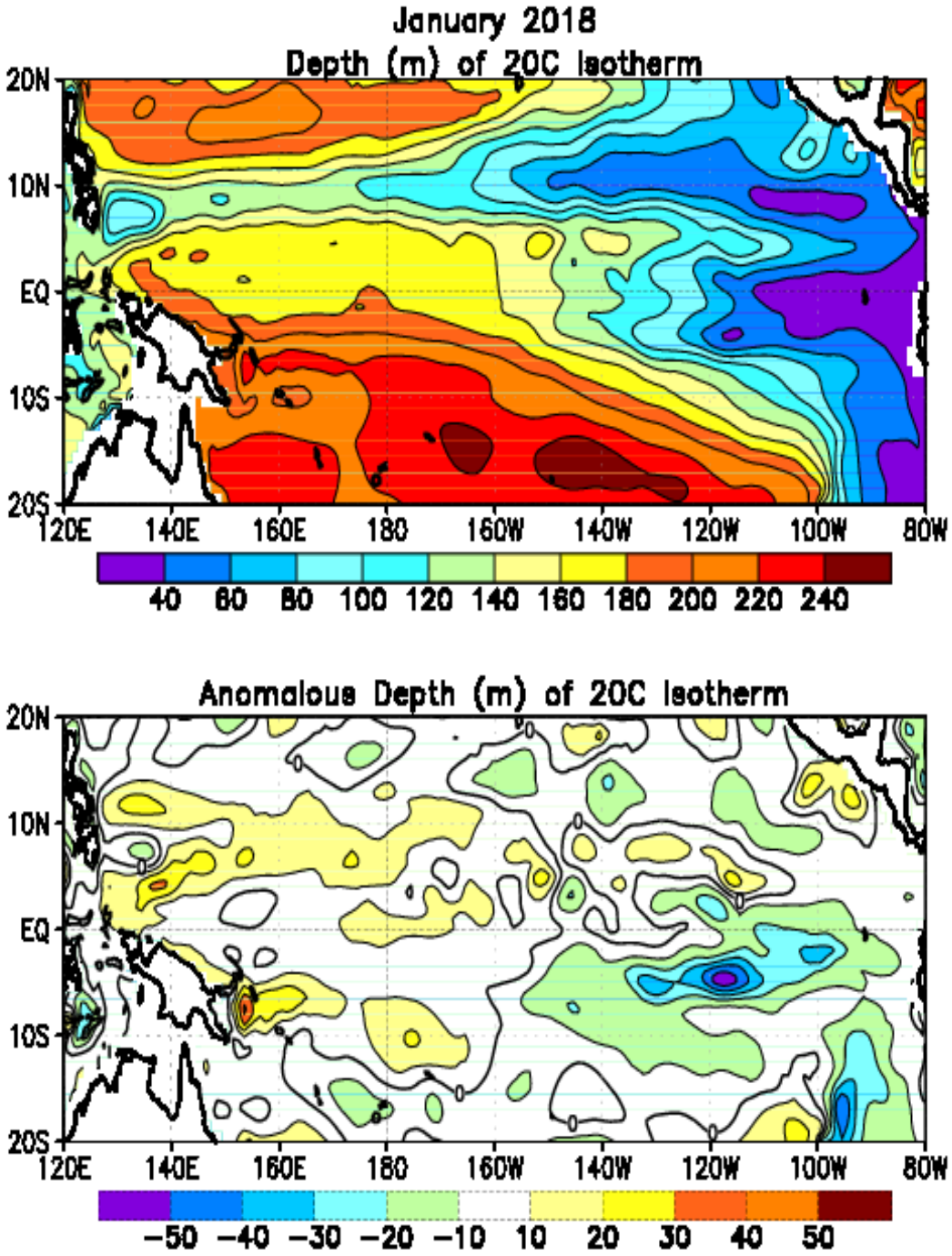

FIGURE T16. Mean (top) and anomalous (bottom) depth of the 20°C isotherm for JAN 2018. Contour interval is 40 m (top) and 10 m (bottom). Dashed contours in bottom panel indicate negative anomalies. Data are derived from the NCEP's global ocean data assimilation system version 2 which assimilates oceanic observations into an oceanic GCM (Xue, Y. and Behringer, D.W., 2006: Operational global ocean data assimilation system at NCEP, to be submitted to BAMS). Anomalies are departures from the 1981–2010 base period means.

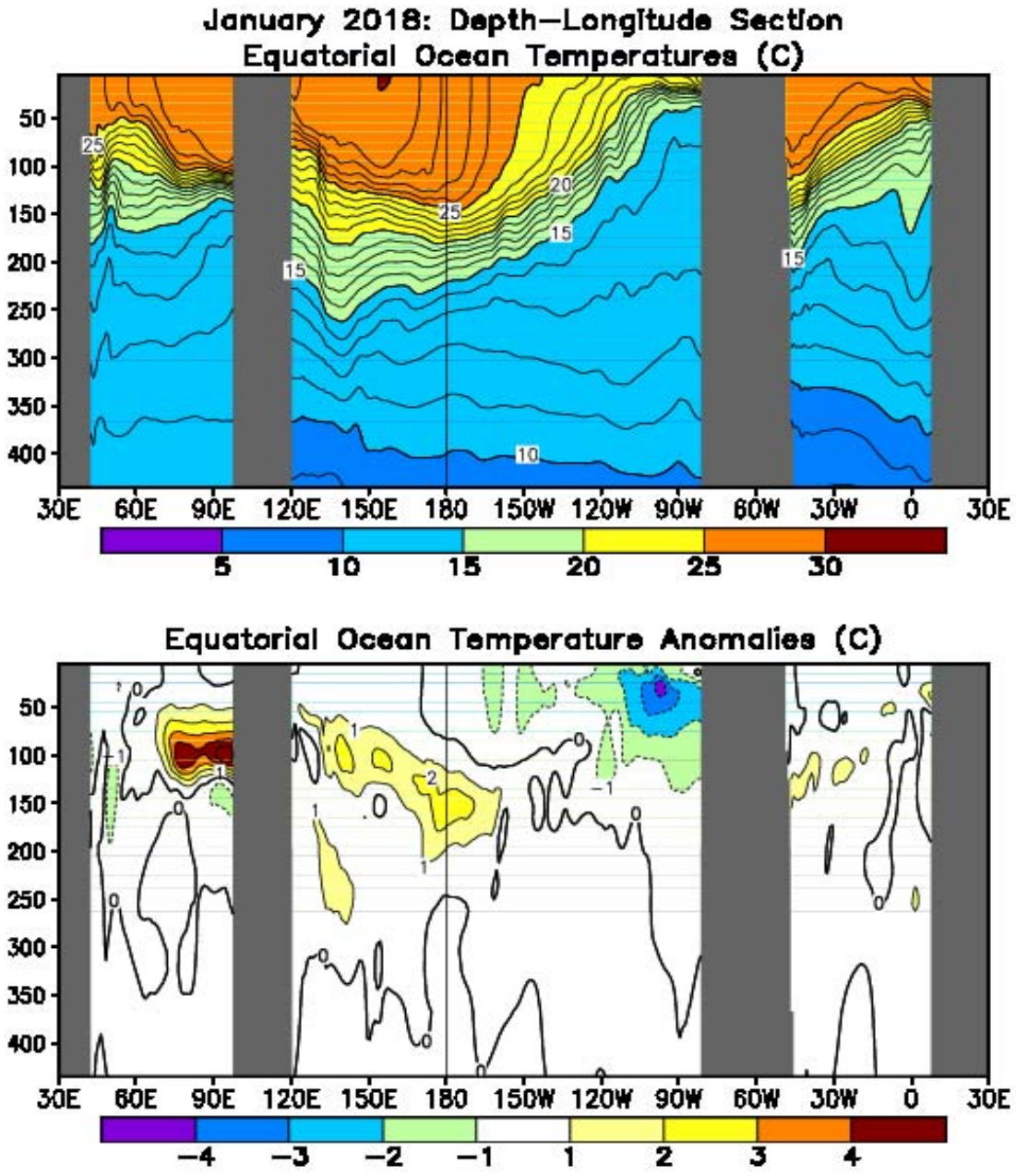

FIGURE T17. Equatorial depth-longitude section of ocean temperature (top) and ocean temperature anomalies (bottom) for JAN 2018. Contour interval is 1°C. Dashed contours in bottom panel indicate negative anomalies. Data are derived from the NCEP's global ocean data assimilation system version 2 which assimilates oceanic observations into an oceanic GCM (Xue, Y. and Behringer, D.W., 2006: Operational global ocean data assimilation system at NCEP, to be submitted to BAMS). Anomalies are departures from the 1981–2010 base period means.

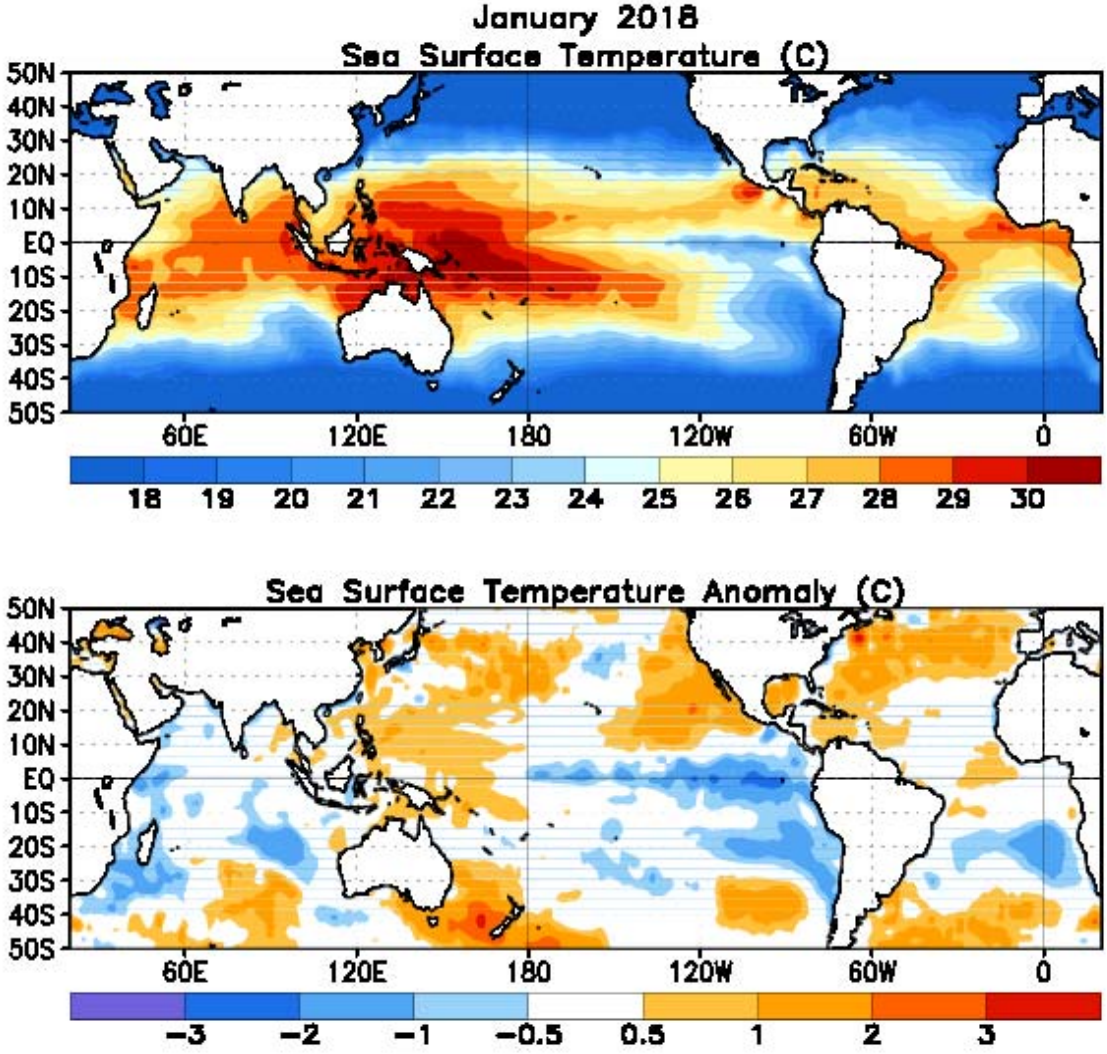

FIGURE T18. Mean (top) and anomalous (bottom) sea surface temperature (SST). Anomalies are departures from the 1981-2010 base period monthly means (Smith and Reynolds 1998, *J. Climate*, **11**, 3320-3323).

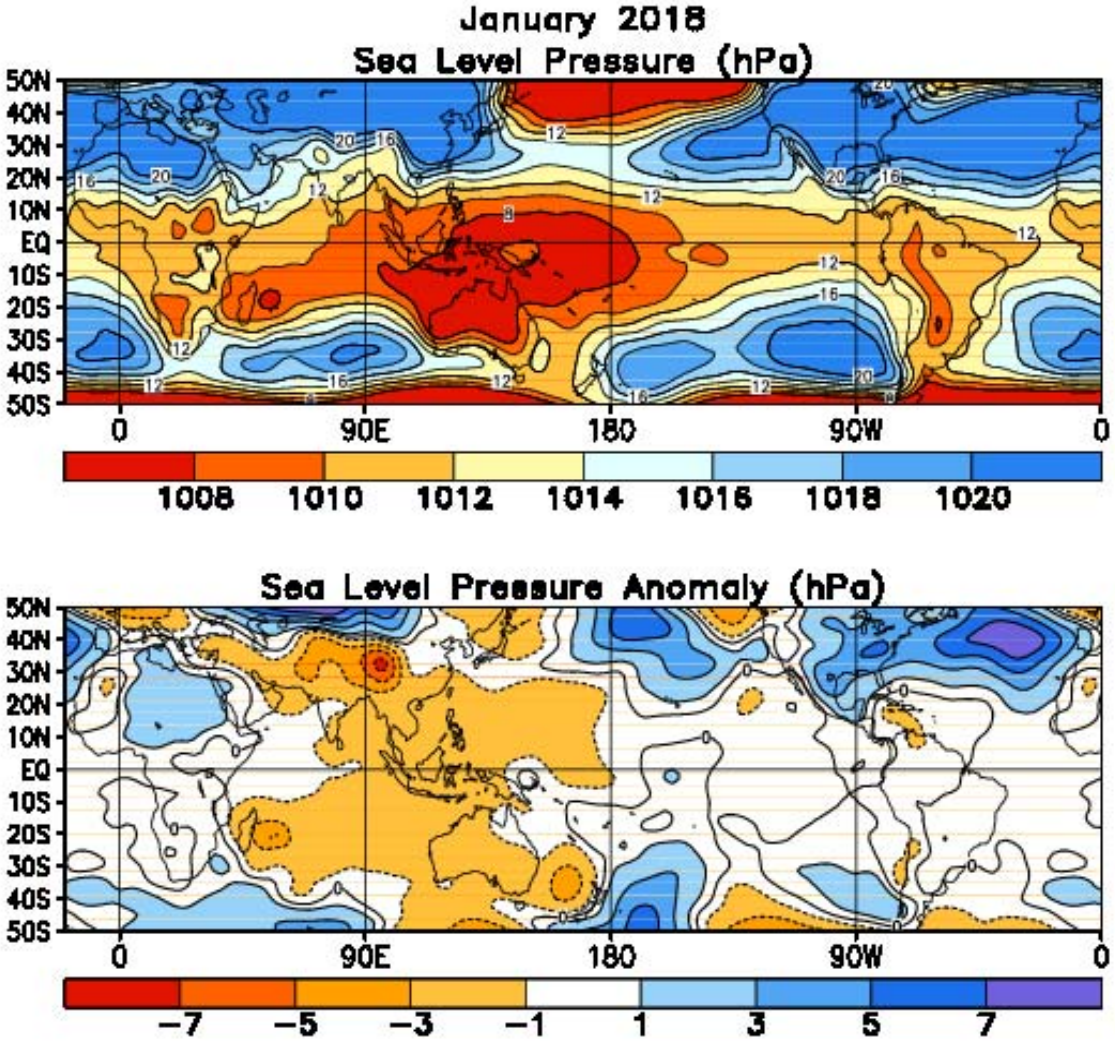

FIGURE T19. Mean (top) and anomalous (bottom) sea level pressure (SLP) (CDAS/Reanalysis). In top panel, 1000 hPa has been subtracted from contour labels, contour interval is 2 hPa, and values below 1000 hPa are indicated by dashed contours. In bottom panel, anomaly contour interval is 1 hPa and negative anomalies are indicated by dashed contours. Anomalies are departures from the 1981-2010 base period monthly means.

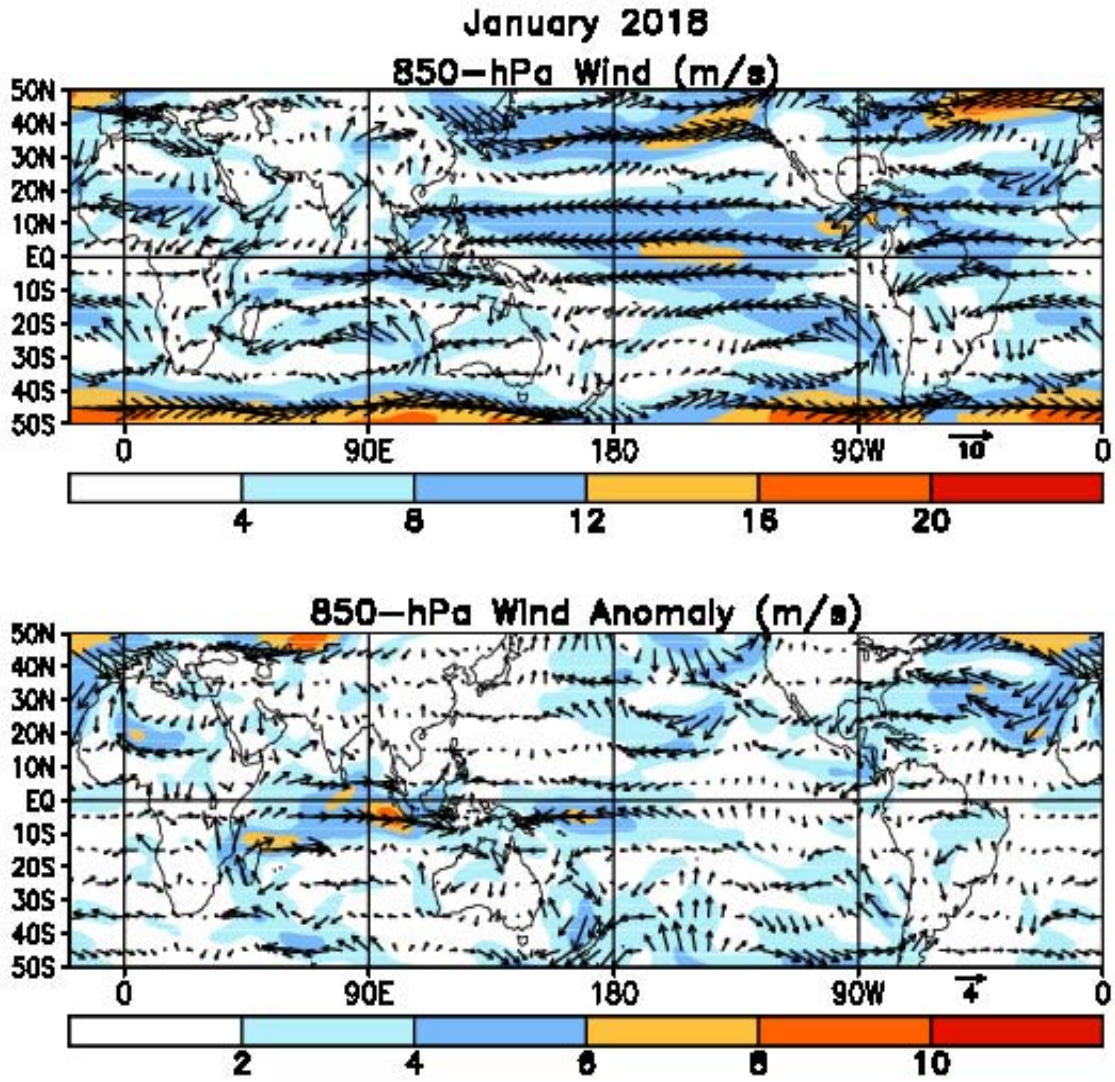

FIGURE T20. Mean (top) and anomalous (bottom) 850-hPa vector wind (CDAS/Reanaysis) for JAN 2018. Contour interval for isotachs is 4 ms^{-1} (top) and 2 ms^{-1} (bottom). Anomalies are departures from the 1981-2010 base period monthly means.

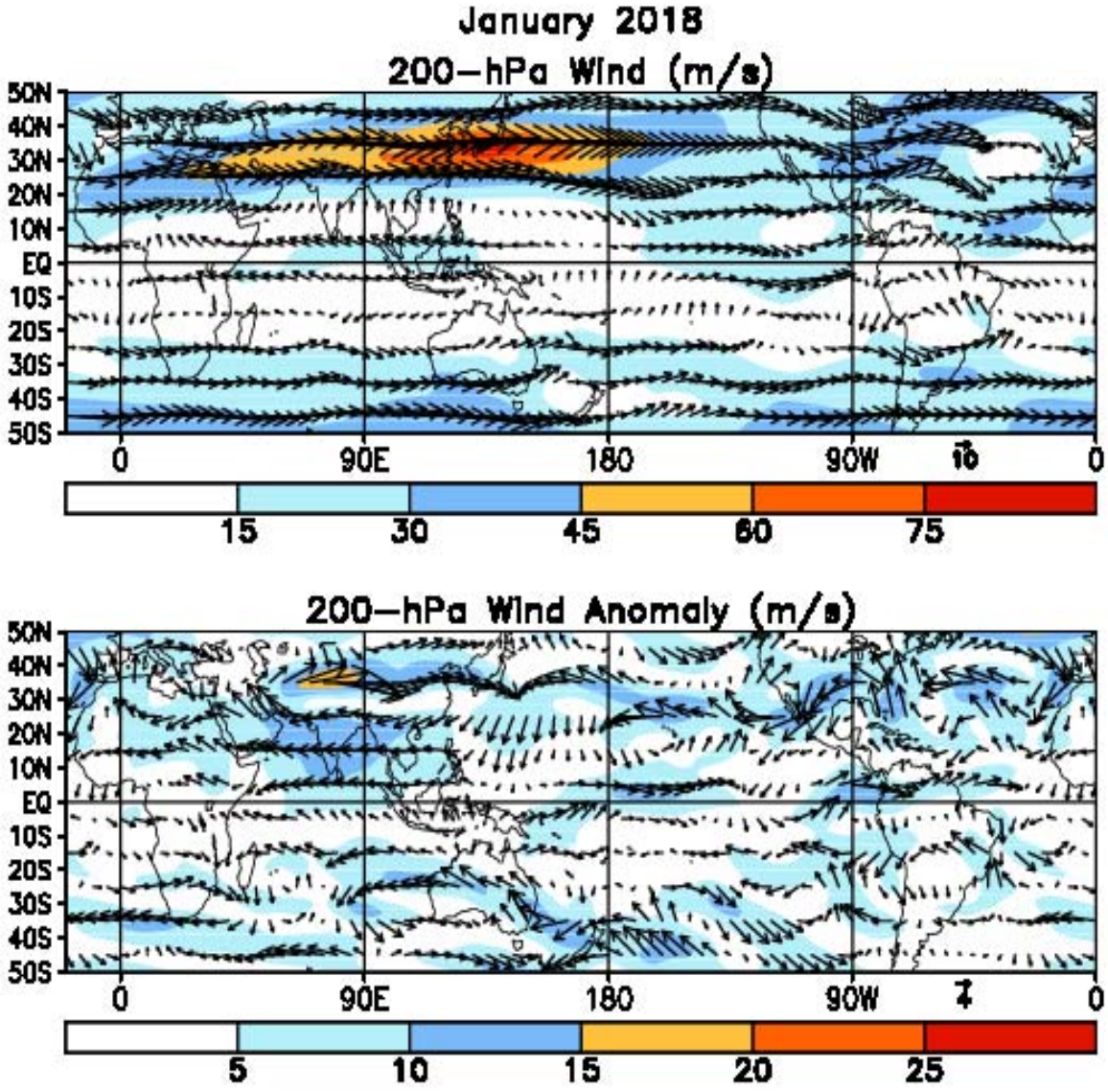

FIGURE T21. Mean (top) and anomalous (bottom) 200-hPa vector wind (CDAS/Reanalysis) for JAN 2018. Contour interval for isotachs is 15 ms^{-1} (top) and 5 ms^{-1} (bottom). Anomalies are departures from 1981-2010 base period monthly means.

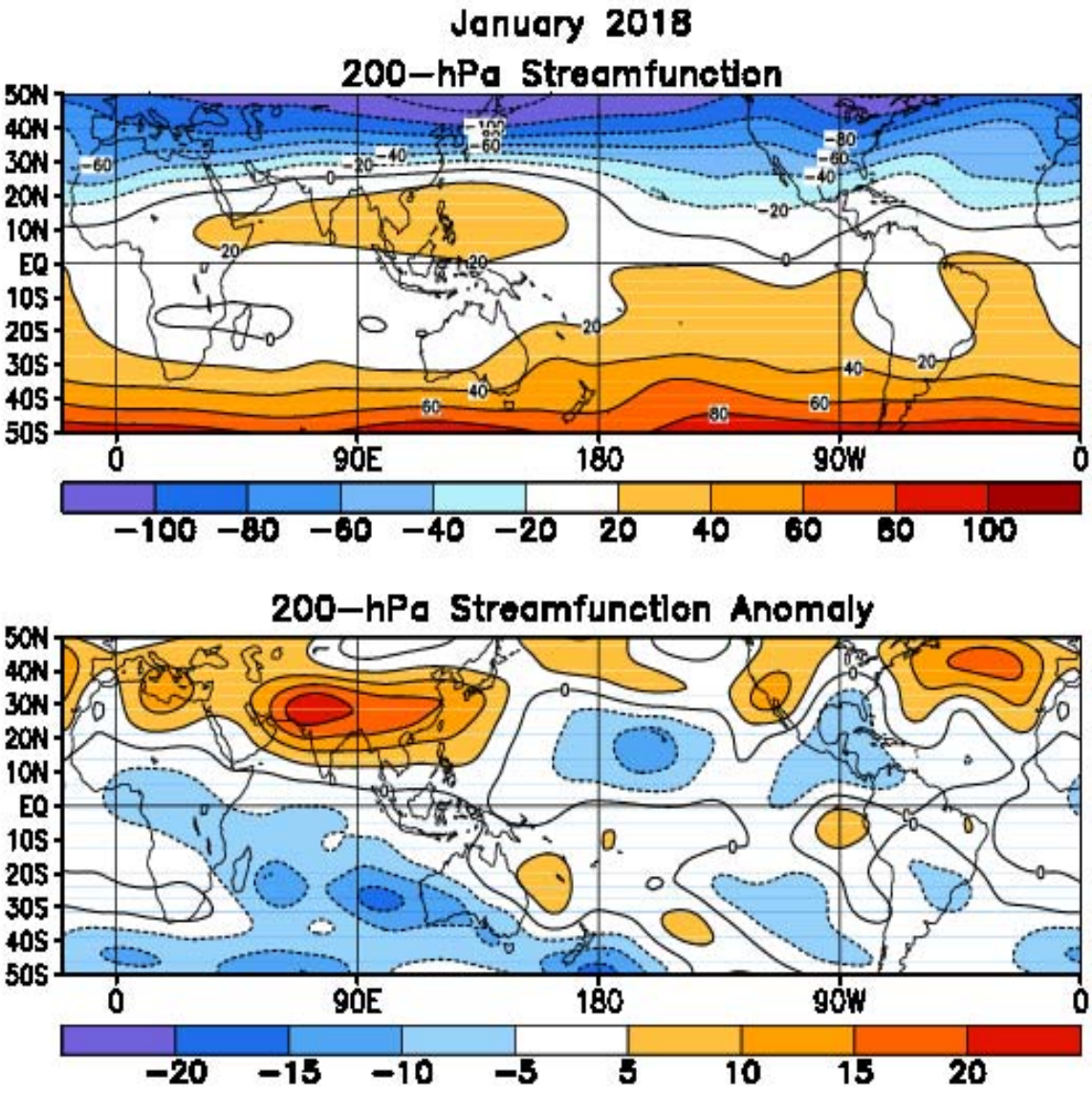

FIGURE T22. Mean (top) and anomalous (bottom) 200-hPa streamfunction (CDAS/Reanalysis). Contour interval is 20 x 10^6 m^2s^{-1} (top) and 5 x 10^6 m^2s^{-1} (bottom). Negative (positive) values are indicated by dashed (solid) lines. The non-divergent component of the flow is directed along the contours with speed proportional to the gradient. Thus, high (low) stream function corresponds to high (low) geopotential height in the Northern Hemisphere and to low (high) geopotential height in the Southern Hemisphere. Anomalies are departures from the 1981-2010 base period monthly means.

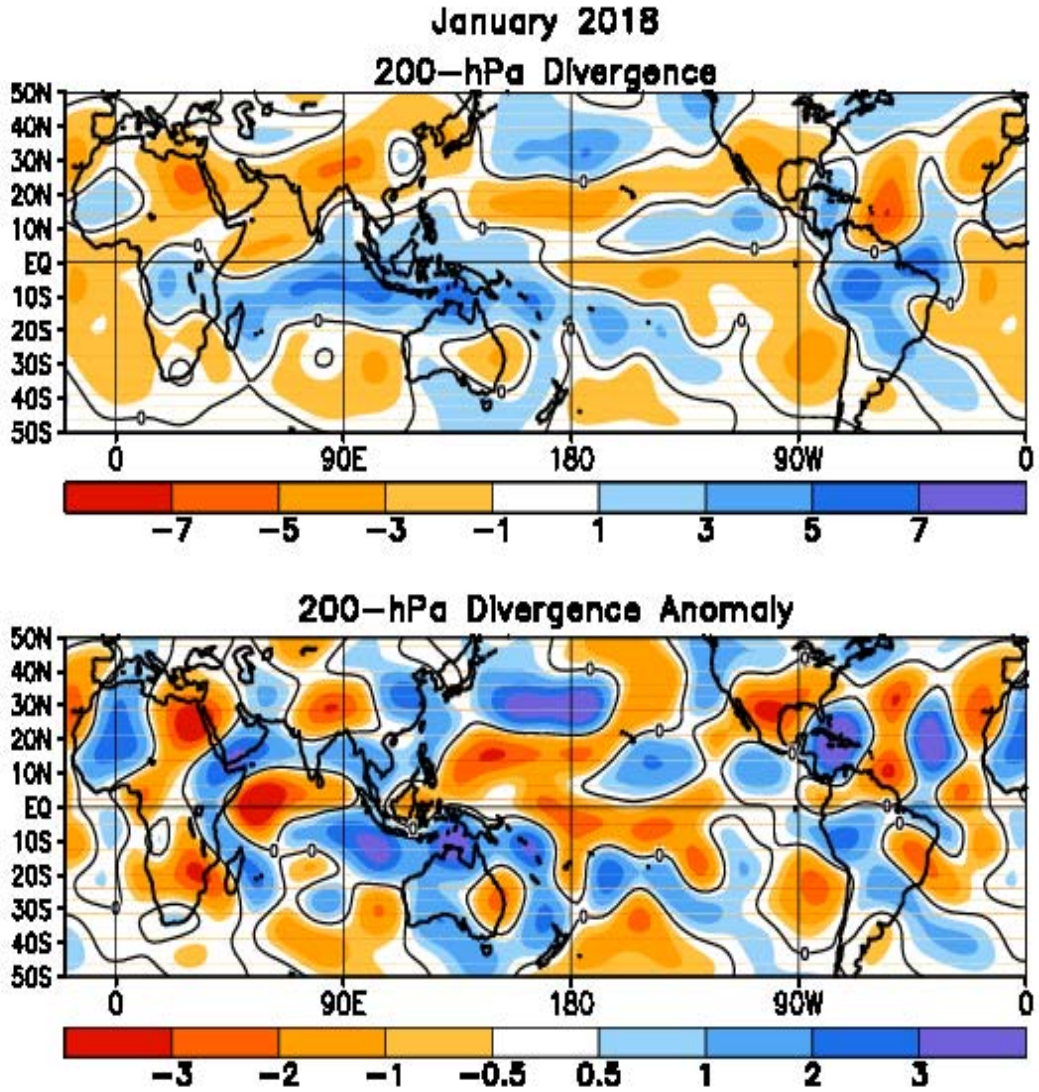

FIGURE T23. Mean (top) and anomalous (bottom) 200-hPa divergence (CDAS/Reanalysis). Divergence and anomalous divergence are shaded blue. Convergence and anomalous convergence are shaded orange. Anomalies are departures from the 1981-2010 base period monthly means.

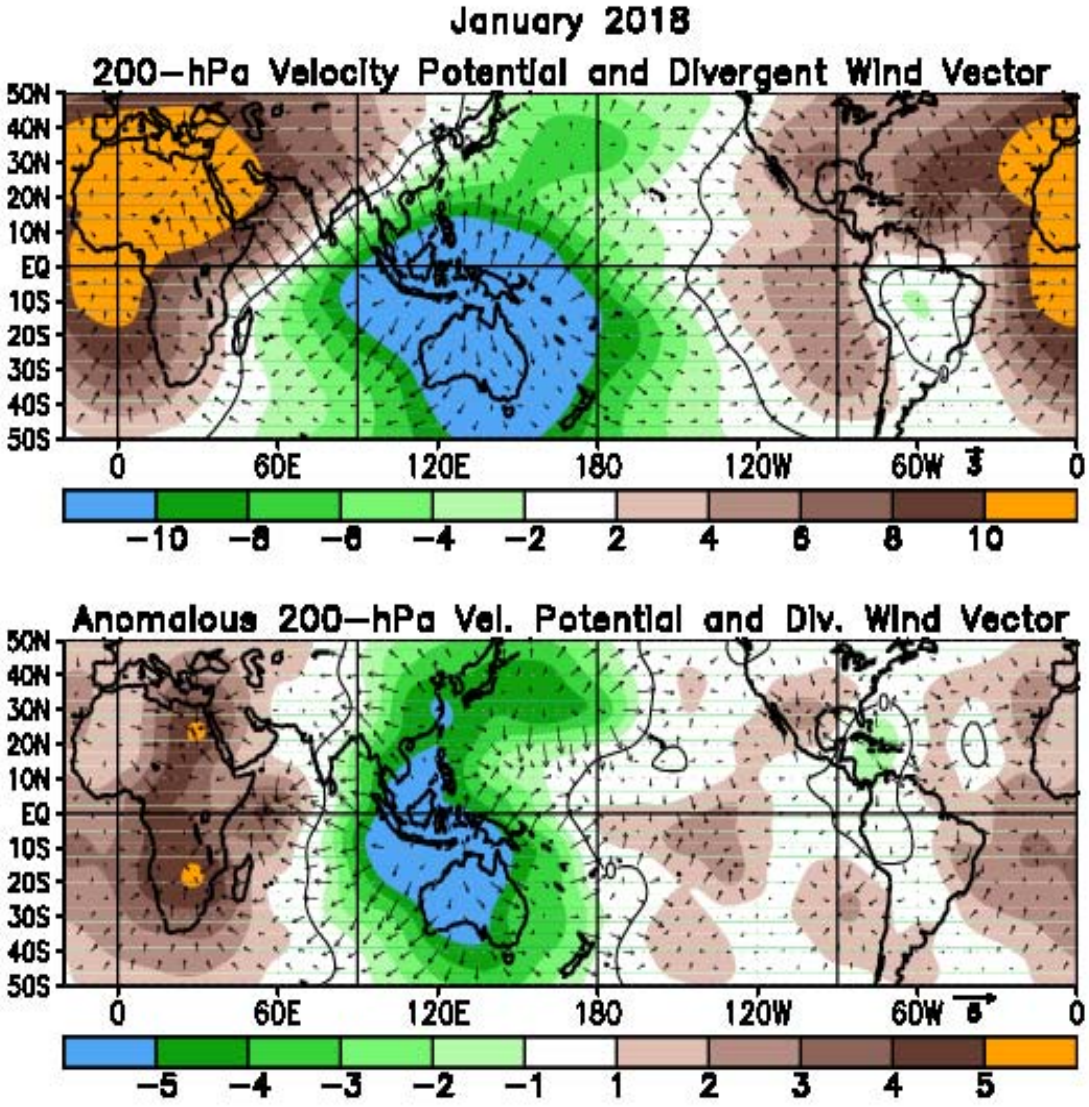

FIGURE T24. Mean (top) and anomalous (bottom) 200-hPa velocity potential ($10^6 m^2 s$) and divergent wind (CDAS/ Reanalysis). Anomalies are departures from the 1981-2010 base period monthly means.

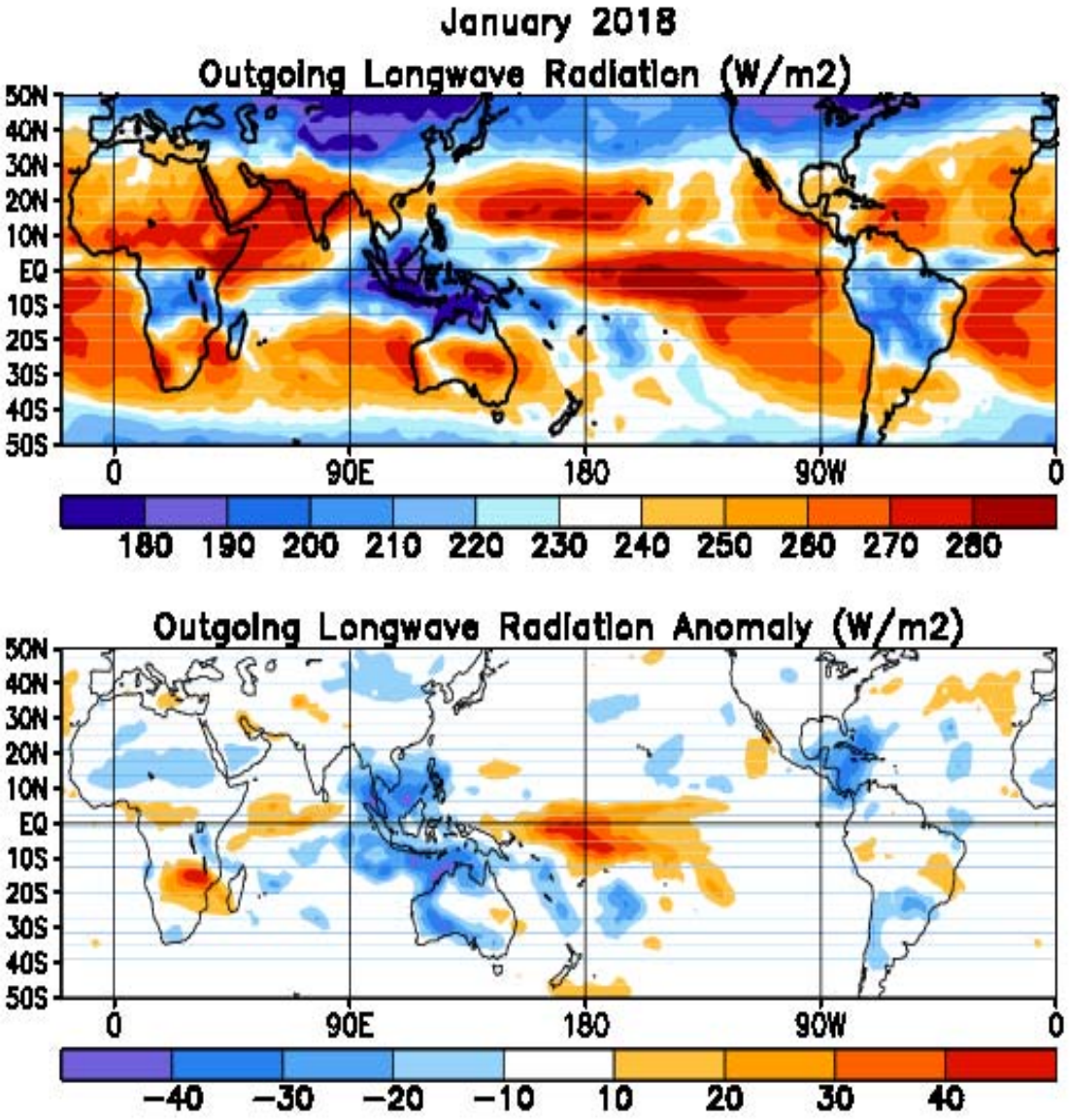

FIGURE T25. Mean (top) and anomalous (bottom) outgoing longwave radiation for JAN 2018 (NOAA 18 AVHRR IR window channel measurements by NESDIS/ORA). OLR contour interval is 20 Wm^{-2} with values greater than 280 Wm^{-2} indicated by dashed contours. Anomaly contour interval is 15 Wm^{-2} with positive values indicated by dashed contours and light shading. Anomalies are departures from the 1981-2010 base period monthly means.

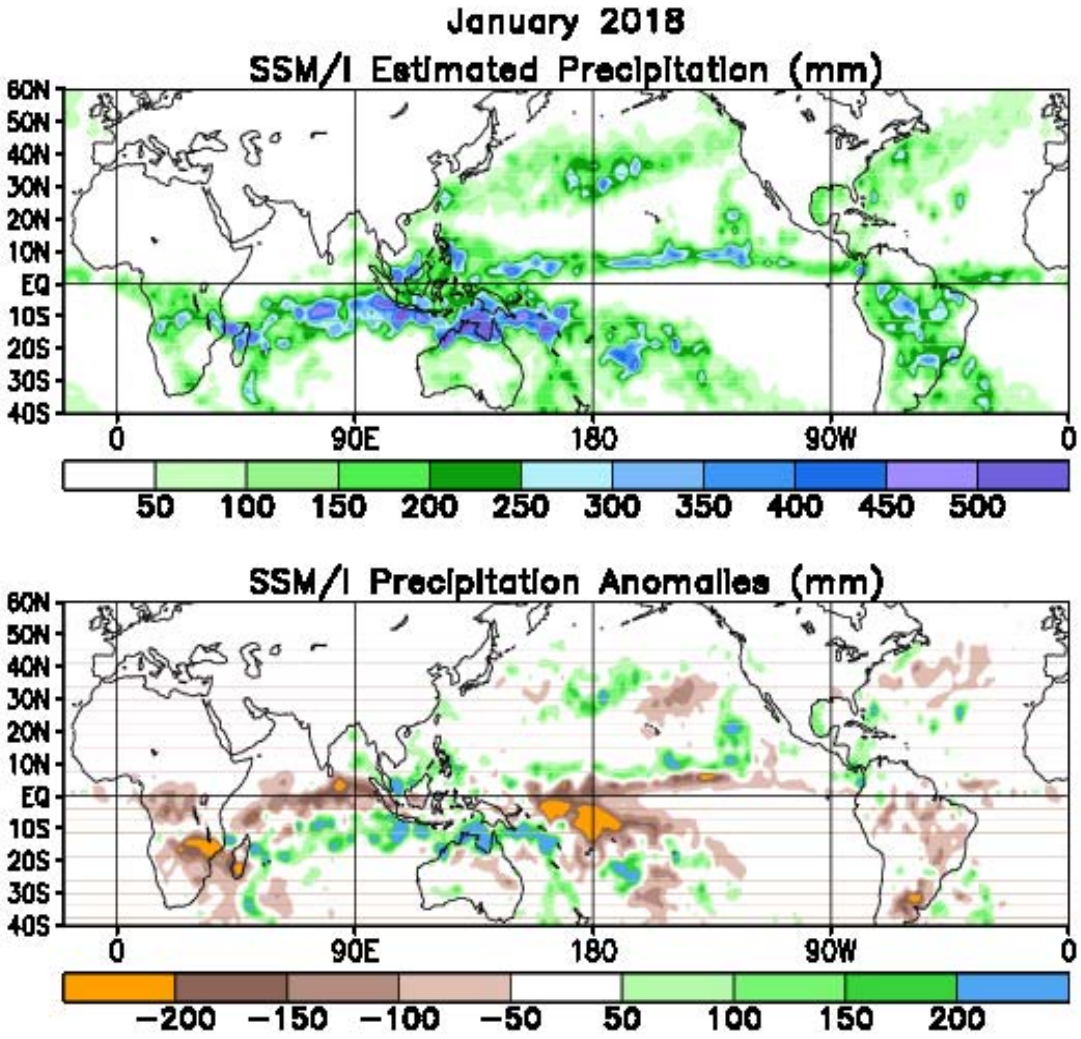

FIGURE T26. Estimated total (top) and anomalous (bottom) rainfall (mm) based on the Special Sensor Microwave/ Imager (SSM/S) precipitation index (Ferraro 1997, *J. Geophys. Res.*, **102**, 16715-16735). Anomalies are computed from the SSM/I 1987-2010 base period monthly means. Anomalies have been smoothed for display purposes.

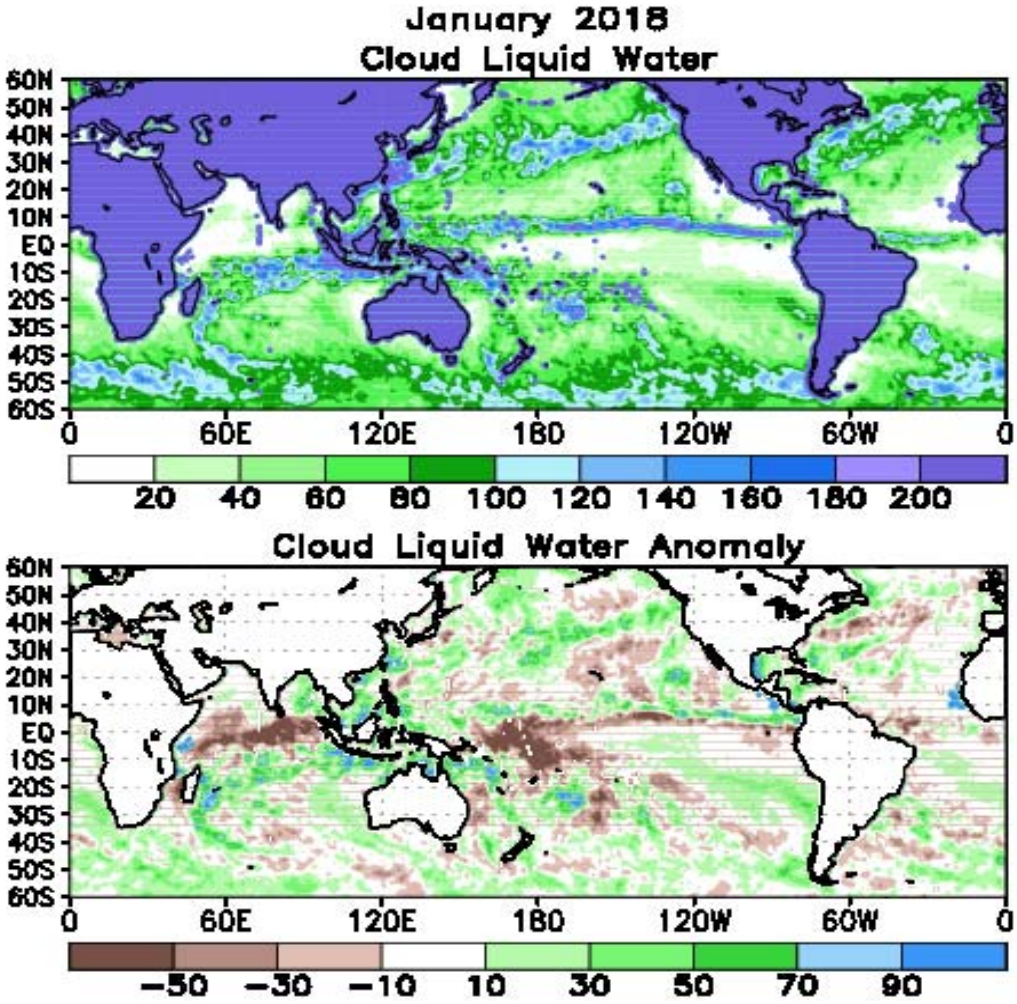

FIGURE T27. Mean (top) and anomalous (bottom) cloud liquid water (g m^{-2}) based on the Special Sensor Microwave/ Imager (SSM/I) (Weng et al 1997: *J. Climate*, **10**, 1086-1098). Anomalies are calculated from the 1987-2010 base period means.

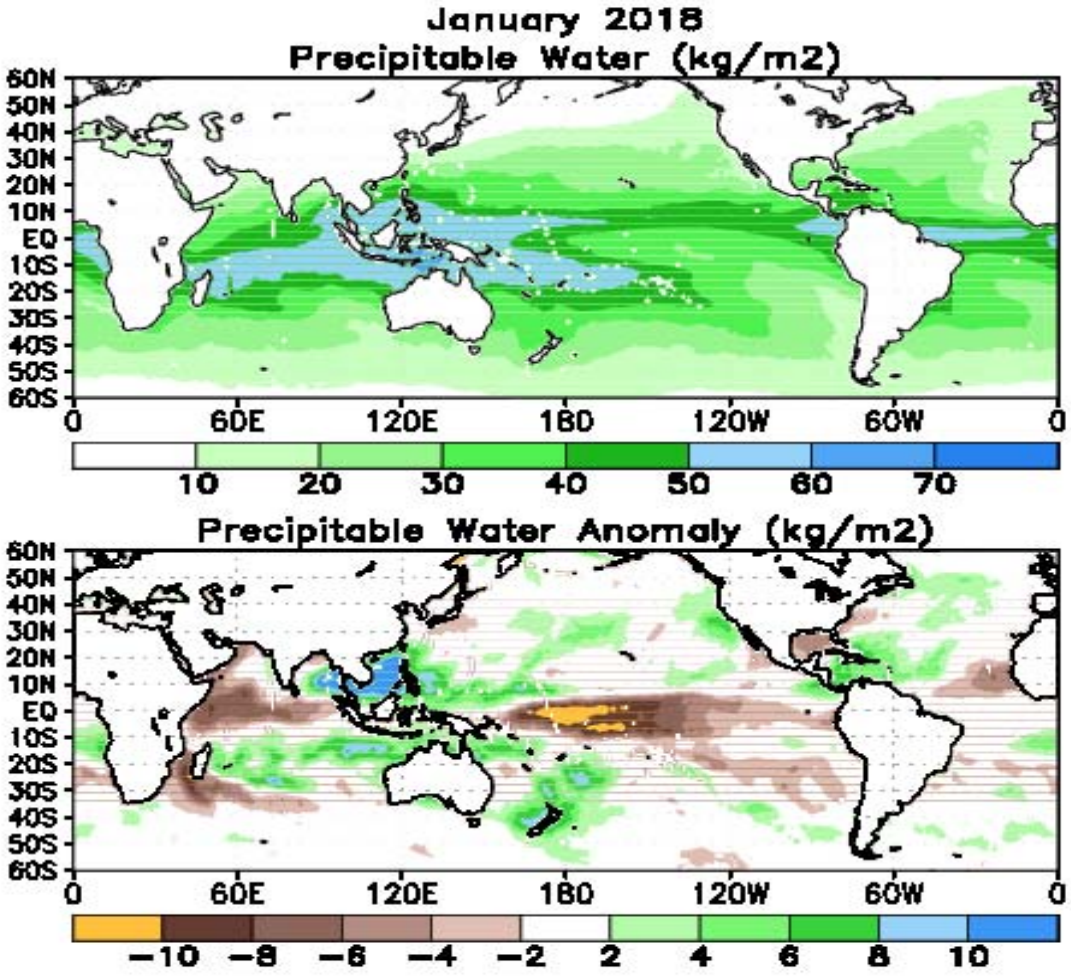

FIGURE T28. Mean (top) and anomalous (bottom) vertically integrated water vapor or precipitable water (kg m^{-2}) based on the Special Sensor Microwave/Imager (SSM/I) (Ferraro et. al, 1996: *Bull. Amer. Meteor. Soc.*, **77**, 891-905). Anomalies are calculated from the 1987-2010 base period means.

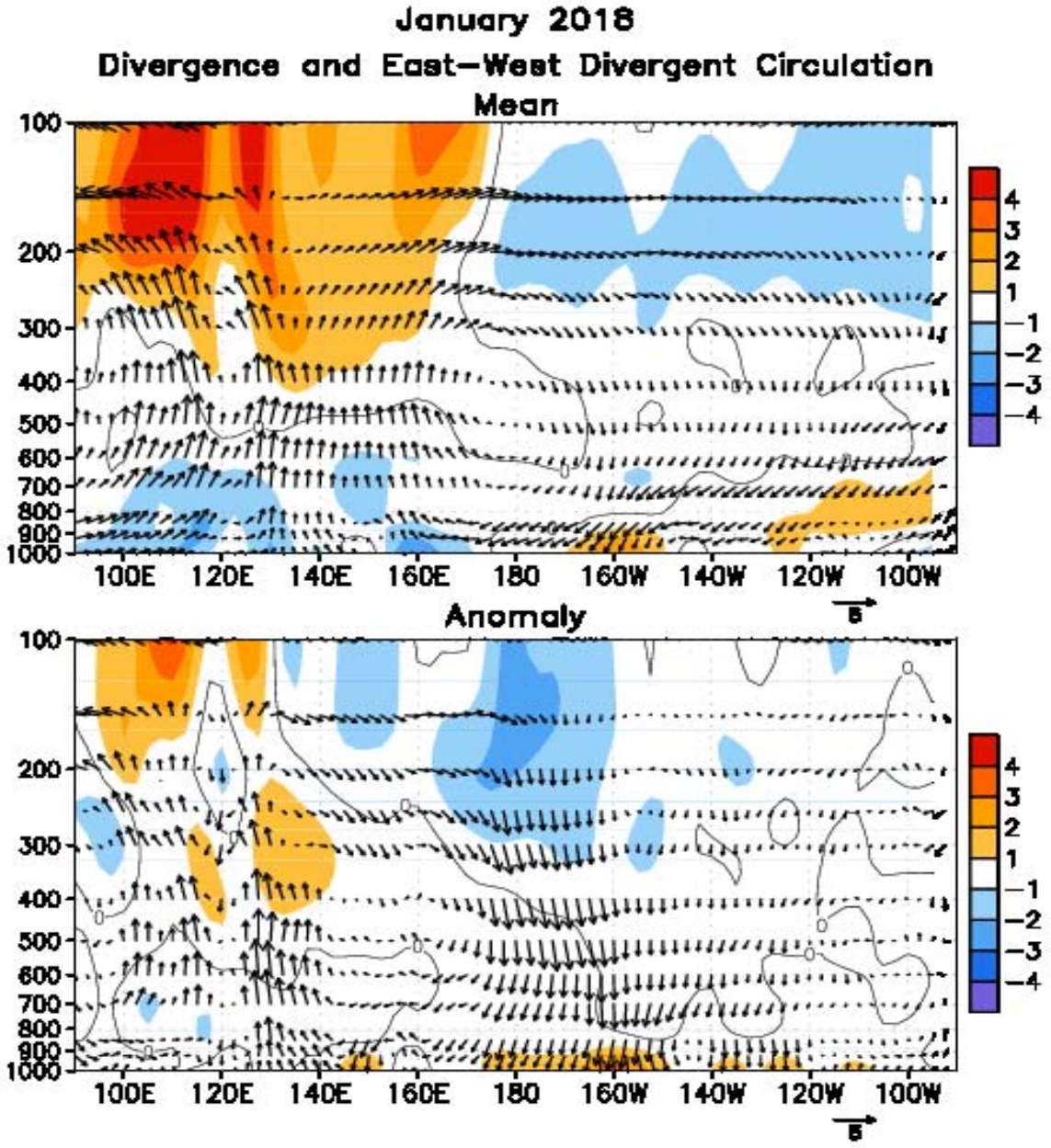

FIGURE T29. Pressure-longitude section (100E-80W) of the mean (top) and anomalous (bottom) divergence (contour interval is 1 x 10^{-6} s^{-1}) and divergent circulation averaged between 5N-5S. The divergent circulation is represented by vectors of combined pressure vertical velocity and the divergent component of the zonal wind. Red shading and solid contours denote divergence (top) and anomalous divergence (bottom). Blue shading and dashed contours denote convergence (top) and anomalous convergence (bottom). Anomalies are departures from the 1981-2010 base period monthly means.

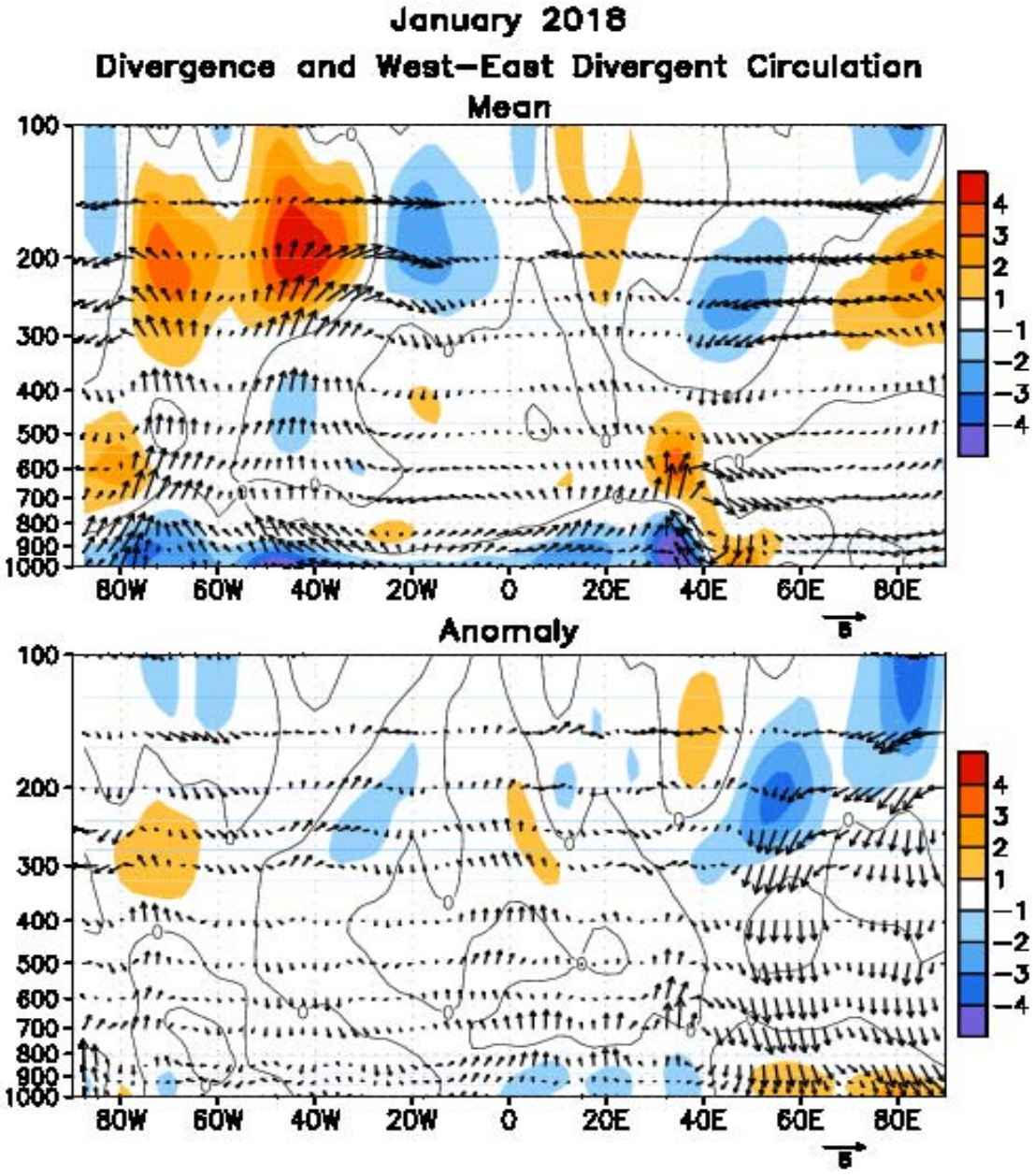

FIGURE T30. Pressure-longitude section (80W-100E) of the mean (top) and anomalous (bottom) divergence (contour interval is 1 x 10^{-6} s^{-1}) and divergent circulation averaged between 5N-5S. The divergent circulation is represented by vectors of combined pressure vertical velocity and the divergent component of the zonal wind. Red shading and solid contours denote divergence (top) and anomalous divergence (bottom). Blue shading and dashed contours denote convergence (top) and anomalous convergence (bottom). Anomalies are departures from the 1981-2010 base period monthly means.

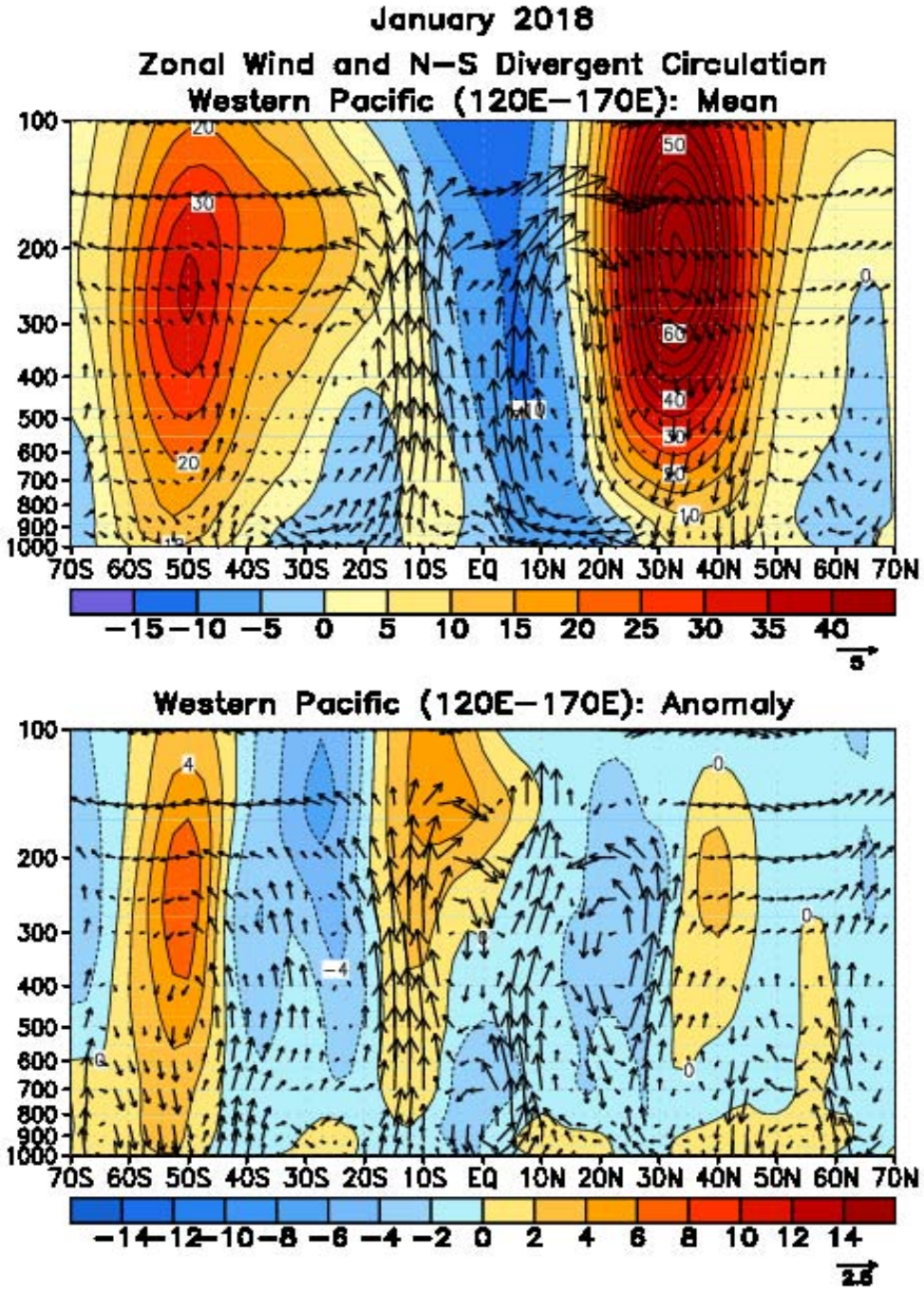

FIGURE T31. Pressure-latitude section of the mean (top) and anomalous (bottom) zonal wind (m s^{-1}) and divergent circulation averaged over the west Pacific sector (120E-170E). The divergent circulation is represented by vectors of combined pressure vertical velocity and the divergent component of the meridional wind. Red shading and solid contours denote a westerly (top) or anomalous westerly (bottom) zonal wind. Blue shading and dashed contours denote an easterly (top) or anomalous easterly (bottom) zonal wind. Anomalies are departures from the 1981-2010 base period monthly means.

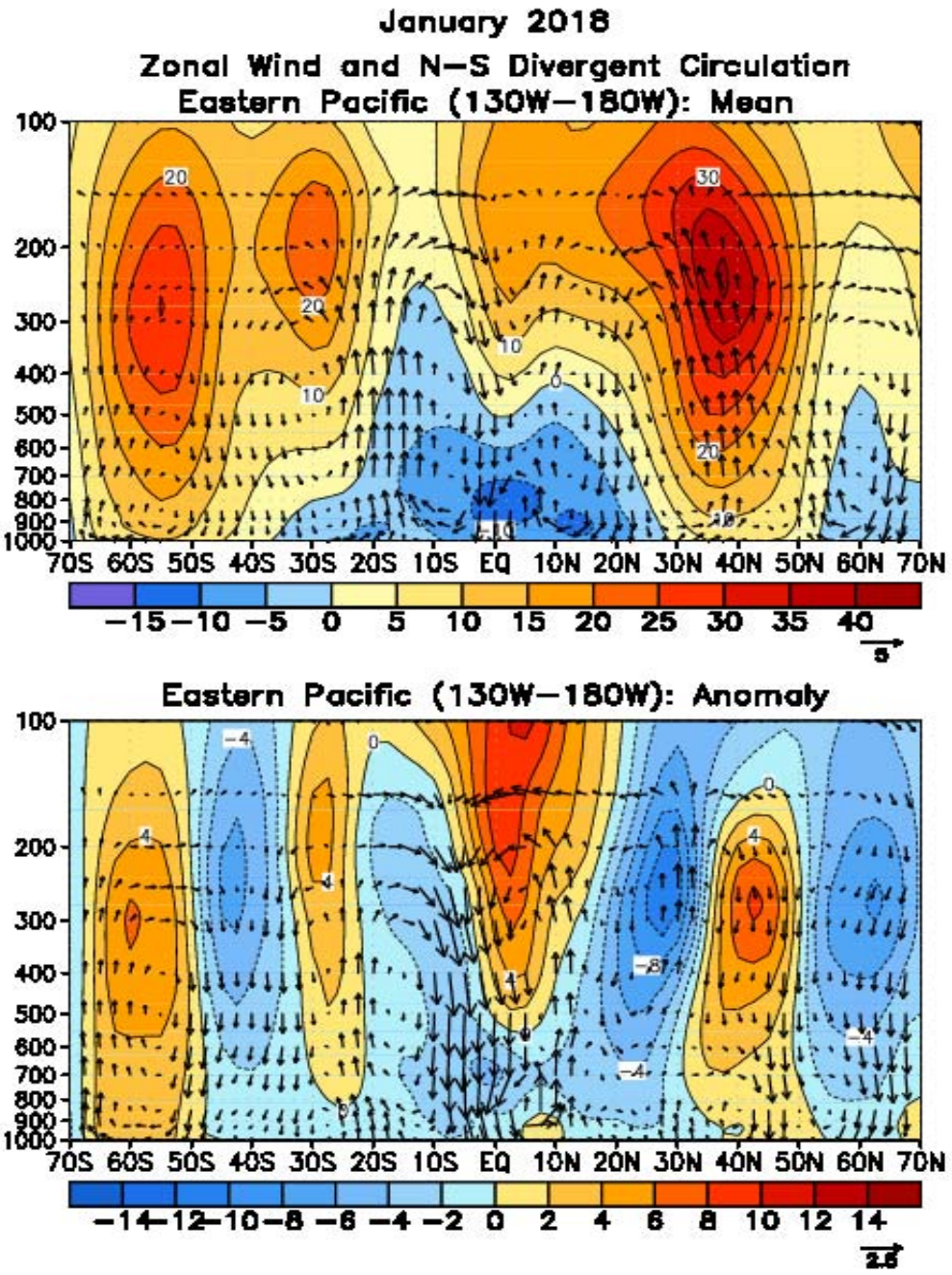

FIGURE T32. Pressure-latitude section of the mean (top) and anomalous (bottom) zonal wind (m s^{-1}) and divergent circulation averaged over the central Pacific sector (130W-180W). The divergent circulation is represented by vectors of combined pressure vertical velocity and the divergent component of the meridional wind. Red shading and solid contours denote a westerly (top) or anomalous westerly (bottom) zonal wind. Blue shading and dashed contours denote an easterly (top) or anomalous easterly (bottom) zonal wind. Anomalies are departures from the 1981-2010 base period monthly means.

Tropical Pacific Drifting Buoys R. Lumpkin/M. Pazos, AOML, Miami

During January 2018, 1466 satellite-tracked surface drifting buoys were reporting from the tropical Pacific. The drifter array did not reveal any large-scale current anomalies in the basin, while several drifters in the eastern basin exhibited very strong anomalies associated with tropical instability waves.

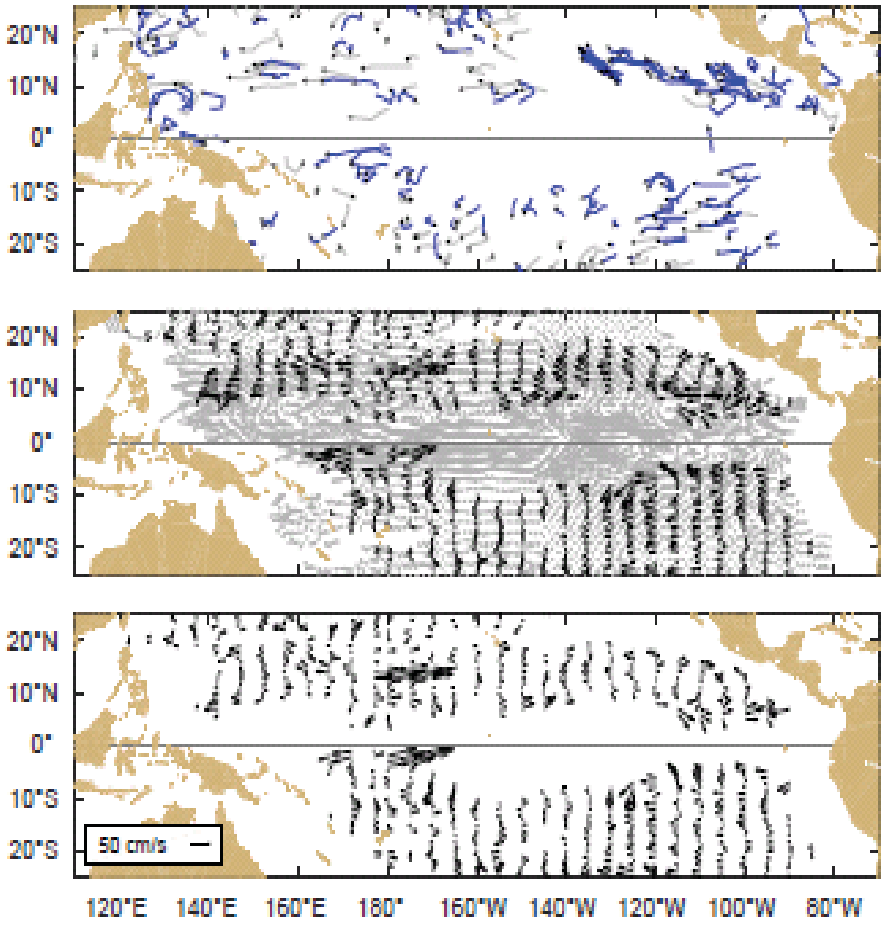

Figure A1.1 Top: Movements of drifting buoys in the tropical Pacific Ocean during January 2018. The linear segments of each trajectory represent a one week displacement. Trajectories of buoys which have lost their subsurface drogues are gray; those with drogues are black.
Middle: Monthly mean currents calculated from all buoys 1993-2002 (gray), and currents measured by the drogued buoys this month (black) smoothed by an optimal filter.
Bottom: Anomalies from the climatological monthly mean currents for this month.

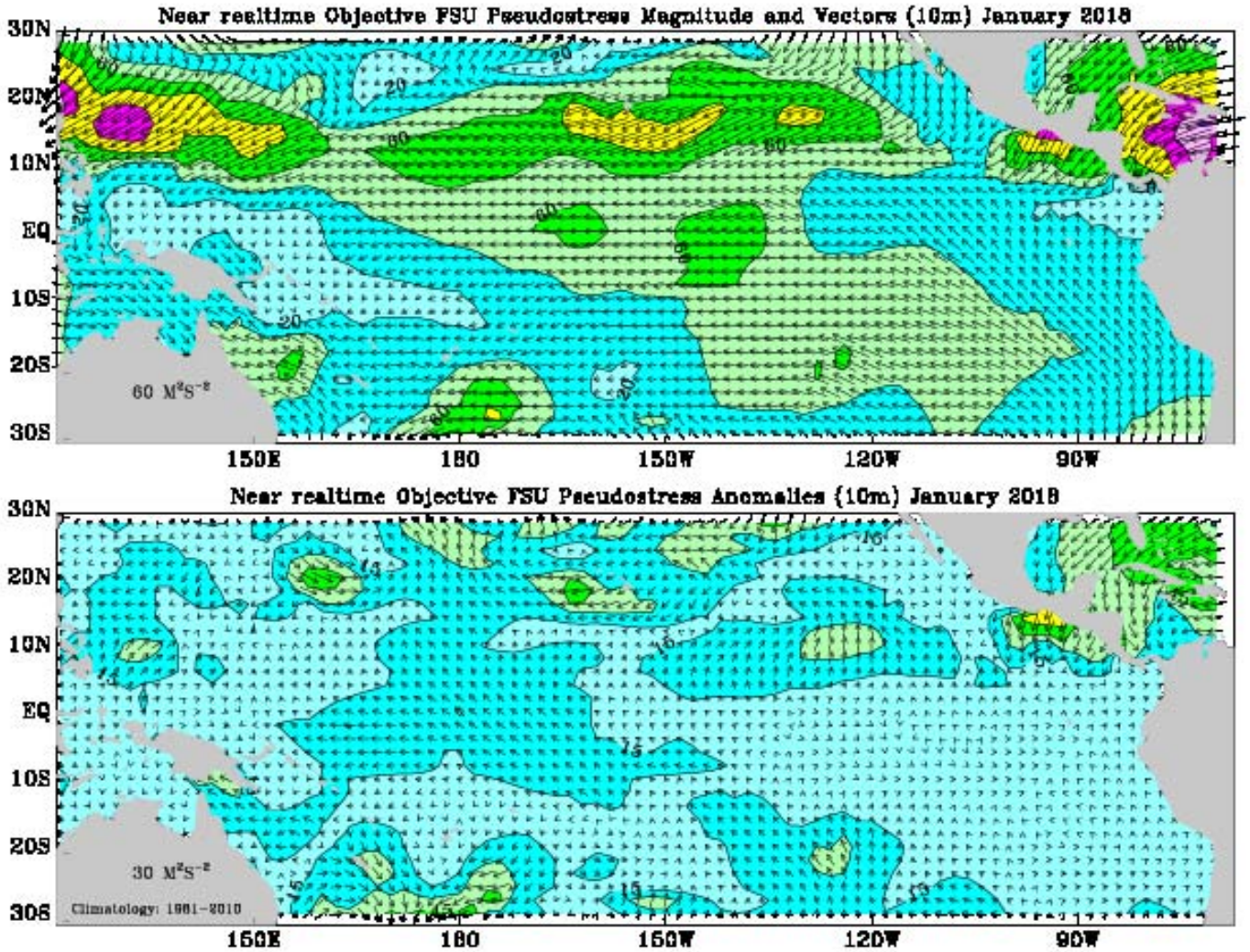

FSU SURFACE PSEUDO-STRESS VECTORS AND ANOMALIES: January 2018. Pseudo-stress vectors (top) are objectively analyzed from ship and buoy winds on a 2° grid. Ship and buoy data are independently weighted and the background field is created from the data. Contour interval of the vector magnitudes is 20 M^2S^{-2}. Anomalies (bottom) are departures from 1981-2010 mean. The contour interval is 15 M^2S^{-2}. For more information, please visit our web site at http://www.coaps.fsu.edu/RVSMDC/html/winds.shtml. Produced by Jeremy Ralph, Mark A. Bourassa, and Shawn R. Smith, Center for Ocean-Atmospheric Prediction Studies, Florida State University, Tallahassee, FL 32306-2840, USA.

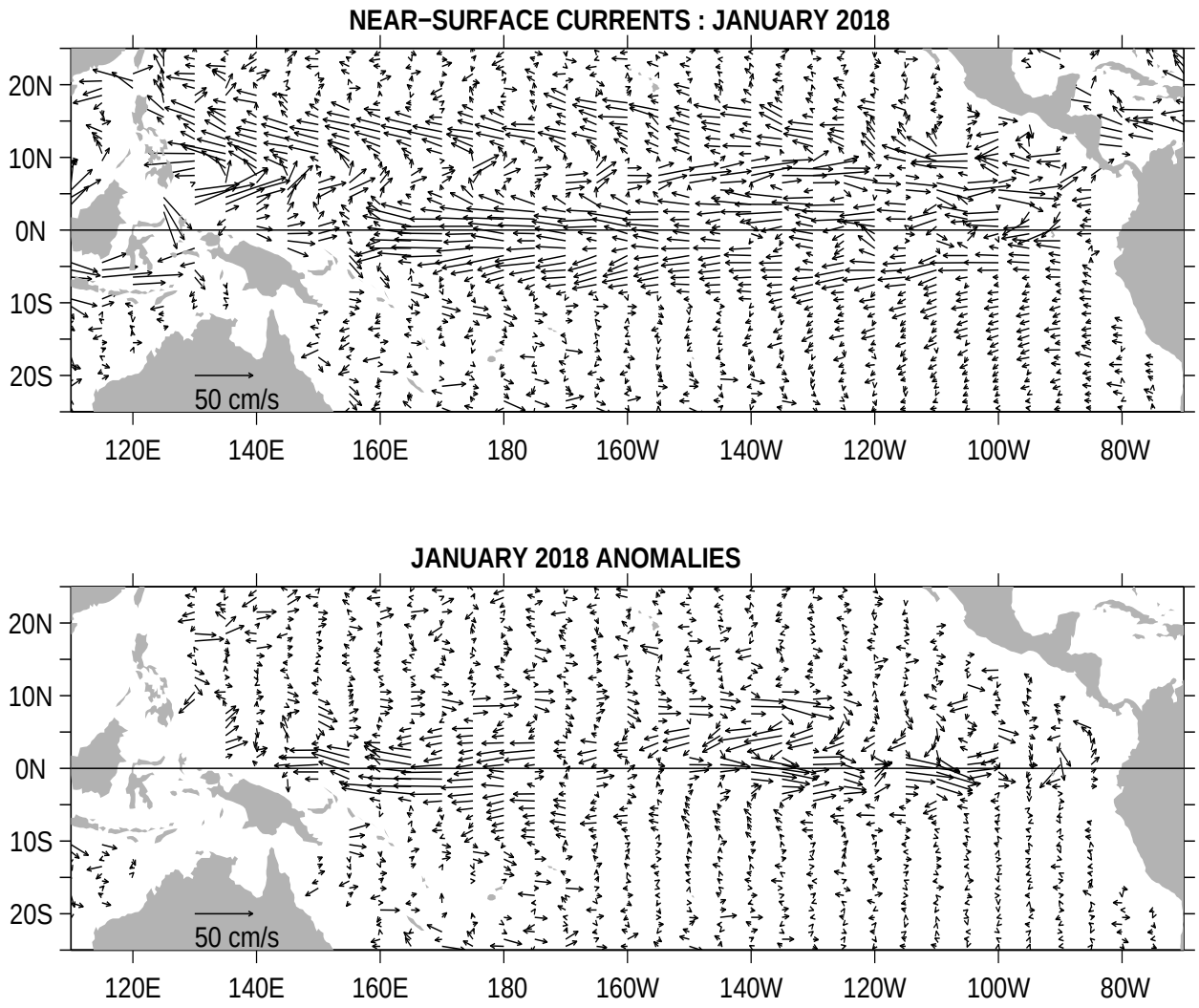

FIGURE A1.3. Ocean Surface Current Analysis-Real-time (OSCAR) for JAN 2018 (Bonjean and Lagerloef 2002, J. Phys. Oceanogr., Vol. 32, No. 10, 2938-2954; Lagerloef et al. 1999, JGR-Oceans, 104, 23313-23326). (top) Total velocity. Surface currents are calculated from satellite data including Jason sea level anomalies and NCEP winds. (bottom) Velocity anomalies. The subtracted climatology was based on SSM/I and QuickScat winds and Topex/ Poseidon and Jason from 1993-2003. See also http://www.oscar.noaa.gov.

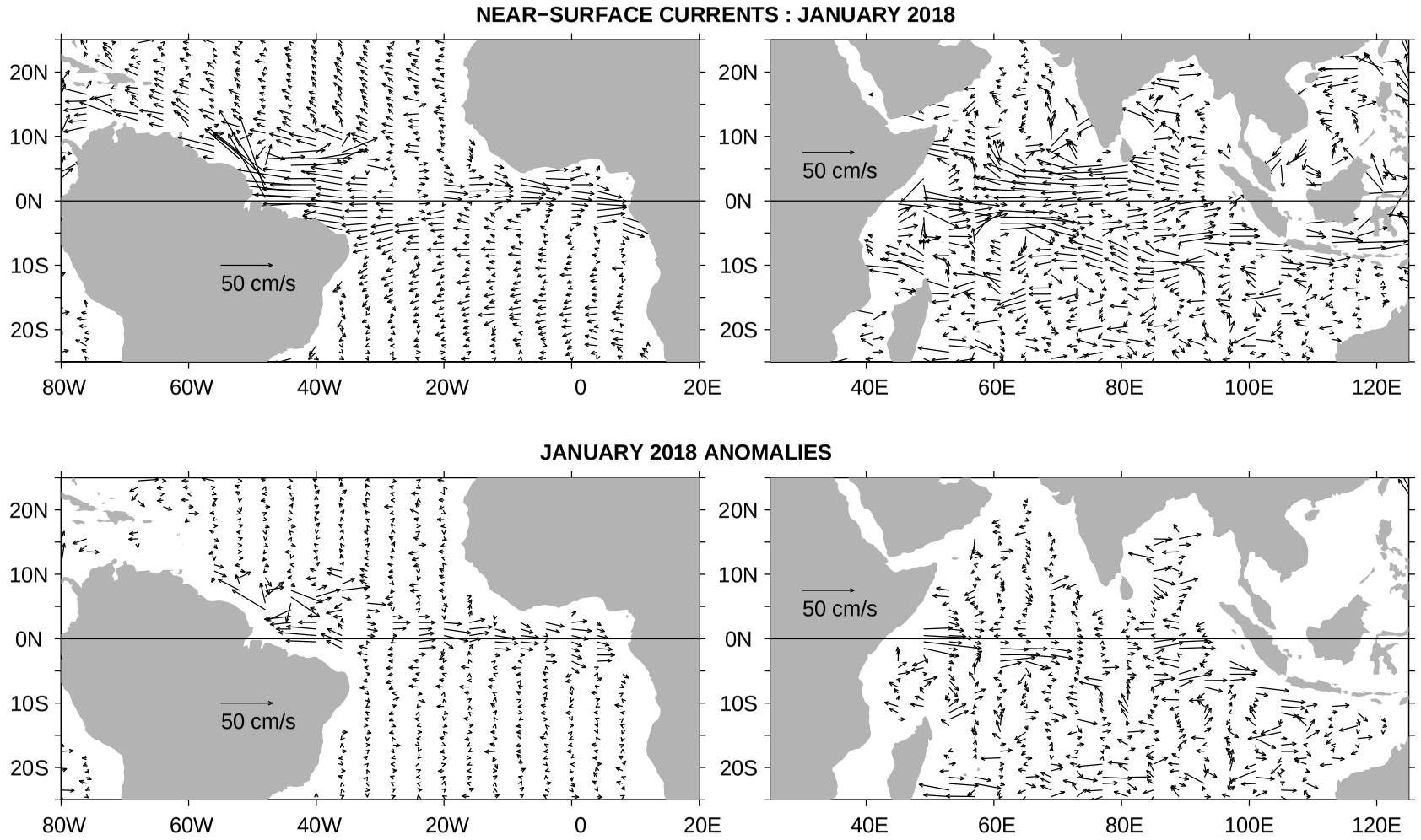

FIGURE A1.4. Ocean Surface Current Analysis-Real-time (OSCAR) for JAN 2018 (Bonjean and Lagerloef 2002, J. Phys. Oceanogr., Vol. 32, No. 10, 2938-2954; Lagerloef et al. 1999, JGR-Oceans, 104, 23313-23326). (top) Total velocity. Surface currents are calculated from satellite data including Jason sea level anomalies and NCEP winds. (bottom) Velocity anomalies. The subtracted climatology was based on SSM/I and QuickScat winds and Topex/Poseidon and Jason from 1993-2003. See also http://www.oscar.noaa.gov.

Forecast Forum

The canonical correlation analysis (CCA) forecast of SST in the central Pacific (Barnett et al. 1988, *Science*, **241**, 192196; Barnston and Ropelewski 1992, *J. Climate*, **5**, 13161345), is shown in **Figs. F1 and F2.** This forecast is produced routinely by the Prediction Branch of the Climate Prediction Center. The predictions from the National Centers for Environmental Prediction (NCEP) Coupled Forecast System Model (CFS03) are presented in **Figs. F3 and F4a, F4b**. Predictions from the Markov model (Xue, et al. 2000: *J. Climate*, **13**, 849871) are shown in **Figs. F5 and F6.** Predictions from the latest version of the LDEO model (Chen et al. 2000: *Geophys. Res. Let*., **27**, 25852587) are shown in **Figs. F7 and F8**. Predictions using linear inverse modeling (Penland and Magorian 1993: *J. Climate*, **6**, 10671076) are shown in **Figs. F9 and F10.** Predictions from the Scripps / Max Planck Institute (MPI) hybrid coupled model (Barnett et al. 1993: *J. Climate*, **6**, 15451566) are shown in **Fig. F11.** Predictions from the ENSOCLIPER statistical model (Knaff and Landsea 1997, *Wea. Forecasting*, **12**, 633652) are shown in **Fig. F12.** Niño 3.4 predictions are summarized in **Fig. F13**, provided by the Forecasting and Prediction Research Group of the IRI.

The CPC and the contributors to the **Forecast Forum** caution potential users of this predictive information that they can expect only modest skill.

ENSO Alert System Status: La Niña Advisory

Outlook

A transition from La Niña to ENSO-neutral is most likely during the Northern Hemisphere spring (~55% chance of ENSO-neutral during the March-May season).

Discussion

During January 2018, La Niña was evident in the pattern of below-average sea surface temperatures (SSTs) across the central and eastern equatorial Pacific Ocean (Fig. T18). The monthly index values were close to -1.0C in the Niño-1+2, Niño-3, and Niño-3.4 regions, while the western-most Niño-4 region was -0.3C (Table 2). While negative anomalies were maintained near the surface, the sub-surface temperatures in the eastern Pacific Ocean returned to near average during the last month. This was due to the eastward propagation of above-average temperatures in association with a downwelling equatorial oceanic Kelvin wave, which undercut the below-average temperatures near the surface (Fig. T17). The atmospheric conditions over the tropical Pacific Ocean also reflected La Niña, with suppressed convection near and east of the International Date Line and enhanced

convection around Indonesia (Fig. T25). Also, the low-level trade winds remained stronger than average over the western and central Pacific, while upper-level winds were anomalously westerly (Figs. T20 & T21). Overall, the ocean and atmosphere system remained consistent with La Niña.

Most models in the IRI/CPC plume predict La Niña will decay and return to ENSO-Neutral during the Northern Hemisphere spring 2018 (Figs. F1-F13). The forecast consensus also favors a transition during the spring with a continuation of ENSO-neutral conditions thereafter. In summary, a transition from La Niña to ENSO-neutral is most likely during the Northern Hemisphere spring (~55% chance of ENSO-neutral during the March-May season).

Weekly updates of oceanic and atmospheric conditions are available on the Climate Prediction Center homepage (El Niño/La Niña Current Conditions and Expert Discussions).

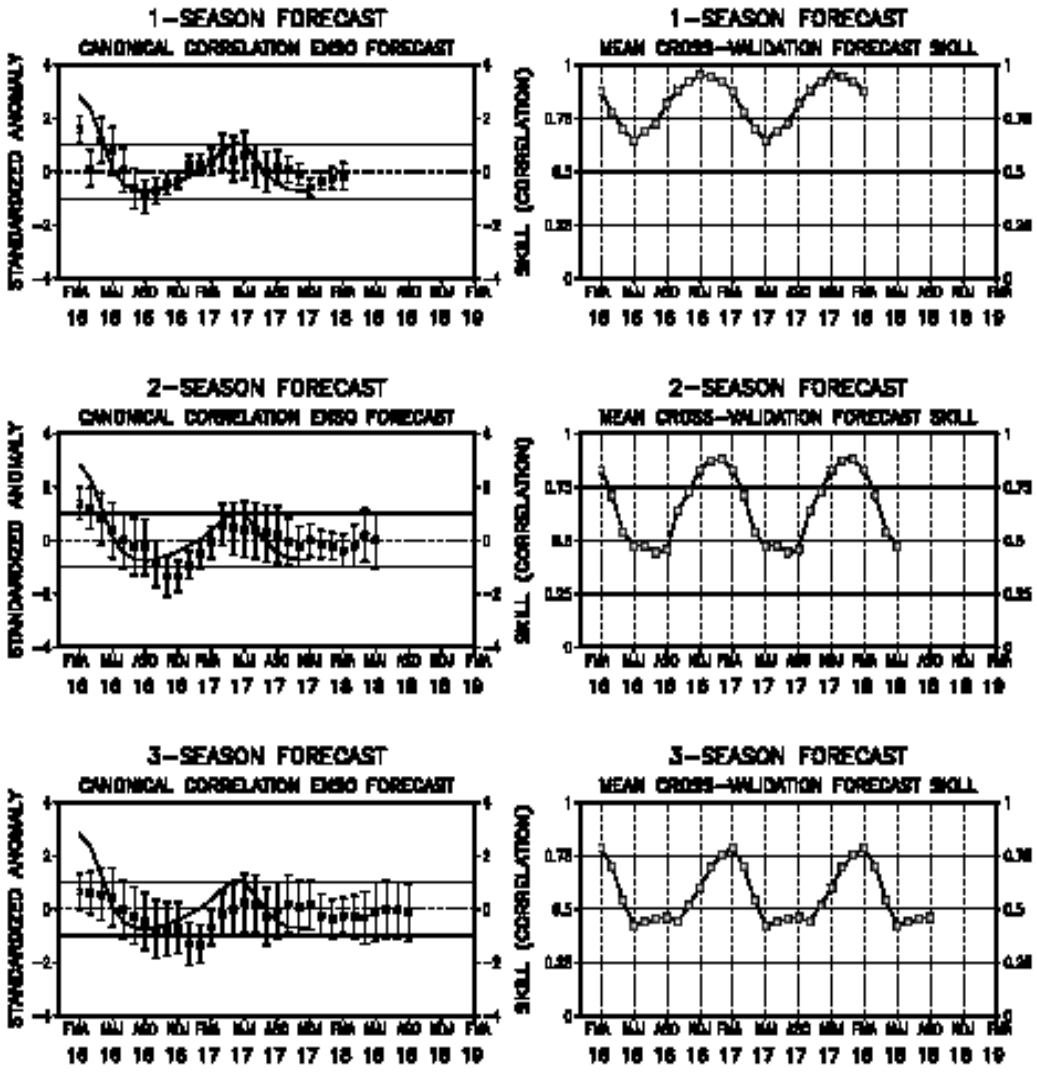

FIGURE F1. Canonical correlation analysis (CCA) sea surface temperature (SST) anomaly prediction for the central Pacific (5˚N to 5˚S, 120˚W to 170˚W (Barnston and Ropelewski, 1992, *J. Climate*, **5**, 1316-1345). The three plots on the left hand side are, from top to bottom, the 1-season, 2-season, and 3-season lead forecasts. The solid line in each forecast represents the observed SST standardized anomaly through the latest month. The small squares at the mid-points of the forecast bars represent the real-time CCA predictions based on the anomalies of quasi-global sea level pressure and on the anomalies of tropical Pacific SST, depth of the 20˚C isotherm and sea level height over the prior four seasons. The vertical lines represent the one standard deviation error bars for the predictions based on past performance. The three plots on the right side are skills, corresponding to the predicted and observed SST. The skills are derived from cross-correlation tests from 1956 to present. These skills show a clear annual cycle and are inversely proportional to the length of the error bars depicted in the forecast time series.

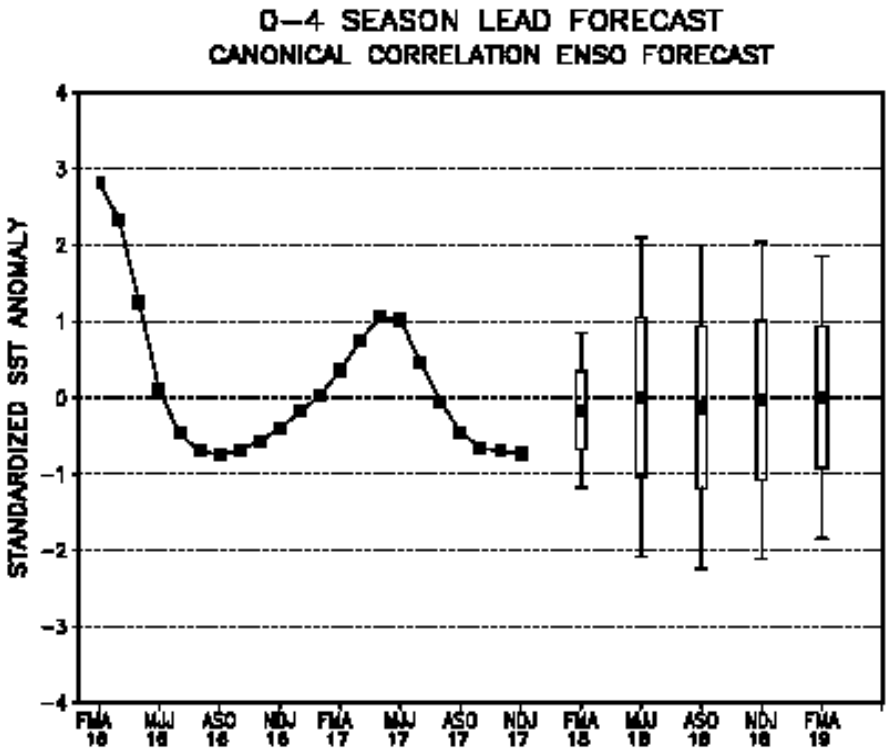

FIGURE F2. Canonical Correlation Analysis (CCA) forecasts of sea-surface temperature anomalies for the Nino 3.4 region (5N-5S, 120W-170W) for the upcoming five consecutive 3-month periods. Forecasts are expressed as standardized SST anomalies. The CCA predictions are based on anomaly patterns of SST, depth of the 20C isotherm, sea level height, and sea level pressure. Small squares at the midpoints of the vertical forecast bars represent the CCA predictions, and the bars show the one (thick) and two (thin) standard deviation errors. The solid continuous line represents the observed standardized three-month mean SST anomaly in the Nino 3.4 region up to the most recently available data.

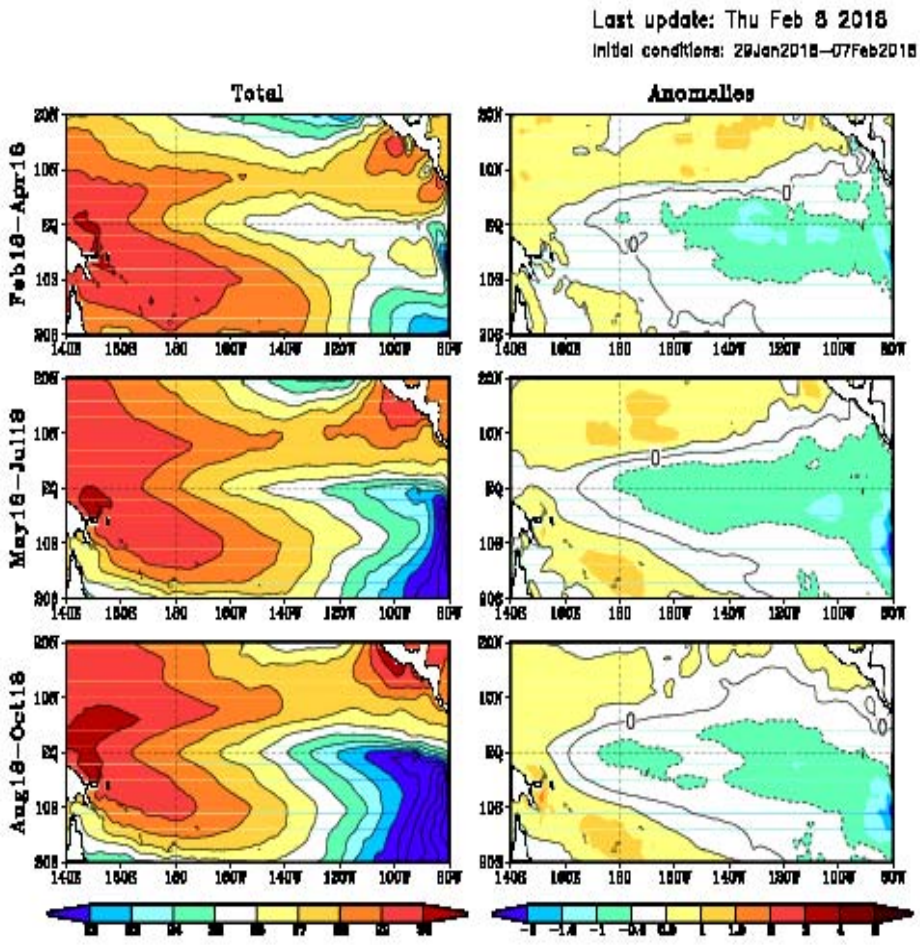

FIGURE F3. Predicted 3-month average sea surface temperature (left) and anomalies (right) from the NCEP Coupled Forecast System Model (CFS03). The forecasts consist of 40 forecast members. Contour interval is 1°C, with additional contours for 0.5°C and -0.5°C. Negative anomalies are indicated by dashed contours.

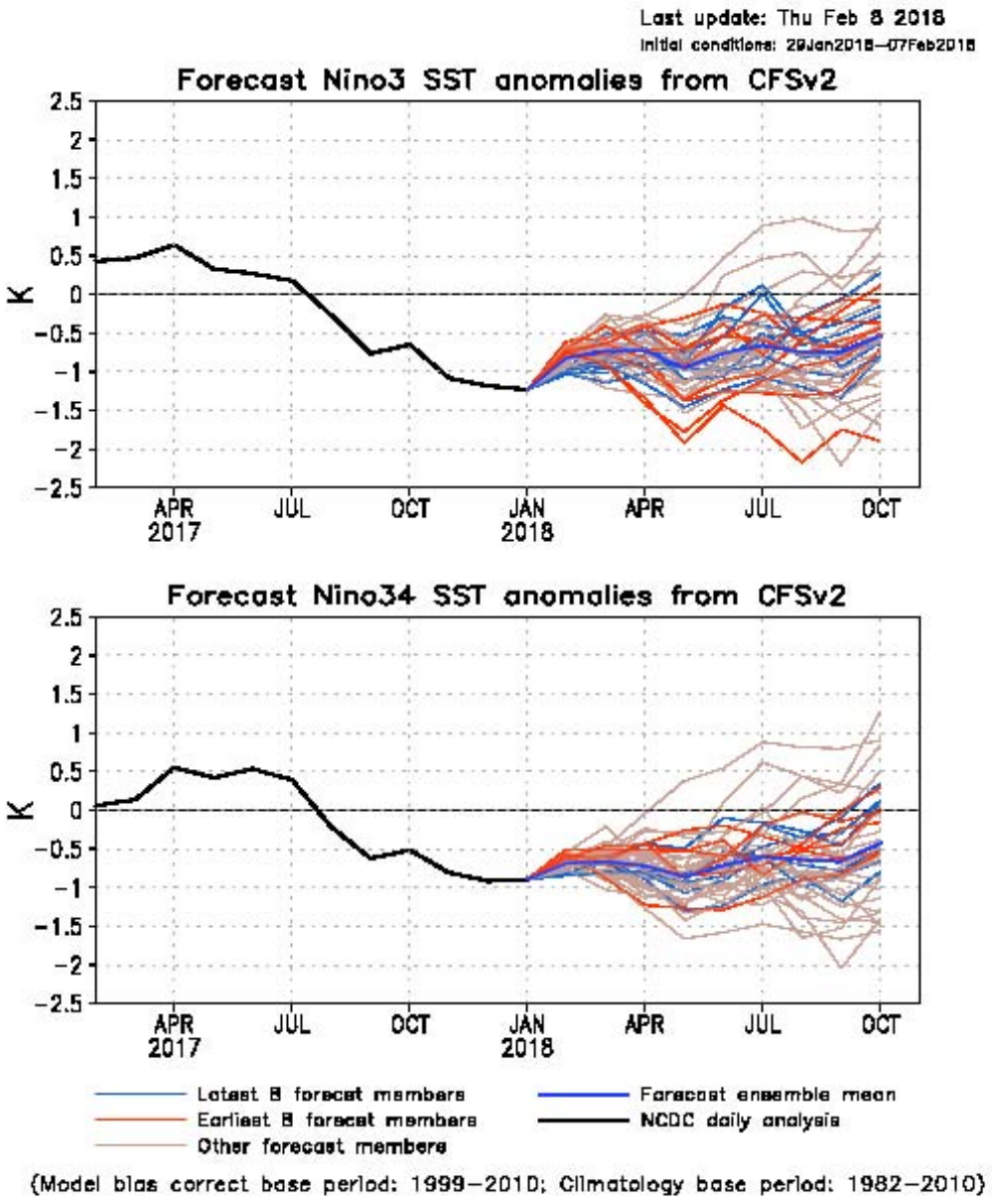

FIGURE F4. Predicted and observed sea surface temperature (SST) anomalies for the Nino 3 (top) and Nino 3.4 (bottom) regions from the NCEP Coupled Forecast System Model (CFS03). The forecasts consist of 40 forecast members. The ensemble mean of all 40 forecast members is shown by the blue line, individual members are shown by thin lines, and the observation is indicated by the black line. The Nino-3 region spans the eastern equatorial Pacific between 5N-5S, 150W-90W. The Nno 3.4 region spans the east-central equatorial Pacific between 5N-5S, 170W-120W.

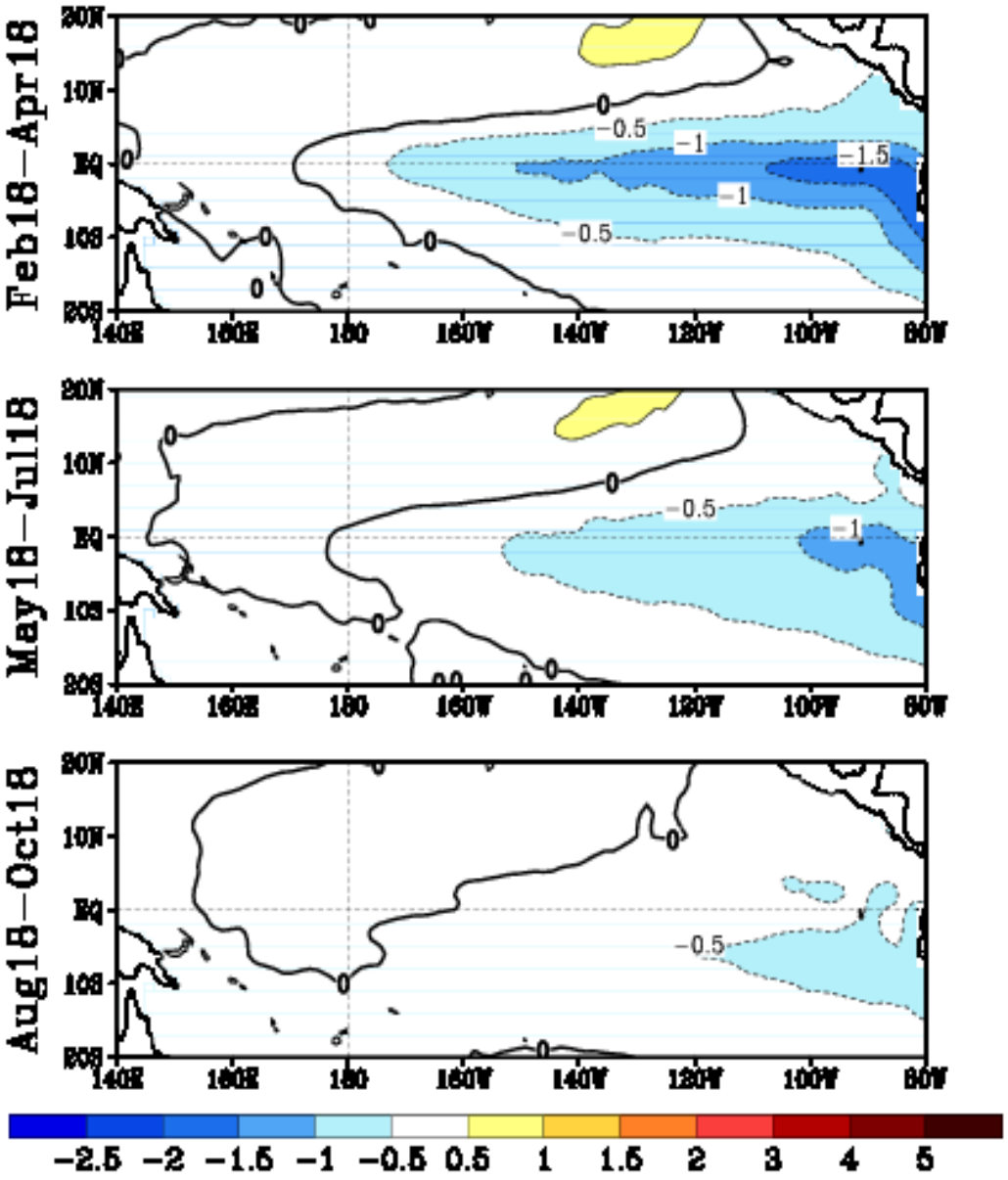

FIGURE F5. Predicted 3-month average sea surface temperature anomalies from the NCEP/CPC Markov model (Xue et al. 2000, *J. Climate*, **13**, 849-871). The forecast is initiated in JAN 2018 . Contour interval is 0.3C and negative anomalies are indicated by dashed contours. Anomalies are calculated relative to the 1971-2000 climatology.

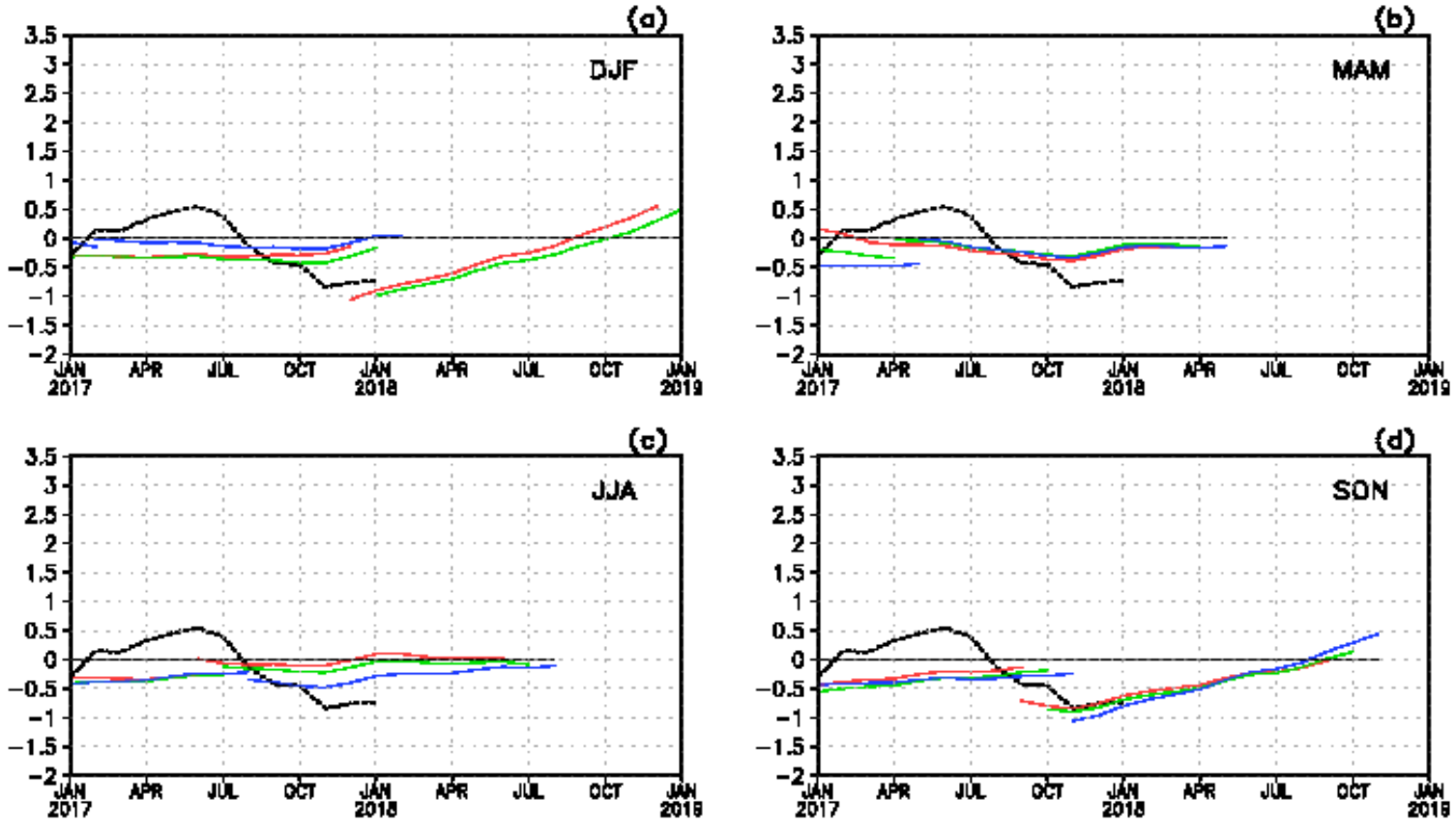

FIGURE F6. Time evolution of observed and predicted SST anomalies in the Nino 3.4 region (up to 12 lead months) by the NCEP/CPC Markov model (Xue et al. 2000, *J. Climate*, **13**, 849-871). Anomalies are calculated relative to the 1971-2000 climatology. Shown in each panel are the forecasts grouped by three consecutive starting months: (a) is for December, January, and February, (b) is for March, April, and May, (c) is for June, July, and August, and (d) is for September, October, and November. The observed Nino 3.4 SST anomalies are indicated by the black dashed lines. The Nino 3.4 region spans the east-central equatorial Pacific between 5N-5S, 170W-120W.

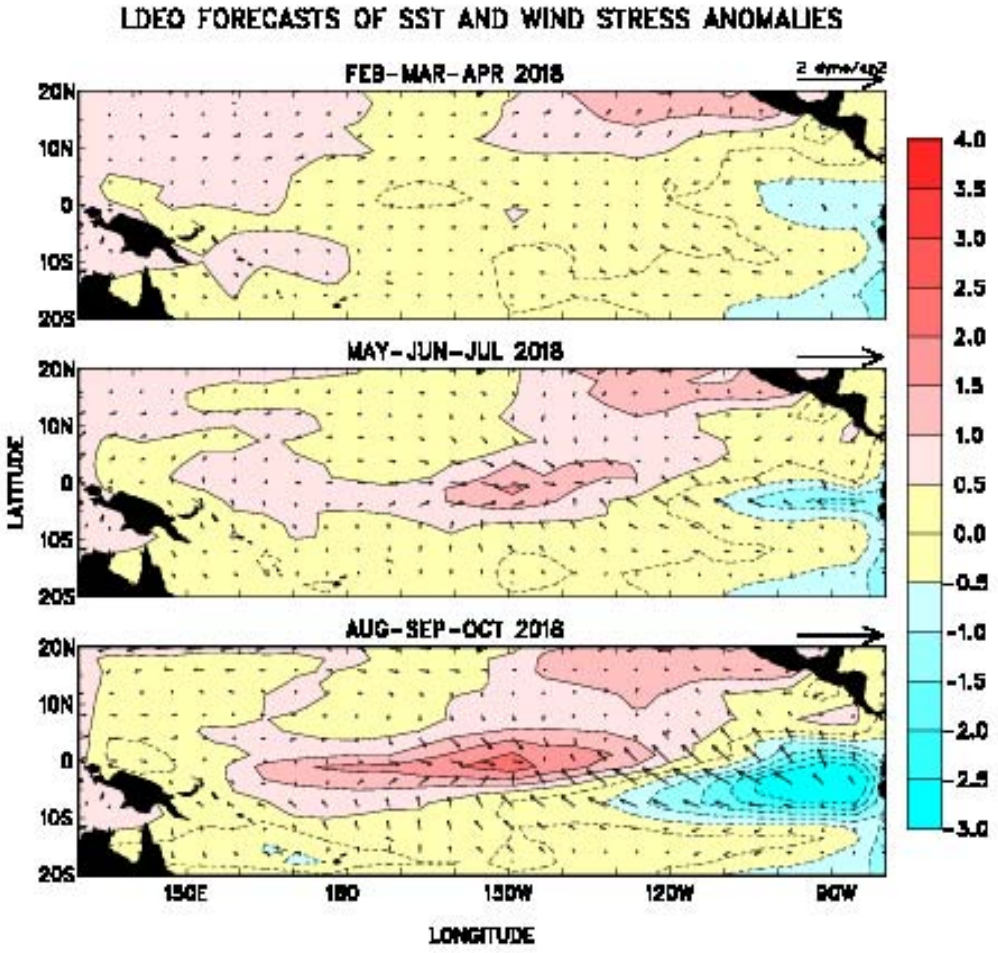

FIGURE F7. Forecasts of the tropical Pacific Predicted SST (shading) and vector wind anomalies for the next 3 seasons based on the LDEO model. Each forecast represents an ensemble average of 3 sets of predictions initialized during the last three consecutive months (see Figure F8).

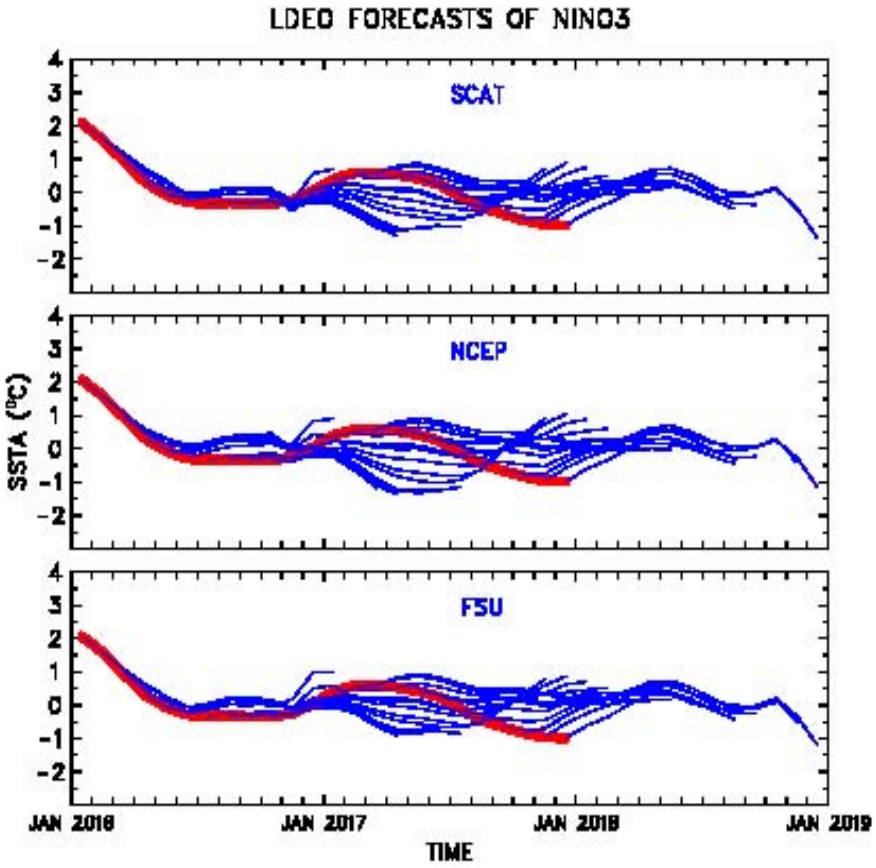

FIGURE F8. LDEO forecasts of SST anomalies for the Nino 3 region using wind stresses obtained from (top) QuikSCAT, (middle) NCEP, and (bottom) Florida State Univ. (FSU), along with SSTs (obtained from NCEP), and sea surface height data (obtained from TOPEX/POSEIDON) data. Each thin blue line represents a 12-month forecast, initialized one month apart for the past 24 months. Observed SST anomalies are indicated by the thick red line. The Nino-3 region spans the eastern equatorial Pacific between 5N-5S, 150W-90W.

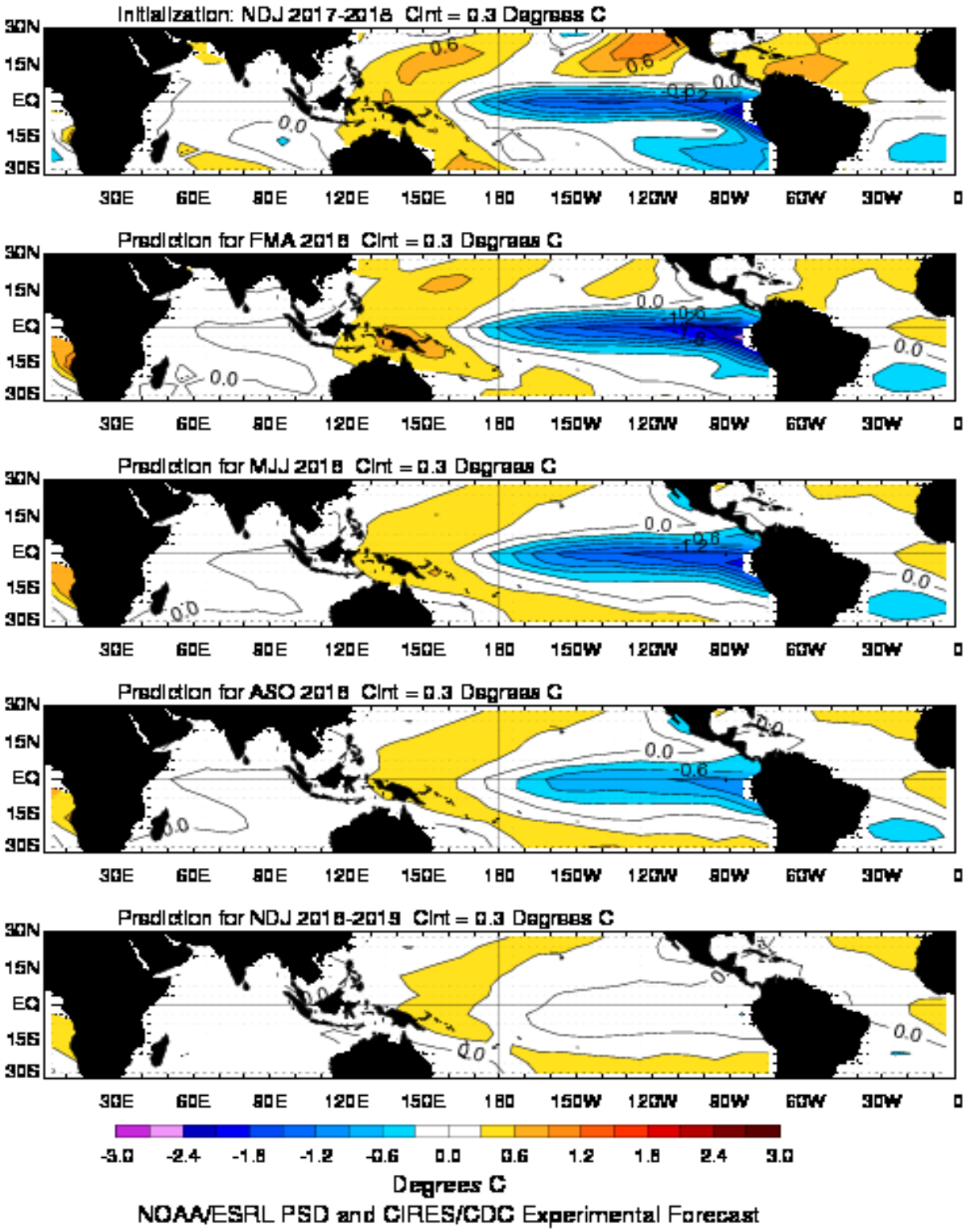

FIGURE F9. Forecast of tropical SST anomalies from the Linear Inverse Modeling technique of Penland and Magorian (1993: *J. Climate*, **6**, 1067-1076). The contour interval is 0.3C. Anomalies are calculated relative to the 1981-2010 climatology and are projected onto 20 leading EOFs.

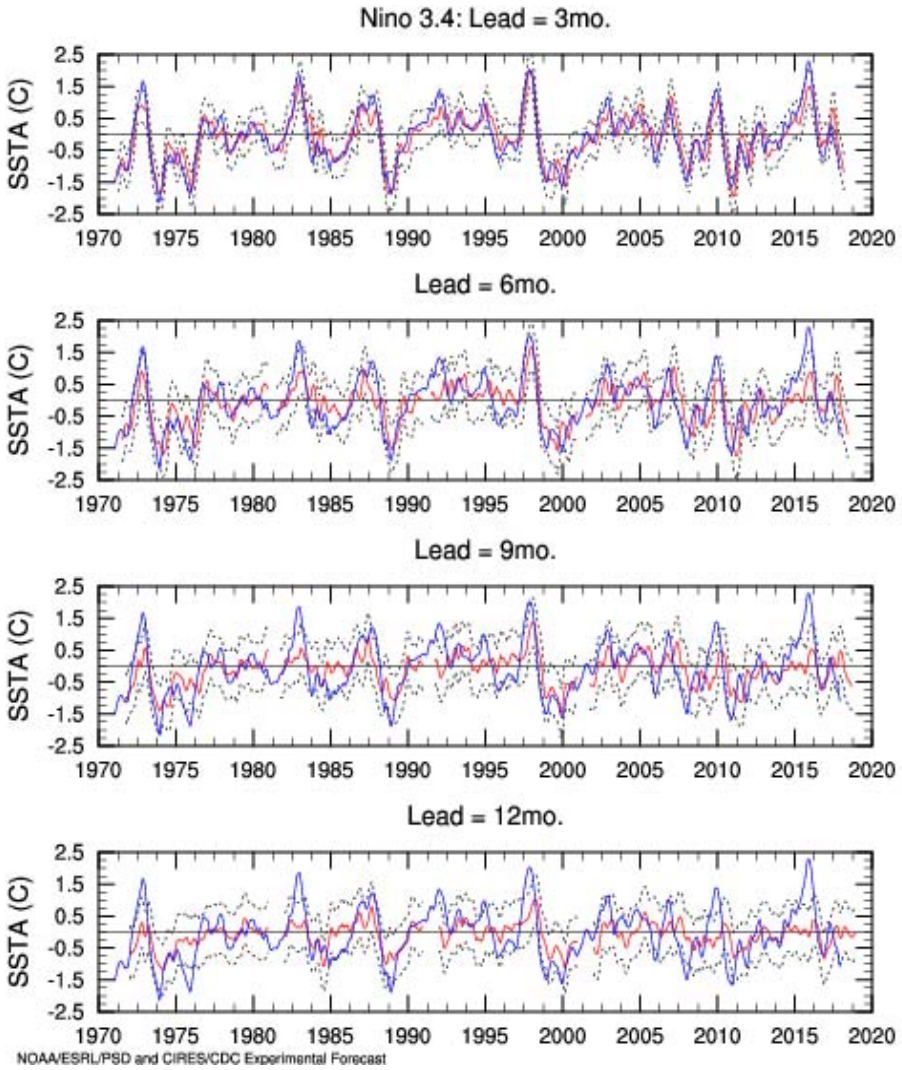

FIGURE F10. Predictions of Niño 3.4 SSTA (blue solid line) and verification (solid red line). The Niño3.4 Index was calculated in the area 6N-6S, 170W-120W. The 1980-2010 climatology was subtracted from ERSST data between 1950 and 2010, after which they were projected onto 20 EOFs containing 90% of thevariance. Significant 1950-2010 trends were subtracted from the corresponding PCs, the forecast was made on the detrended anomalies, after which the trend was added to the forecast. The dotted lines indicate the one standard deviation confidence interval for the forecasts based on a perfect adherence to assumption.

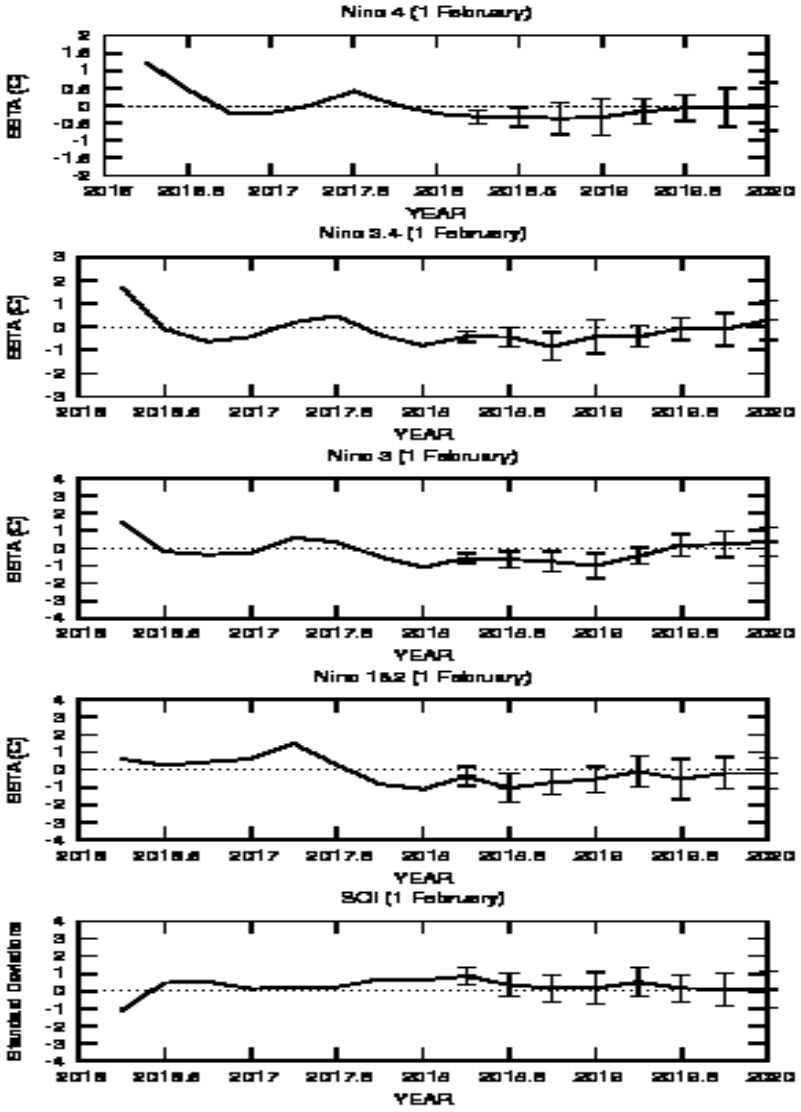

FIGURE F11. ENSO-CLIPER statistical model forecasts of three-month average sea surface temperature anomalies (green lines, deg. C) in (top panel) the Nino 4 region (5N-5S, 160E-150W), (second panel) the Nino 3.4 region (5N-5S, 170W-120W), (third panel) the Nino 3 region (5N-5S, 150W-90W), and (fourth panel) the Nino 1+2 region (0-10S, 90W-80W) (Knaff and Landsea 1997, *Wea. Forecasting*, **12**, 633-652). Bottom panel shows predictions of the three-month standardized Southern Oscillation Index (SOI, green line). Horizontal bars on green line indicate the adjusted root mean square error (RMSE). The Observed three-month average values are indicated by the thick blue line. SST anomalies are departures from the 1981-2010 base period means, and the SOI is calculated from the 1951-1980 base period means.

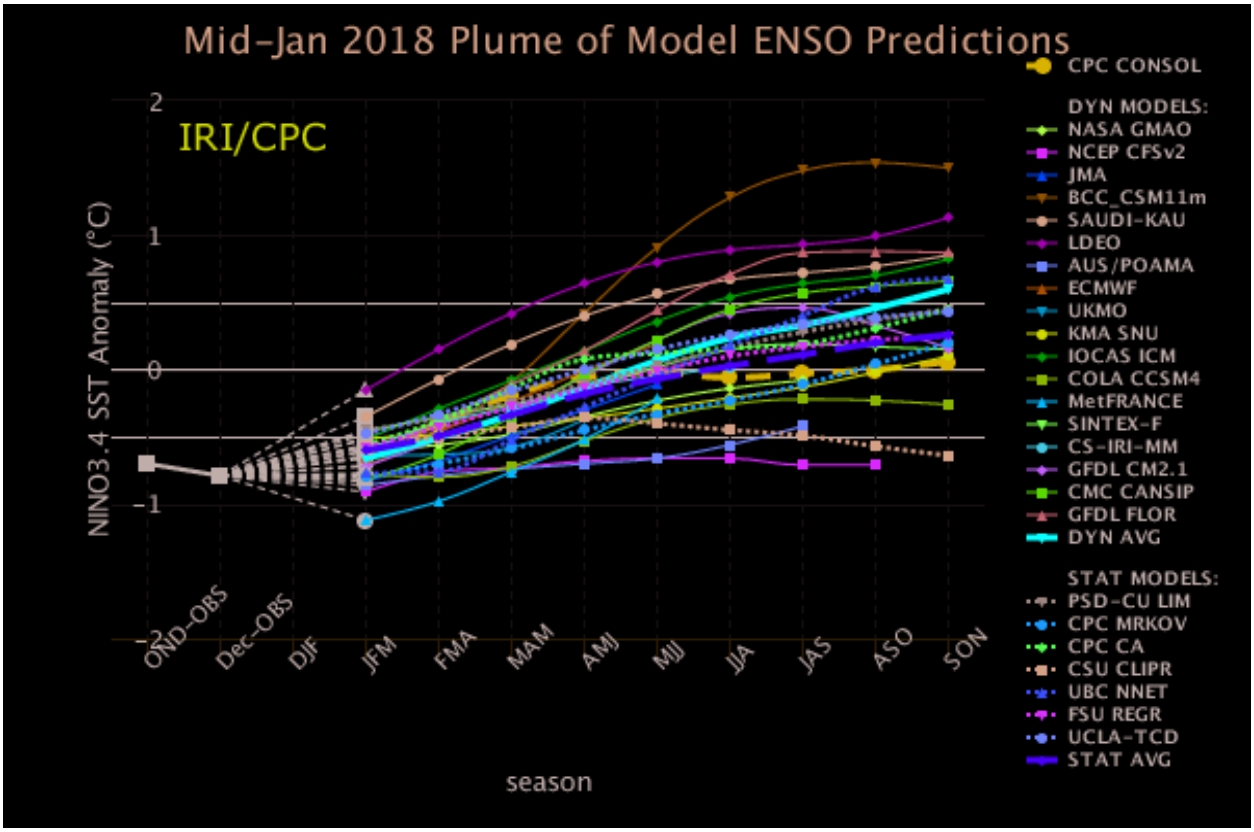

FIGURE F12. Time series of predicted sea surface temperature anomalies for the Nino 3.4 region (deg. C) from various dynamical and statistical models for nine overlapping 3-month periods. The Nino 3.4 region spans the east-central equatorial Pacific between 5N-5S, 170W-120W. Figure provided by the International Research Institute (IRI).

Extratropical Highlights – January 2018

1. Northern Hemisphere

The 500-hPa circulation during January featured an anomalous wave-4 pattern. Above-average heights were present over the high latitudes of the North Pacific, western North America, the central North Atlantic, and northwestern Russia. Below-average heights were present over the Gulf of Alaska, the high latitudes of the North Atlantic, and eastern Asia (Fig. E9).

At 200-hPa, the circulation reflected La Niña. This signal included amplified troughs near and east of the date line across the subtropical Pacific Ocean in both hemispheres, and amplified ridges over Australasia (Fig. T22). The amplified troughs in both hemispheres reflected the disappearance of deep tropical convection from the central equatorial Pacific (Fig. T25). The amplified subtropical ridges reflected enhanced convection over the western tropical Pacific, Indonesia, and the eastern Indian Ocean.

The main land-surface temperature signals during January included above-average temperatures across western North America, Europe, and western Russia, and below-average temperatures in the southeastern and eastern U.S., and in south-central Russia (Fig. E1). The main precipitation signals included above-average totals in the northwestern U.S. and central Europe, and below-average totals in the southern and southeastern U.S. (Fig. E3).

a. North Pacific and North America

The 500-hPa circulation during January featured above-average heights over the high latitudes of the North Pacific and western North America, and below-average heights over the Gulf of Alaska (Fig. E9). This type of highly amplified wave pattern is often seen during La Niña. La Niña produces an enhanced subtropical ridge over southeastern Asia along with an amplified mid-Pacific trough (Fig. T22). These conditions act to retract westward the East Asian jet steam, as seen during January by a confinement of that jet core to the area around Japan and by the location of that jet's exit region being located well west of the date line (Fig. T21). This anomalous jet structure produces the essence of the downstream anomalous 500-hPa circulation pattern seen during January.

This overall pattern contributed to anomalously warm surface temperatures in western North America, and to anomalously cool conditions in the southern and eastern U.S. (Fig. E1). It also contributed to above-average precipitation in the northwestern U.S., and to below-average precipitation in the southern and southeastern U.S. (Fig. E3).

b. Eurasia

An amplified wave pattern at 500-hPa extended from the central North Atlantic Ocean to eastern Asia (Fig. E9). Features of this pattern included an anomalous ridges over the central North Atlantic and northwestern Russia, and anomalous troughs over the high latitudes of the North At-

lantic and eastern Asia (Fig. E9). This pattern was associated with anomalously warm (Fig. E1) and wet (Fig. E3) conditions in Europe, and with anomalously cool and dry conditions in portions of central Russia (Fig. E3).

c. China

At 200-hPa, the subtropical ridge was much stronger than average across southern Asia and China (Fig. T22). This ridge was associated with an enhanced southerly flow at 850-hPa (Fig. T20) of deep tropical moisture into eastern China, along with anomalous upper-level divergence in that region along the equatorward flank of the East Asian jet entrance region (Fig. T23). As a result, eastern China recorded well above-average precipitation during January, with area-averaged totals in the upper 90th percentile of occurrences (Fig. E4).

2. Southern Hemisphere

The mean 500-hPa circulation during January featured above-average heights in the vicinity of New Zealand, and below-average heights over much of the high latitudes (Fig. E15). At 200-hPa, the subtropical circulation featured an amplified trough over the central and eastern South Pacific Ocean, and an amplified ridge over western Australia and the eastern Indian Ocean (Fig. T22). This anomalous subtropical circulation is typical of La Niña.

On the synoptic scale, the upper-level circulation featured a ridge across western Australia and a trough off the coast of eastern Australia. This pattern was associated with weaker upper-level westerlies across the continent (Fig. T21), and with anomalous upper-level convergence (Fig. T23) and below-average precipitation (Fig. E3) across eastern Australia between the mean ridge and trough axes. It was also associated with well above-average surface temperatures in eastern Australia, with many locations recording temperatures in the upper 90th percentile of occurrences (Fig. E1).

The South African monsoon season runs from October to April. This area recorded well below-average precipitation during January, with area-averaged totals in the lowest 10th percentile of occurrences (Fig. E4). The most significant deficits were observed in the northern and western portions of the monsoon region (Fig E3), where they acted to intensify severe drought in areas such as Cape Town. In the north and east, many normally heavy-rainfall areas of Zimbabwe and Mozambique recorded very limited rainfall during January (and December) resulting in 2-month deficits of 400 mm – 500 mm.

TELECONNECTION INDICES

Month	North Atlantic			North Pacific			EURASIA		
	NAO	EA	WP	EP-NP	PNA	TNH	EATL/ WRUS	SCAND	POLEUR
JAN 18	1.2	0.5	0.4	0.7	-0.1	-0.3	-1.6	0.4	-1.5
DEC 17	0.7	-0.5	0.3	---	0.6	1.0	-1.6	-0.5	-1.9
NOV 17	-0.1	0.1	0.7	0.4	-2.0	---	-1.2	-0.1	-2.2
OCT 17	0.7	0.6	0.7	-0.6	-0.3	---	-0.0	0.3	-1.2
SEP 17	-0.5	1.6	-1.2	-0.5	-0.3	---	-2.5	0.5	-1.7
AUG 17	-1.5	2.0	-1.4	-1.6	0.2	---	-2.9	-1.6	1.8
JUL 17	1.3	1.8	0.5	0.0	1.3	---	-0.6	0.0	-0.1
JUN 17	0.4	2.0	-0.8	0.5	1.2	---	0.3	-1.4	-0.1
MAY 17	-1.7	0.5	0.7	-0.7	-0.2	---	1.5	0.9	0.5
APR 17	1.7	-0.6	-0.4	1.0	0.1	---	0.7	-1.4	-1.4
MAR 17	0.4	1.0	-2.1	-1.0	-0.0	---	-1.0	-1.0	0.7
FEB 17	0.7	0.6	-0.1	0.2	-0.1	-0.1	1.1	0.7	-0.4
JAN 17	0.0	-1.1	0.6	0.4	-0.3	-0.3	0.6	0.2	1.0

TABLE E1-Standardized amplitudes of selected Northern Hemisphere teleconnection patterns for the most recent thirteen months (computational procedures are described in Fig. E7). Pattern names and abbreviations are North Atlantic Oscillation (NAO); East Atlantic pattern (EA);West Pacific pattern (WP); East Pacific - North Pacific pattern (EP-NP); Pacific/North American pattern (PNA); Tropical/Northern Hemisphere pattern (TNH);East Atlantic/Western Russia pattern (EATL/WRUS-called Eurasia-2 pattern by Barnston and Livezey, 1987, *Mon. Wea. Rev.*, **115**, 1083-1126); Scandanavia pattern (SCAND-called Eurasia-1 pattern by Barnston and Livezey 1987); and Polar Eurasia pattern (POLEUR). No value is plotted for calendar months in which the pattern does not appear as a leading mode.

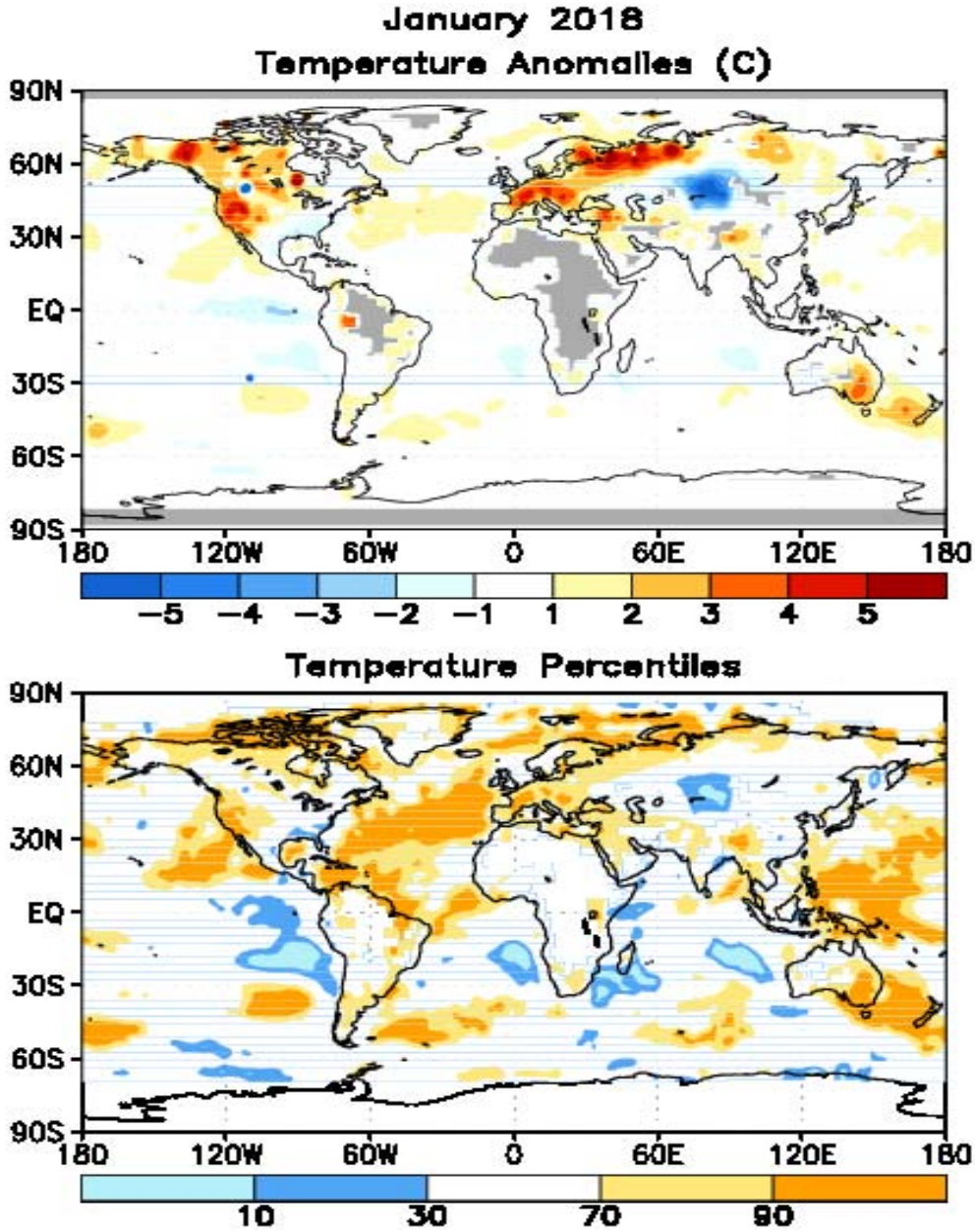

FIGURE E1. Surface temperature anomalies (°C, top) and surface temperature expressed as percentiles of the normal (Gaussian) distribution fit to the 1981–2010 base period data (bottom) for JAN 2018. Analysis is based on station data over land and on SST data over the oceans (top). Anomalies for station data are departures from the 1981–2010 base period means, while SST anomalies are departures from the 1981–2010 adjusted OI climatology. (Smith and Reynolds 1998, *J. Climate*, **11**, 3320-3323). Regions with insufficient data for analysis in both figures are indicated by shading in the top figure only.

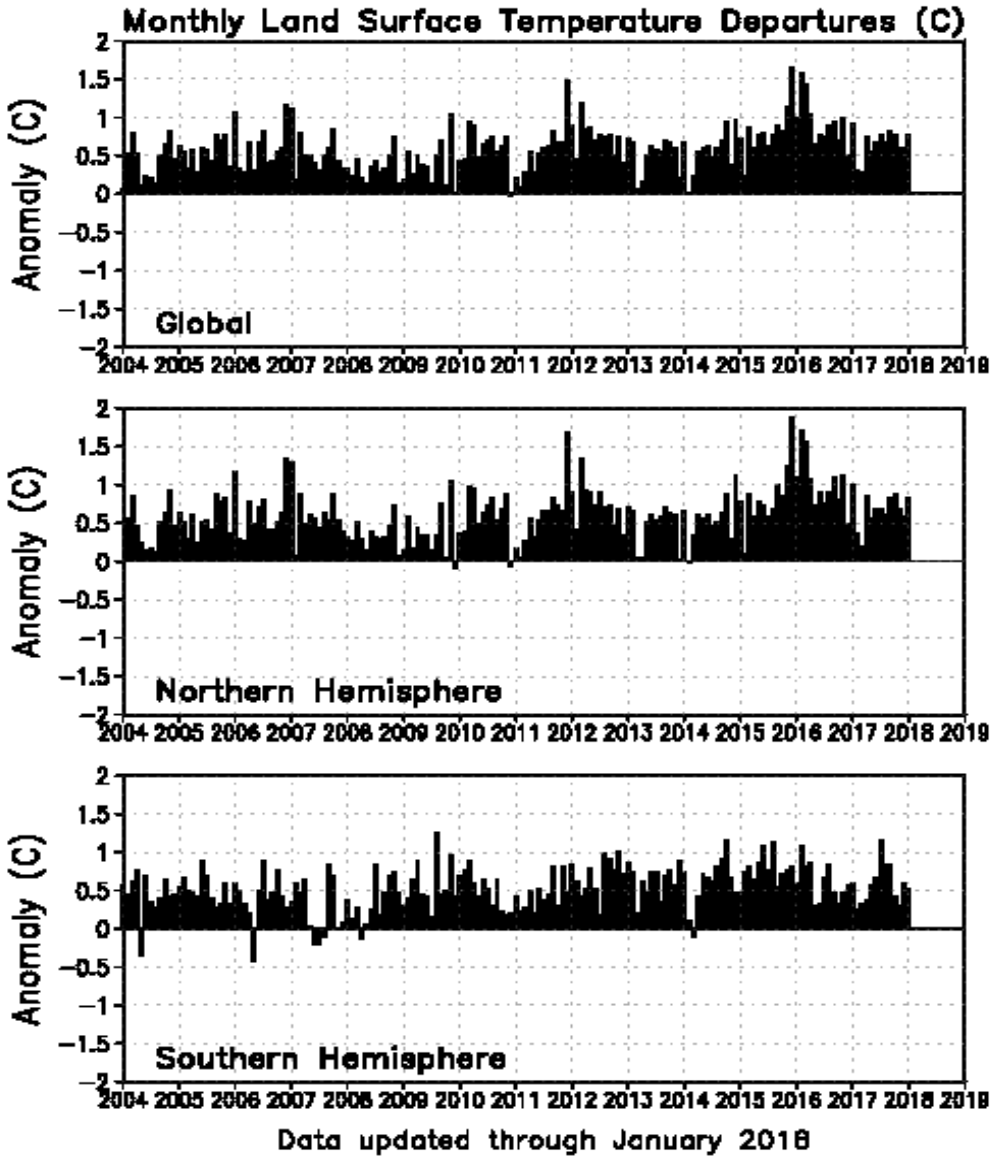

FIGURE E2. Monthly global (top), Northern Hemisphere (middle), and Southern Hemisphere (bottom) surface temperature anomalies (land only, ˚C) from January 1990 - present, computed as departures from the 1981–2010 base period means.

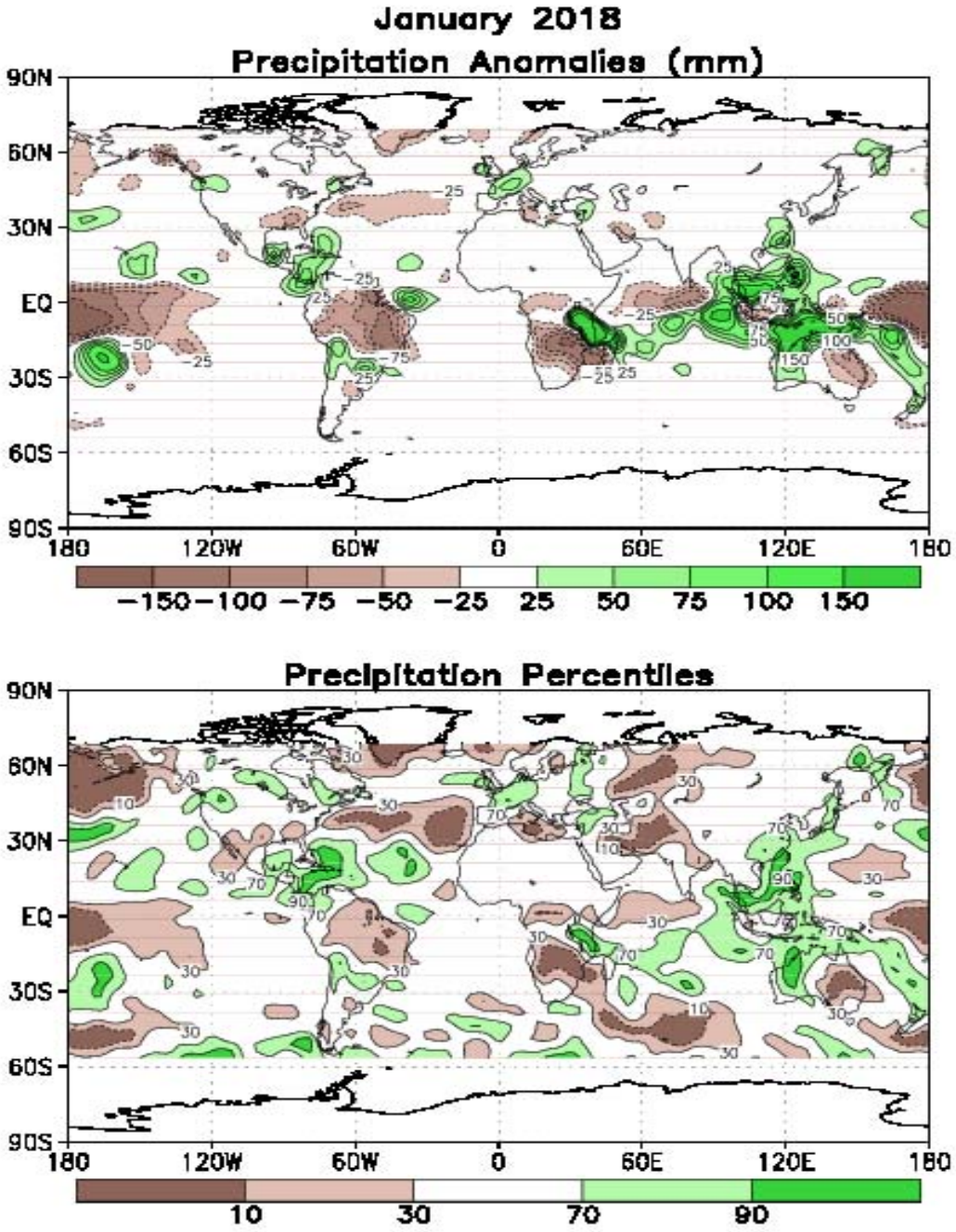

FIGURE E3. Anomalous precipitation (mm, top) and precipitation percentiles based on a Gamma distribution fit to the 1981–2010 base period data (bottom) for JAN 2018. Data are obtained from a merge of raingauge observations and satellite-derived precipitation estimates (Janowiak and Xie 1999, *J. Climate*, **12**, 3335–3342). Contours are drawn at 200, 100, 50, 25, -25, -50, -100, and -200 mm in top panel. Percentiles are not plotted in regions where mean monthly precipitation is <5mm/month.

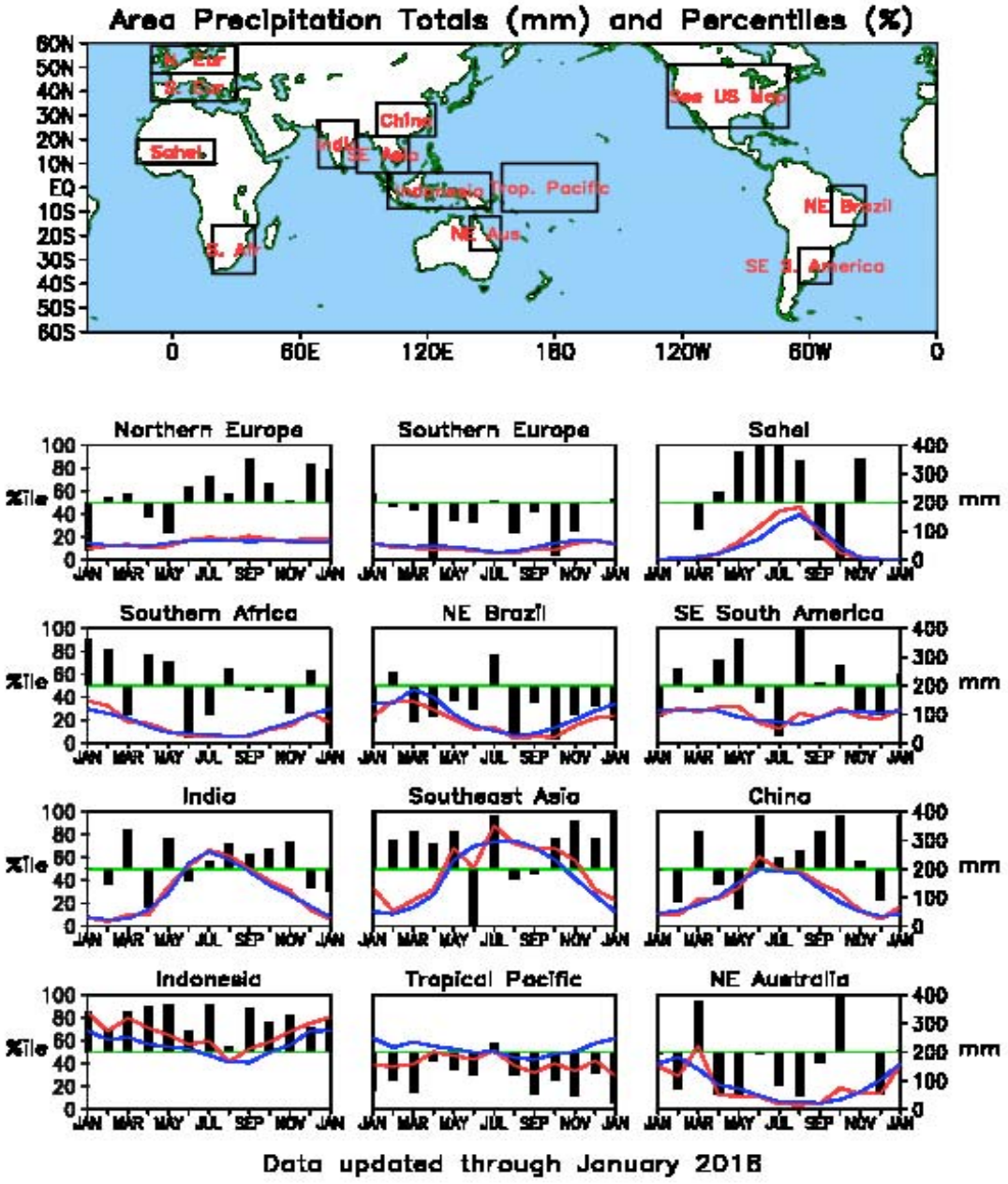

FIGURE E4. Areal estimates of monthly mean precipitation amounts (mm, solid lines) and precipitation percentiles (%, bars) for the most recent 13 months obtained from a merge of raingauge observations and satellite-derived precipitation estimates (Janowiak and Xie 1999, *J. Climate*, **12**, 3335–3342). The monthly precipitation climatology (mm, dashed lines) is from the 1981–2010 base period monthly means. Monthly percentiles are not shown if the monthly mean is less than 5 mm.

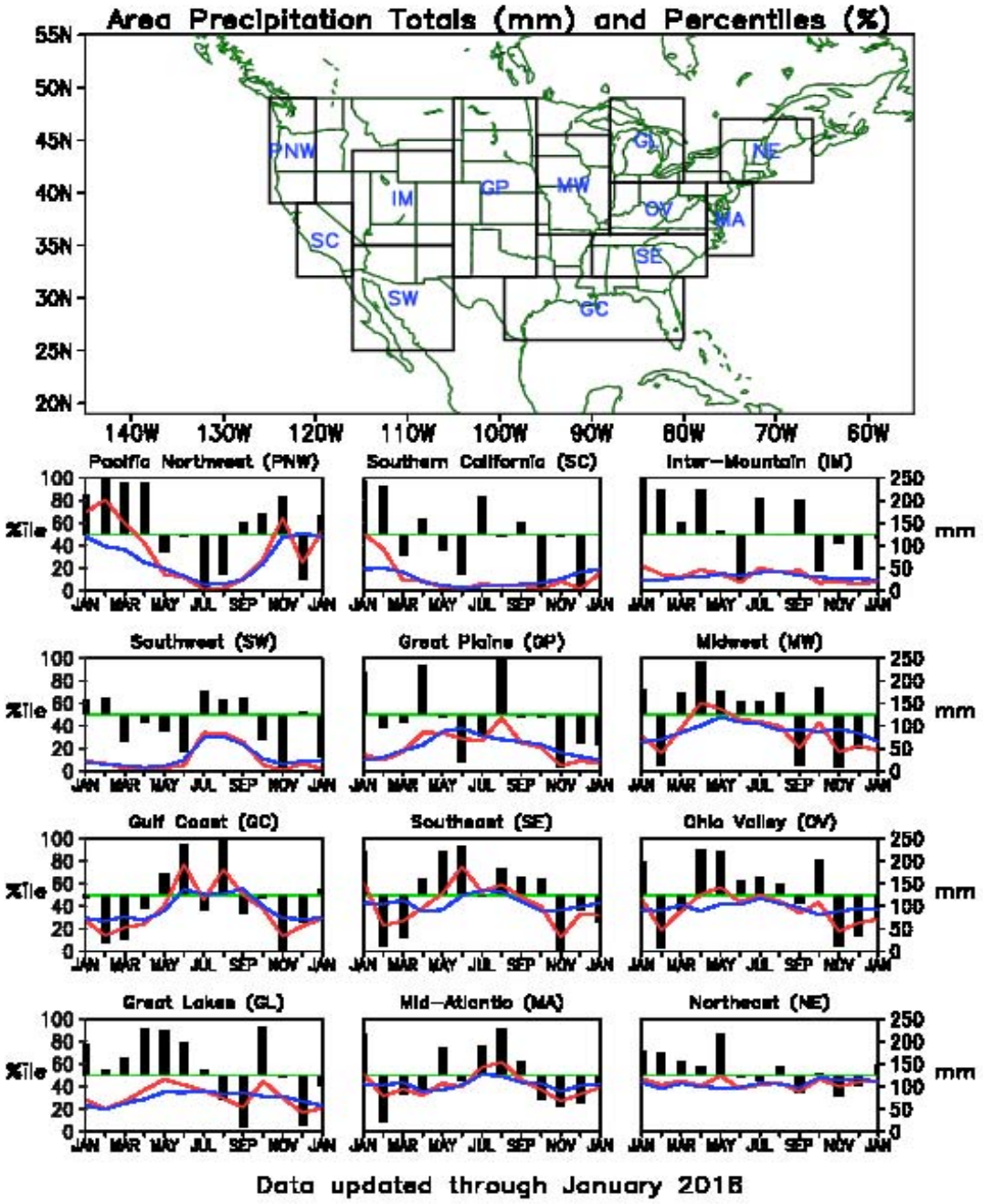

FIGURE E5. Areal estimates of monthly mean precipitation amounts (mm, solid lines) and precipitation percentiles (%, bars) for the most recent 13 months obtained from a merge of raingauge observations and satellite-derived precipitation estimates (Janowiak and Xie 1999, *J. Climate*, **12**, 3335–3342). The monthly precipitation climatology (mm, dashed lines) is from the 1981–2010 base period monthly means. Monthly percentiles are not shown if the monthly mean is less than 5 mm.

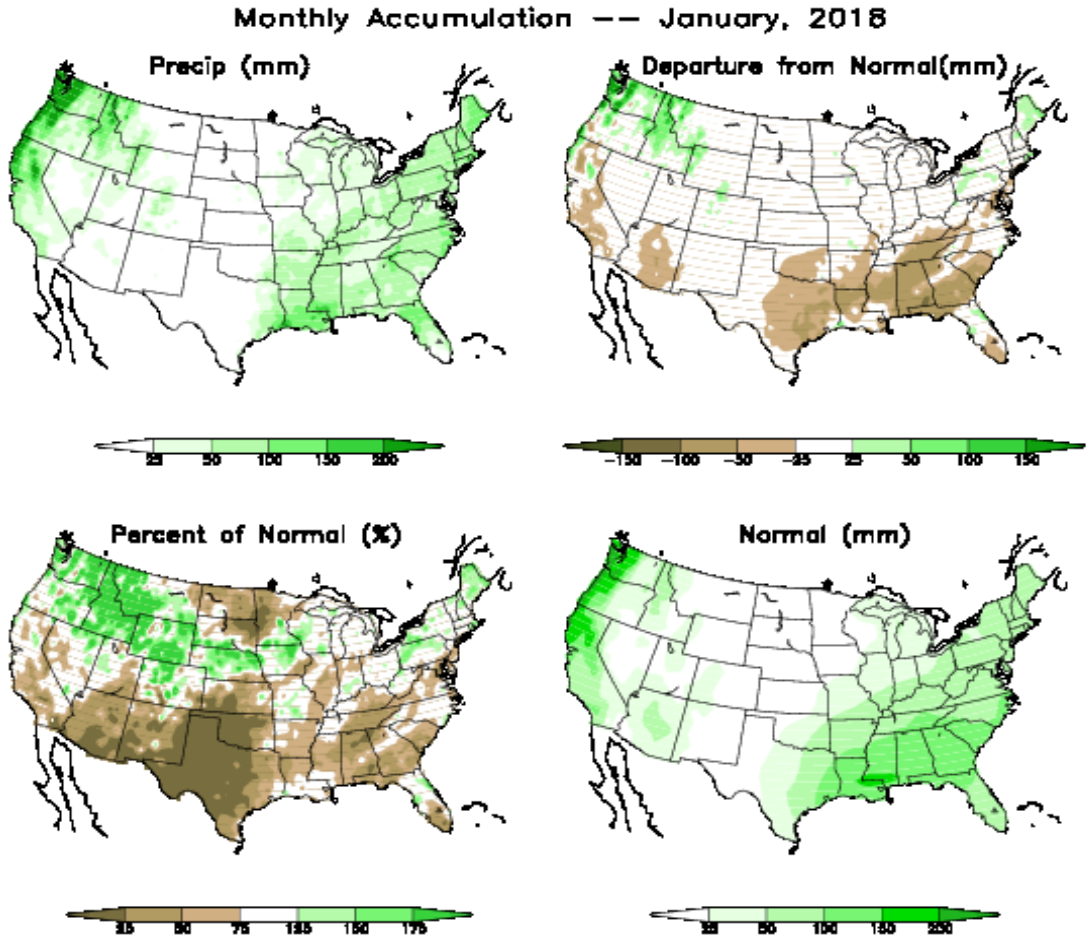

FIGURE E6. Observed precipitation (upper left), departure from average (upper right), percent of average (lower left), and average precipitation (lower right) for JAN 2018. The units are given on each panel. Base period for averages is 1981–2010. Results are based on CPC's U. S. daily precipitation analysis, which is available at http://www.cpc.ncep.noaa.gov/prodcuts/precip/realtime.

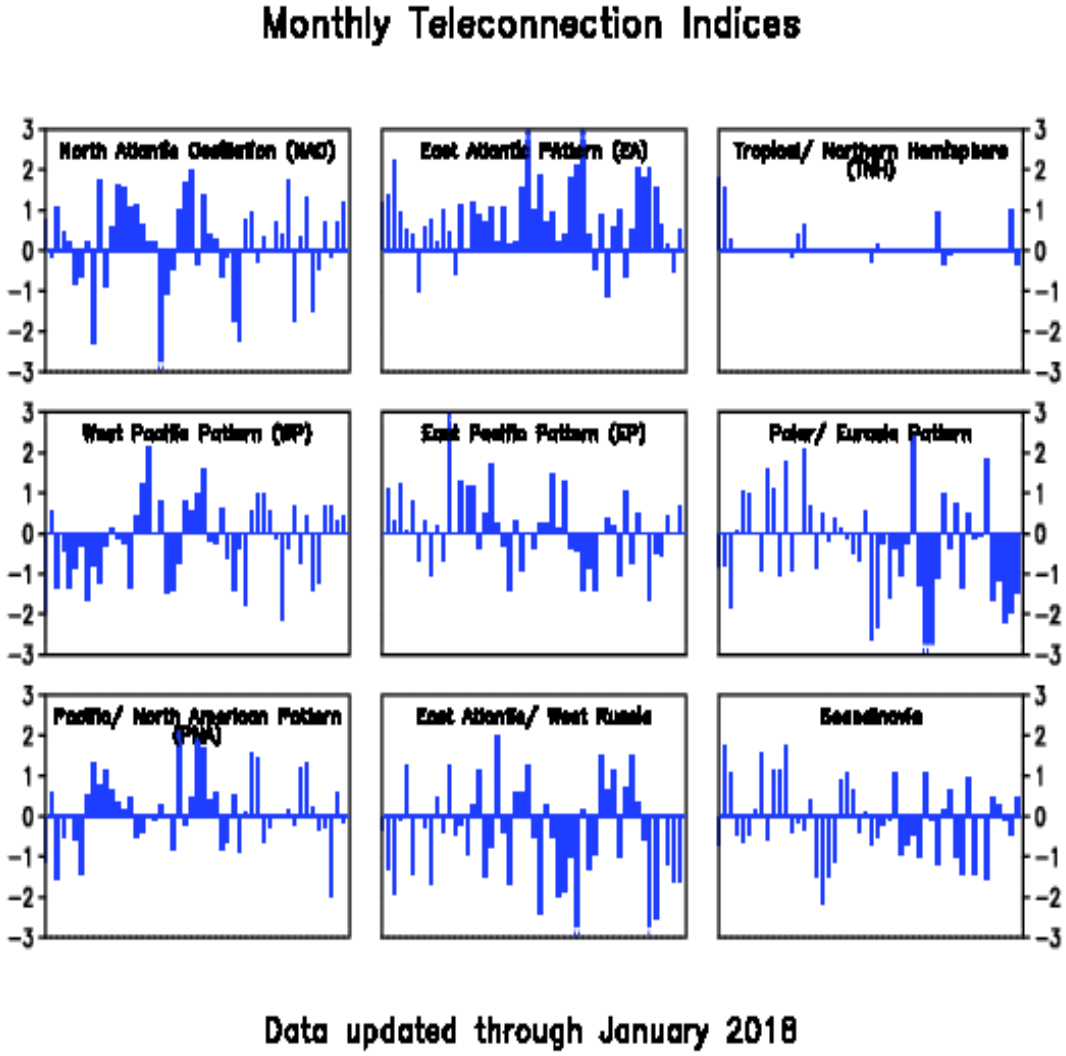

FIGURE E7. Standardized monthly Northern Hemisphere teleconnection indices. The teleconnection patterns are calculated from a Rotated Principal Component Analysis (RPCA) applied to monthly standardized 500-hPa height anomalies during the 1981-2010 base period. To obtain these patterns, ten leading un-rotated modes are first calculated for each calendar month by using the monthly height anomaly fields for the three-month period centered on that month: [i.e., The July modes are calculated from the June, July, and August standardized monthly anomalies]. A Varimax spatial rotation of the ten leading un-rotated modes for each calendar month results in 120 rotated modes (12 months x 10 modes per month) that yield ten primary teleconnection patterns.The teleconnection indices are calculated by first projecting the standardized monthly anomalies onto the teleconnection patterns corresponding to that month (eight or nine teleconnection patterns are seen in each calendar month). The indices are then solved for simultaneously using a Least-Squares approach. In this approach, the indices are the solution to the Least-Squares system of equations which explains the maximum spatial structure of the observed height anomaly field during the month. The indices are then standardized for each pattern and calendar month independently. No index value exists when the teleconnection pattern does not appear as one of the ten leading rotated EOF's valid for that month.

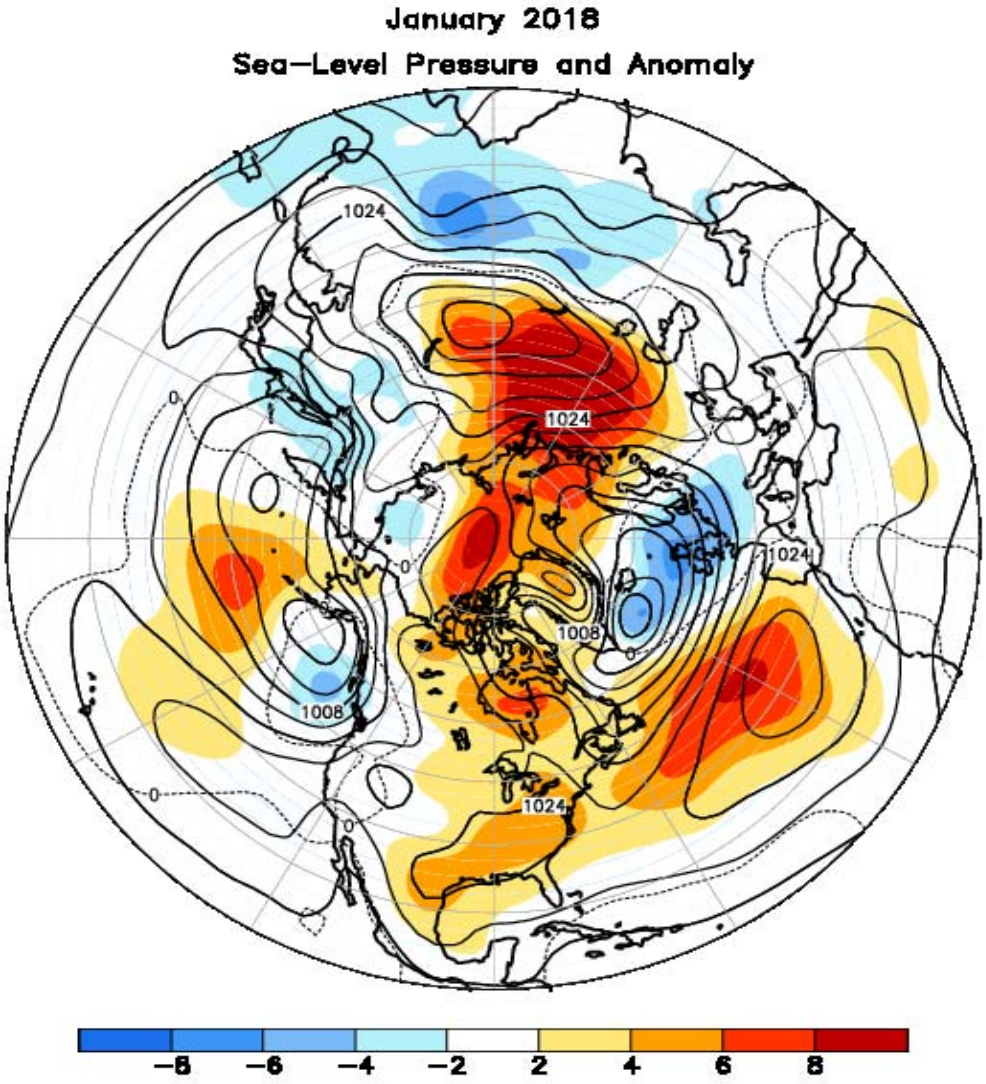

FIGURE E8. Northern Hemisphere mean and anomalous sea level pressure (CDAS/Reanalysis) for JAN 2018. Mean values are denoted by solid contours drawn at an interval of 4 hPa. Anomaly contour interval is 2 hPa with values less (greater) than -2 hPa (2 hPa) indicated by dark (light) shading. Anomalies are calculated as departures from the 1981-2010 base period monthly means.

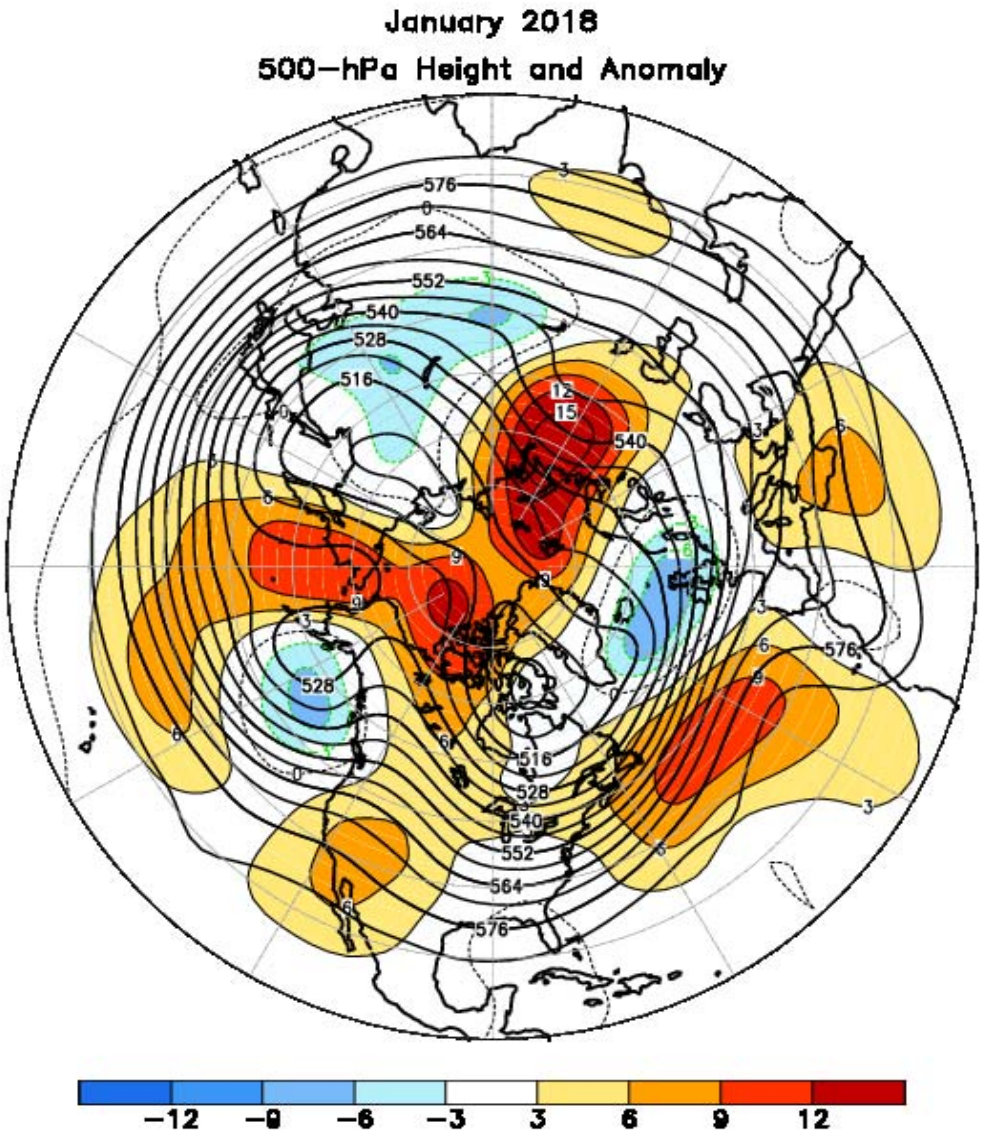

FIGURE E9. Northern Hemisphere mean and anomalous 500-hPa geopotential height (CDAS/Reanalysis) for JAN 2018. Mean heights are denoted by solid contours drawn at an interval of 6 dam. Anomaly contour interval is 3 dam with values less (greater) than -3 dam (3 dam) indicated by dark (light) shading. Anomalies are calculated as departures from the 1981-2010 base period monthly means.

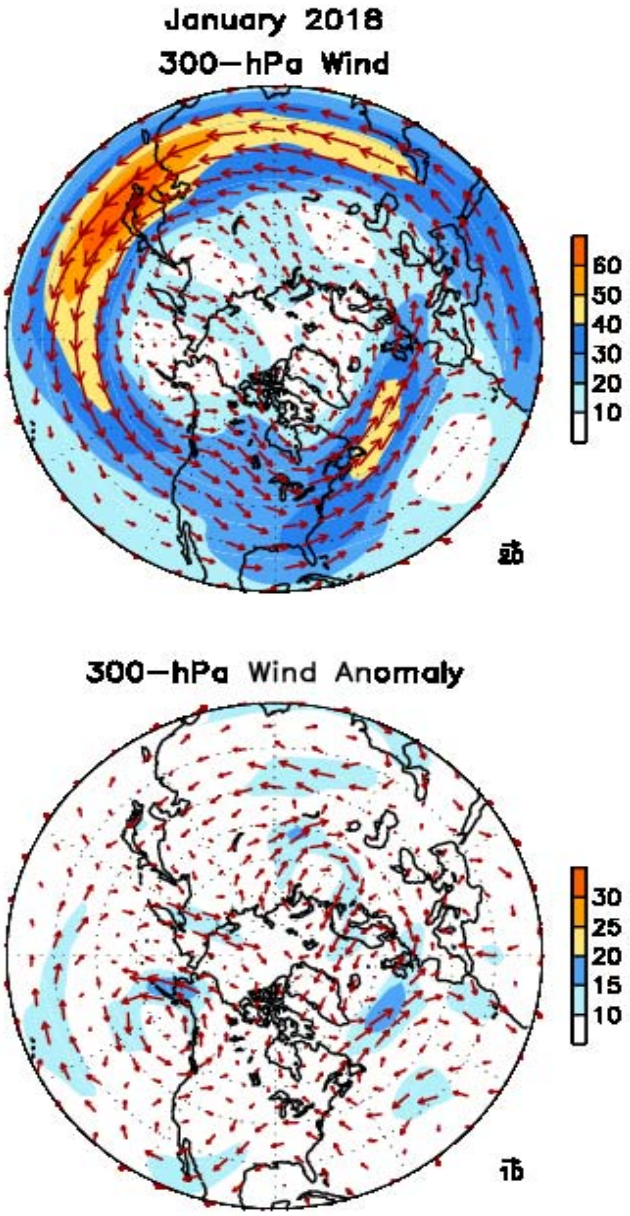

FIGURE E10. Northern Hemisphere mean (left) and anomalous (right) 300-hPa vector wind (CDAS/Reanalysis) for JAN 2018. Mean (anomaly) isotach contour interval is 10 (5) ms^{-1}. Values greater than 30 ms^{-1} (left) and 10 ms^{-1} (rights) are shaded. Anomalies are departures from the 1981-2010 base period monthly means.

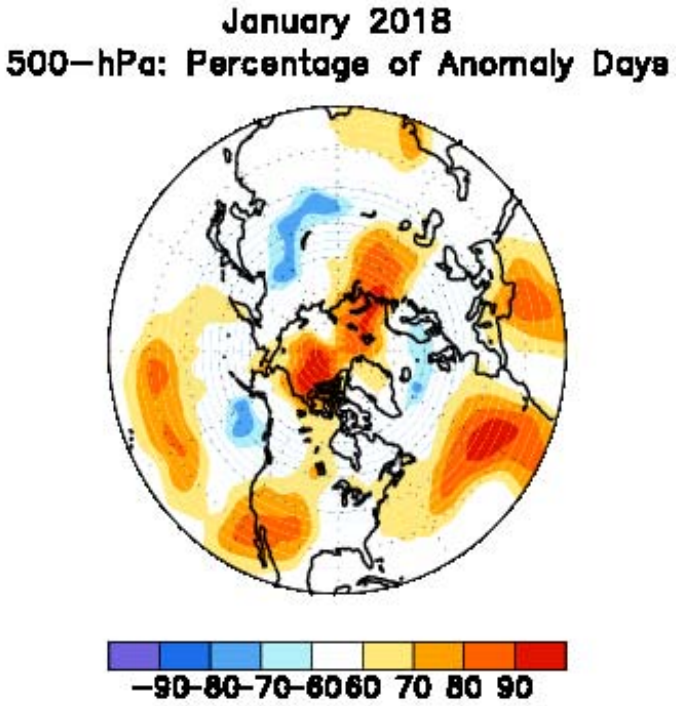

FIGURE E11. Northern Hemisphere percentage of days during JAN 2018 in which 500-hPa height anomalies greater than 15 m (red) and less than -15 m (blue) were observed. Values greater than 70% are shaded and contour in-

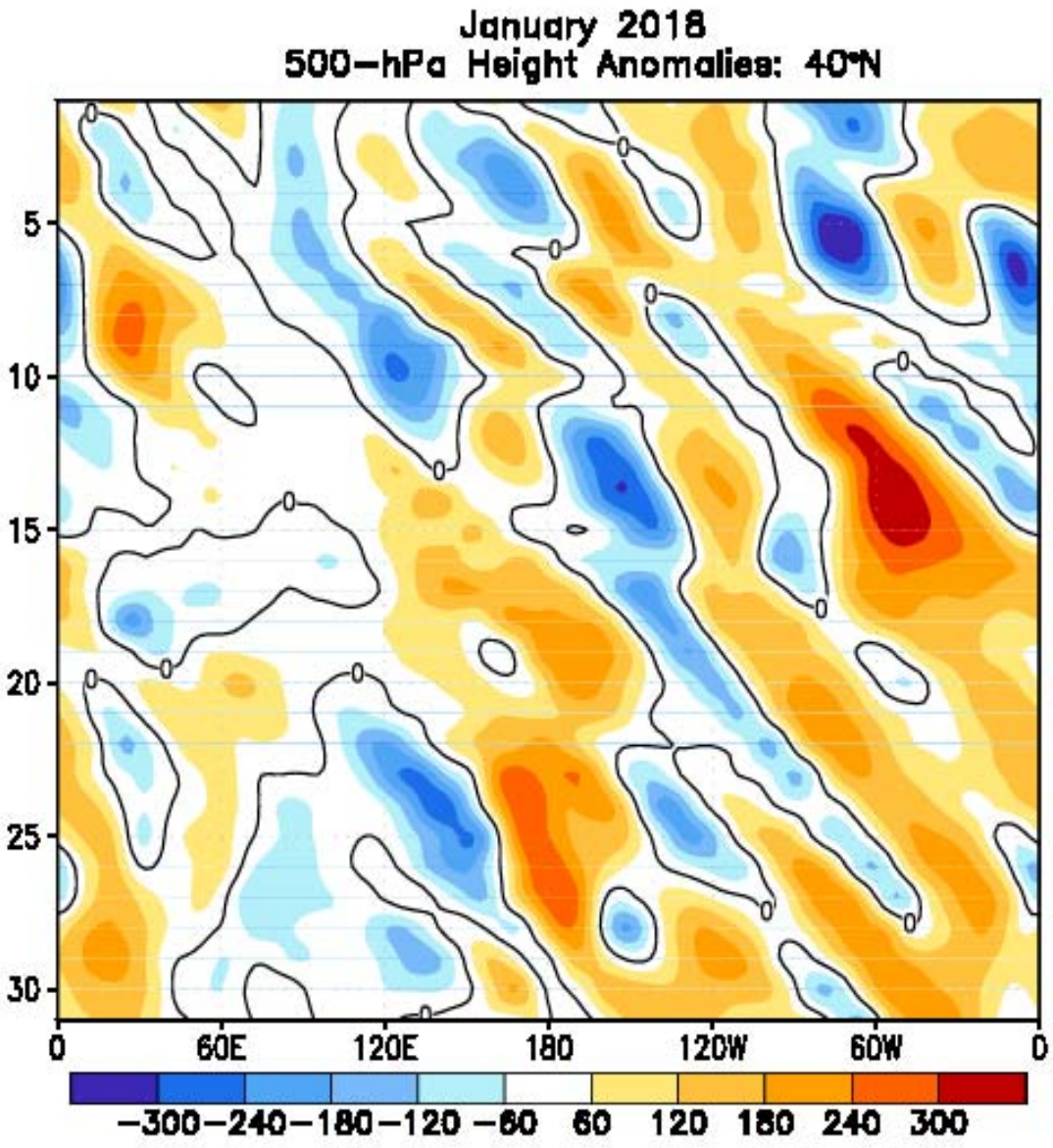

FIGURE E12. Northern Hemisphere: Daily 500-hPa height anomalies for JAN 2018 averaged over the 5° latitude band centered on 40°N. Positive values are indicated by solid contours and dark shading. Negative values are indicated by dashed coutours and light shading. Contour interval is 60 m. Anomalies are departures from the 1981-2010 base period daily means.

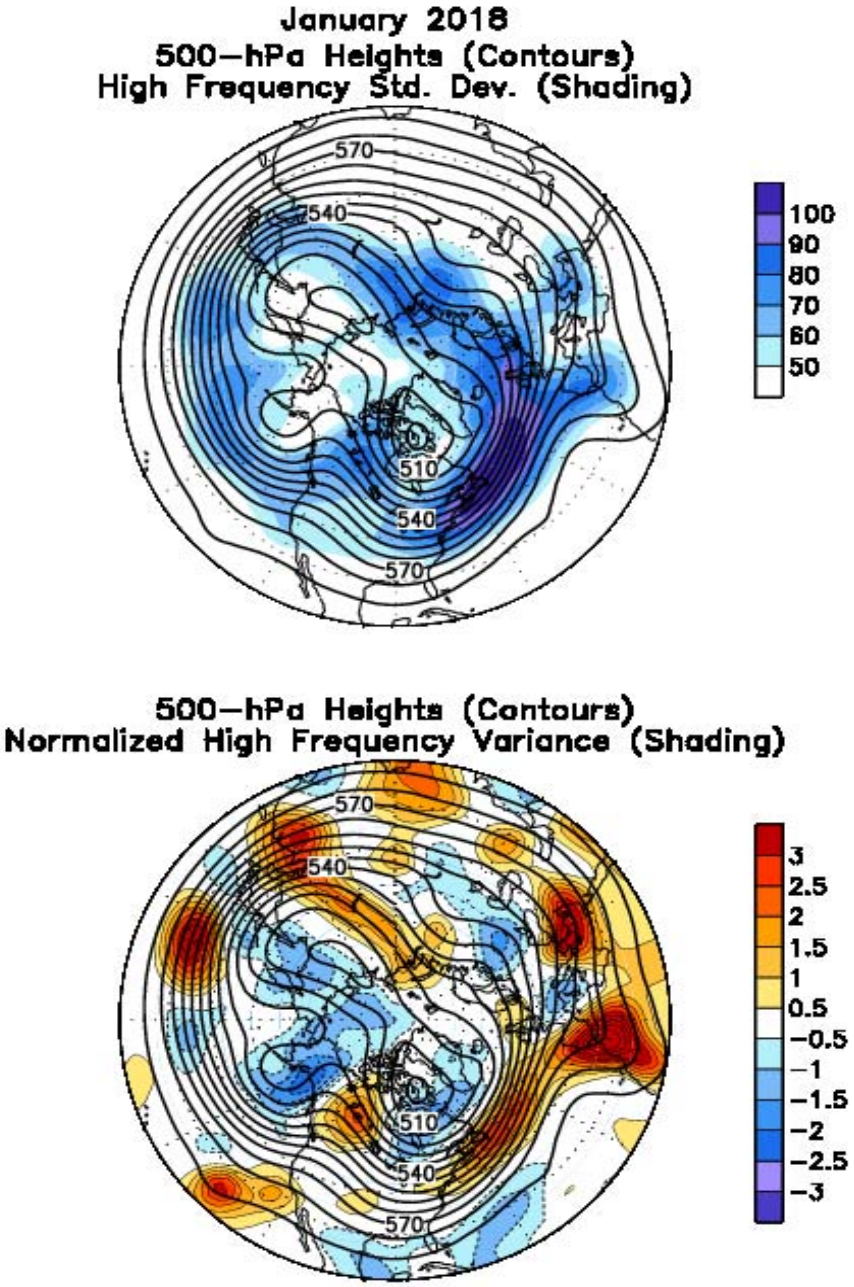

FIGURE E13. Northern Hemisphere 500-hPa heights (thick contours, interval is 6 dam) overlaid with (Top) Standard deviation of 10-day high-pass (HP) filtered height anomalies and (Bottom) Normalized anomalous variance of 10-day HP filtered height anomalies. A Lanczos filter is used to calculate the HP filtered anomalies. Anomalies are departures from the 1981-2010 daily means.

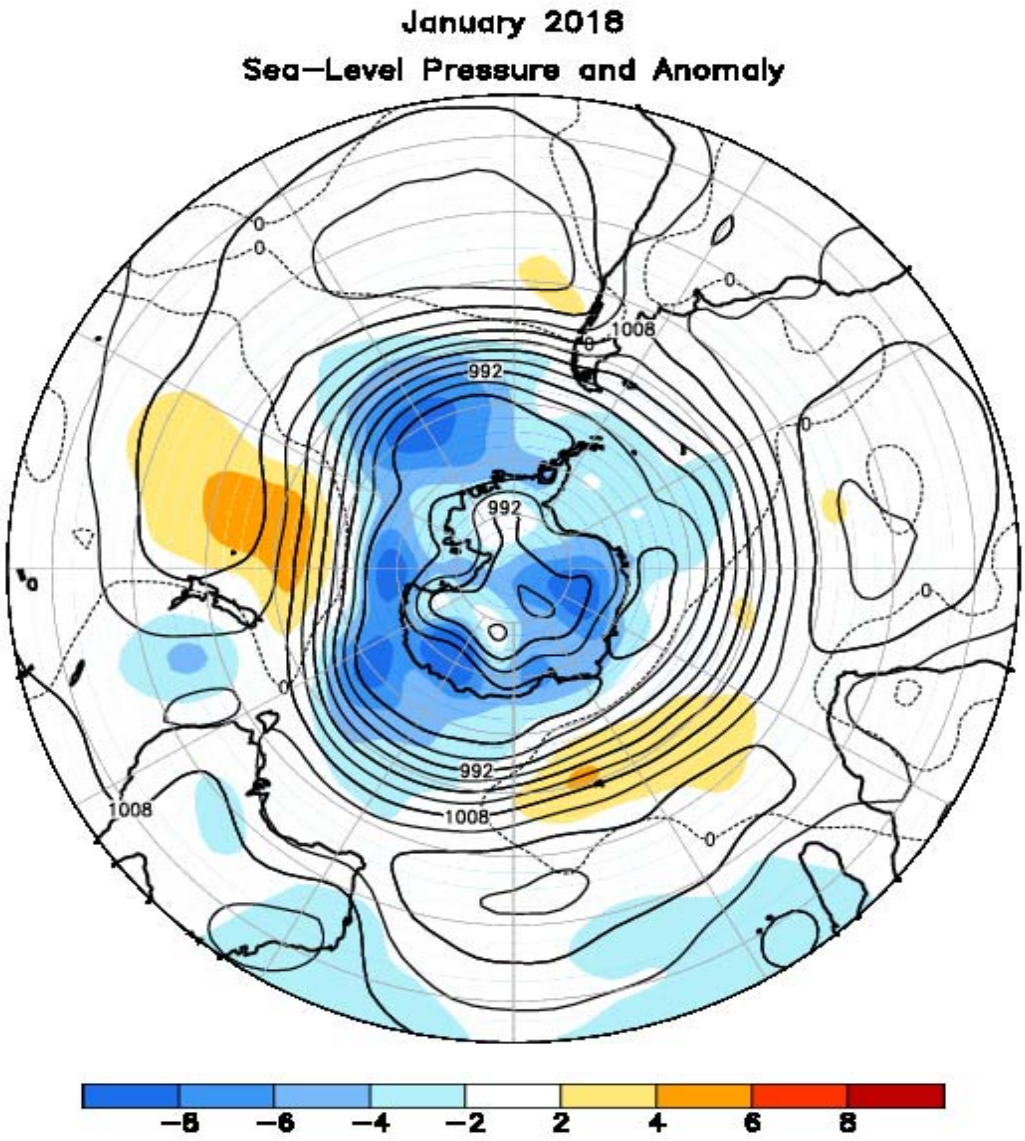

FIGURE E14. Southern Hemisphere mean and anomalous sea level pressure(CDAS/Reanalysis) for JAN 2018. Mean values are denoted by solid contours drawn at an interval of 4 hPa. Anomaly contour interval is 2 hPa with values less (greater) than -2 hPa (2 hPa) indicated by dark (light) shading. Anomalies are calculated as departures from the 1981-2010 base period monthly means.

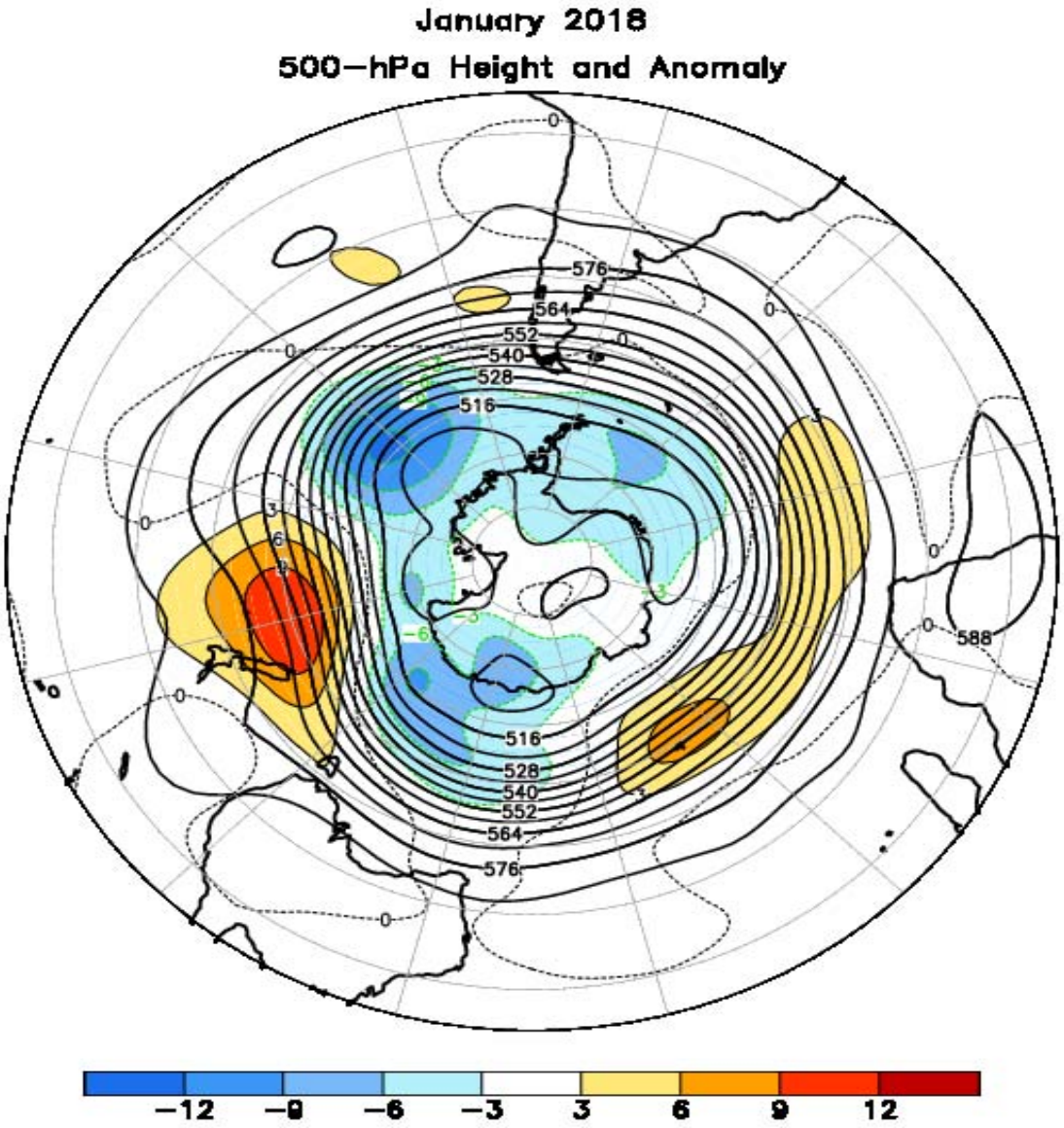

FIGURE E15. Southern Hemisphere mean and anomalous 500-hPa geopotential height (CDAS/Reanalysis) for JAN 2018. Mean heights are denoted by solid contours drawn at an interval of 6 dam. Anomaly contour interval is 3 dam with values less (greater) than -3 dam (3 dam) indicated by dark (light) shading. Anomalies are calculated as departures from the 1981-2010 base period monthly means.

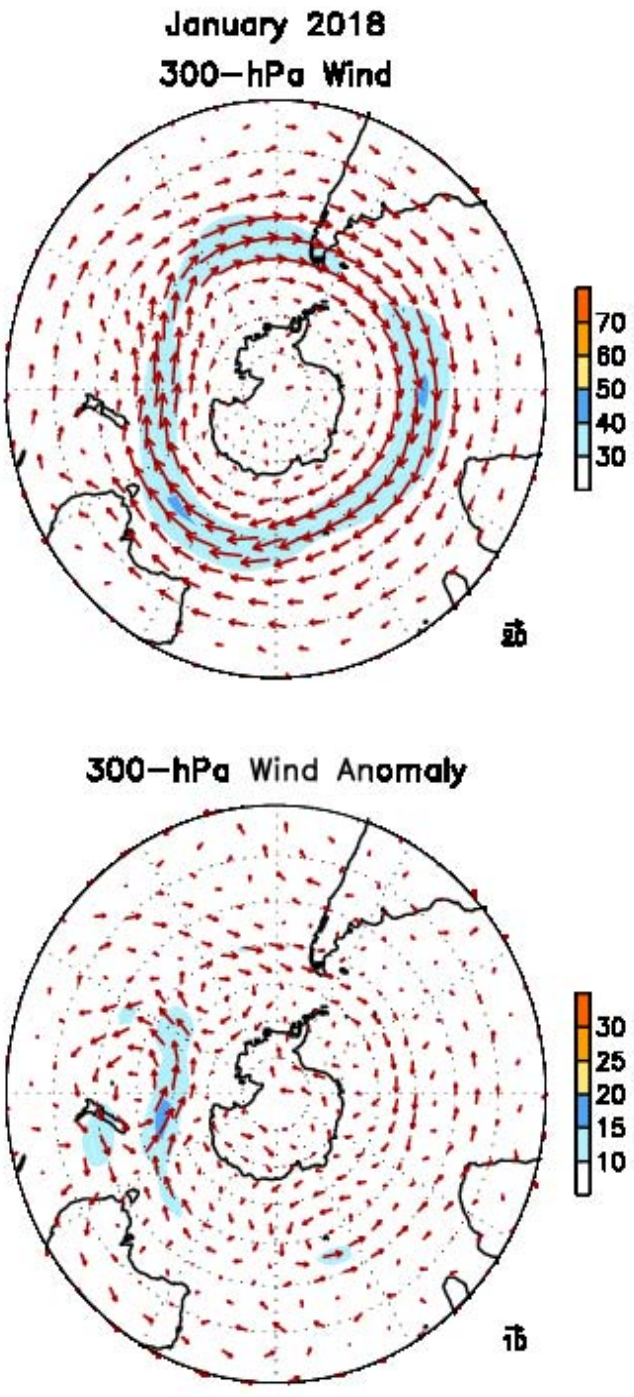

FIGURE E16. Southern Hemisphere mean (left) and anomalous (right) 300-hPa vector wind (CDAS/Reanalysis) for JAN 2018. Mean (anomaly) isotach contour interval is 10 (5) ms^{-1}. Values greater than 30 ms^{-1} (left) and 10 ms^{-1} (rights) are shaded. Anomalies are departures from the 1981-2010 base period monthly means.

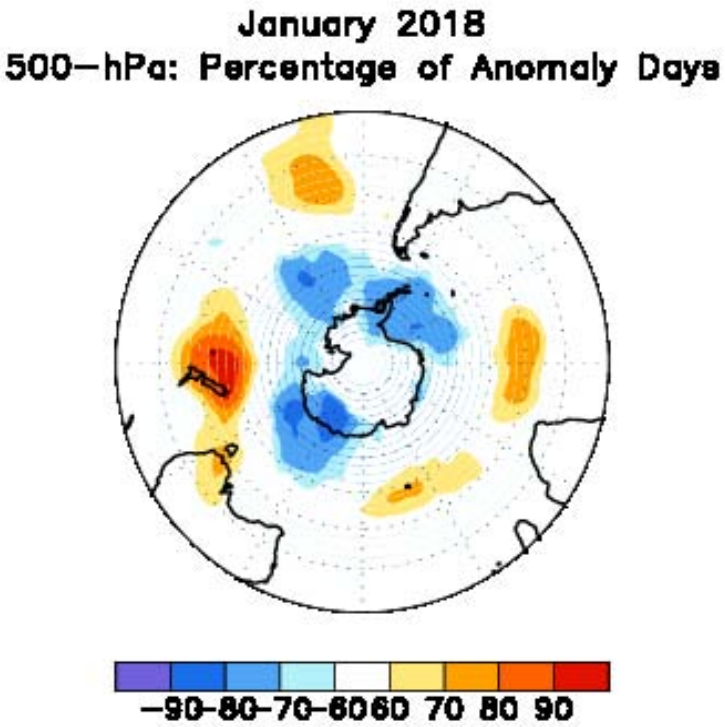

FIGURE E17. Southern Hemisphere percentage of days during JAN 2018 in which 500-hPa height anomalies greater than 15 m (red) and less than -15 m (blue) were observed. Values greater than 70% are shaded and contour in-

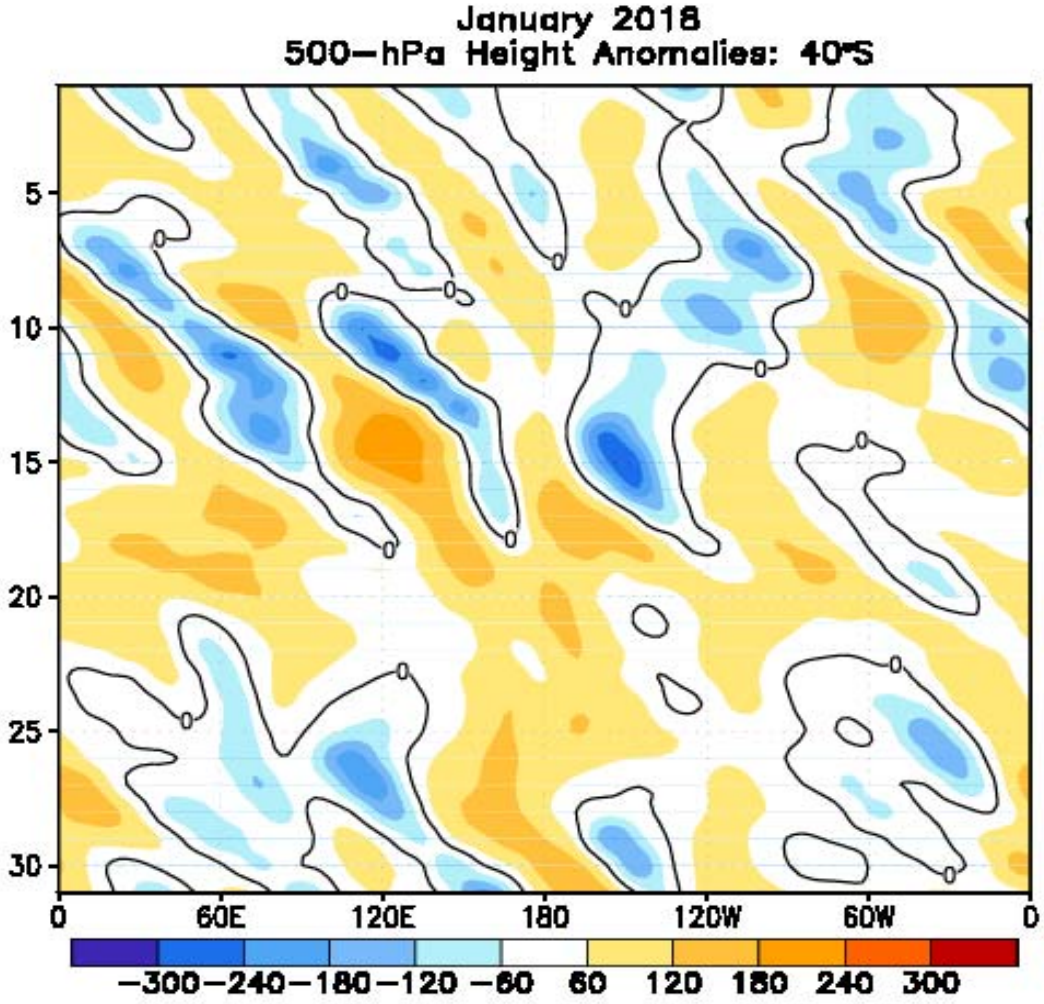

FIGURE E18. Southern Hemisphere: Daily 500-hPa height anomalies for JAN 2018 averaged over the 5° latitude band centered on 40°S. Positive values are indicated by solid contours and dark shading. Negative values are indicated by dashed coutours and light shading. Contour interval is 60 m. Anomalies are departures from the 1981-2010 base period daily means.

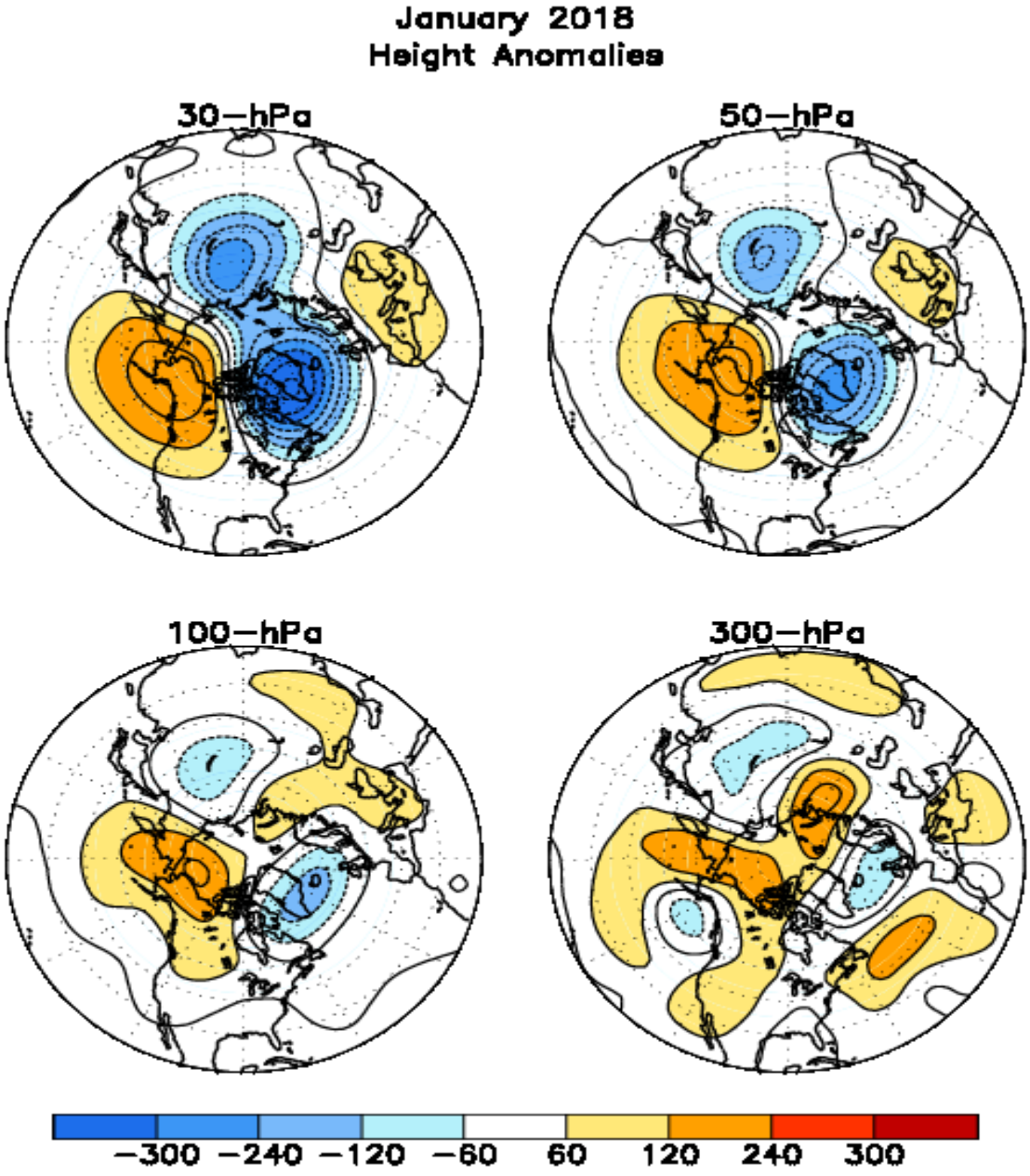

FIGURE S1. Stratospheric height anomalies (m) at selected levels for JAN 2018. Positive values are indicated by solid contours and dark shading. Negative values are indicated by dashed contours and light shading. Contour interval is 60 m. Anomalies are calculated from the 1981-2010 base period means. Winter Hemisphere is shown.

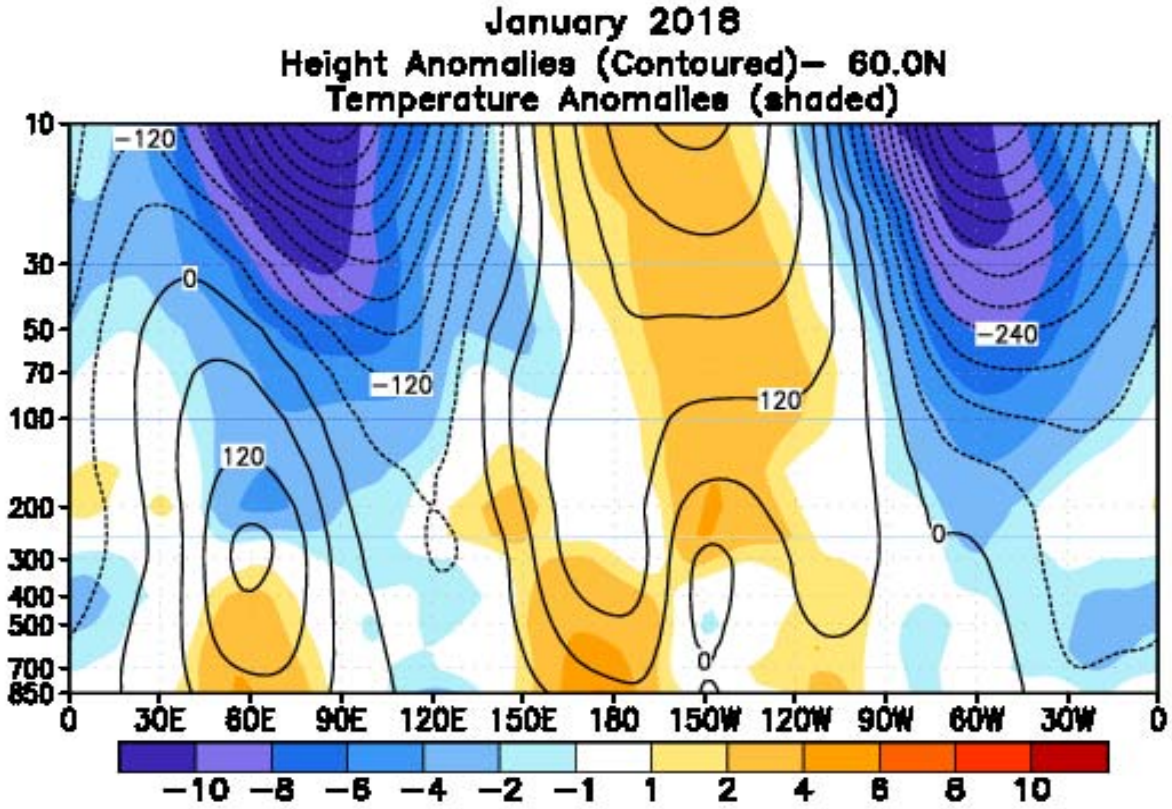

FIGURE S2. Height-longitude sections during JAN 2018 for height anomalies (contour) and temperature anomalies (shaded). In both panels, positive values are indicated by solid contours and dark shading, while negative anomalies are indicated by dashed contours and light shading. Contour interval for height anomalies is 60 m and for temperature anomalies is 2°C. Anomalies are calculated from the 1981-2010 base period monthly means. Winter Hemisphere is shown.

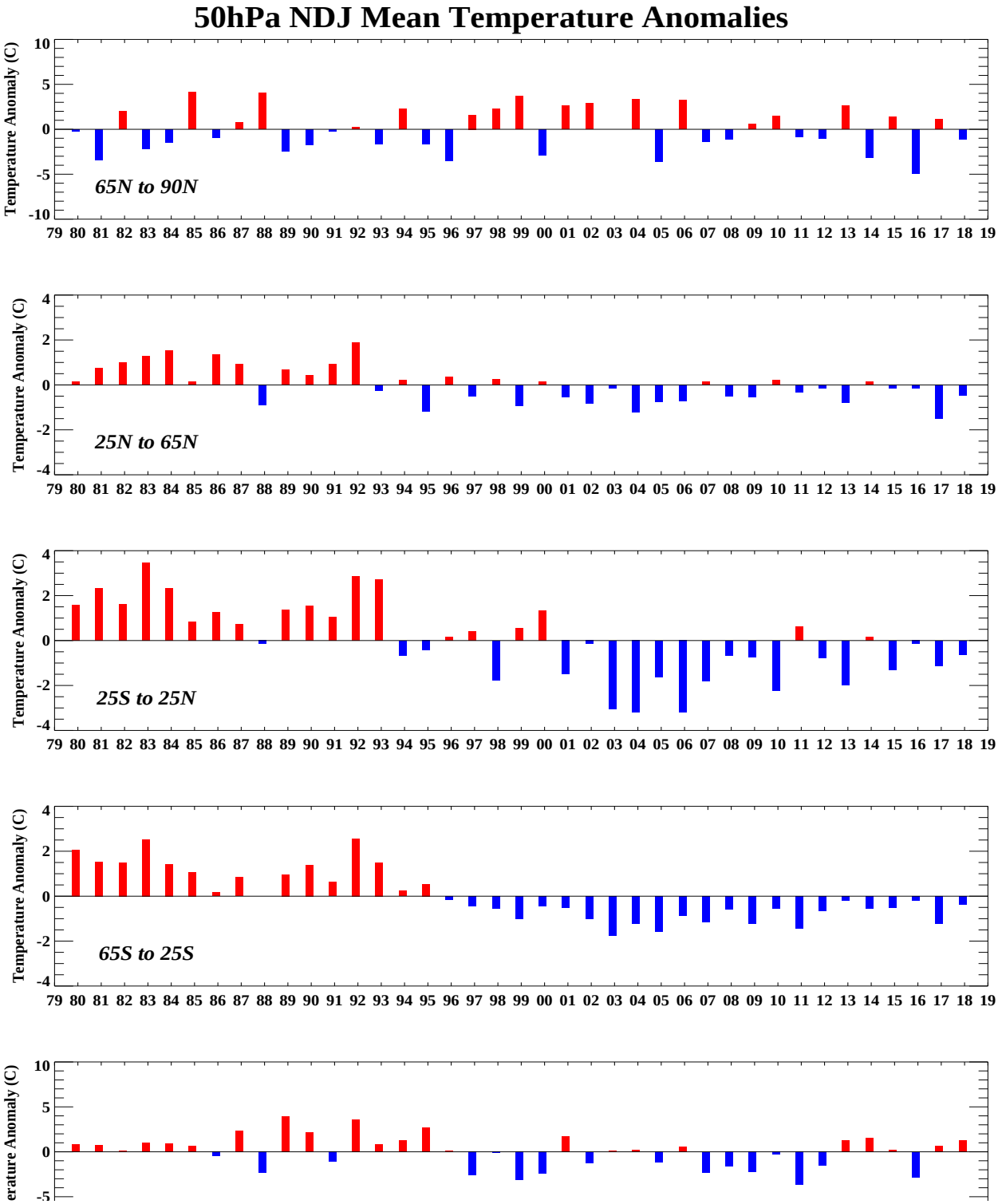

FIGURE S3. Seasonal mean temperature anomalies at 50-hPa for the latitude bands 65°–90°N, 25°–65°N, 25°N–25°S, 25°–65°S, 65°–90°S. The seasonal mean is comprised of the most recent three months. Zonal anomalies are taken from the mean of the entire data set.

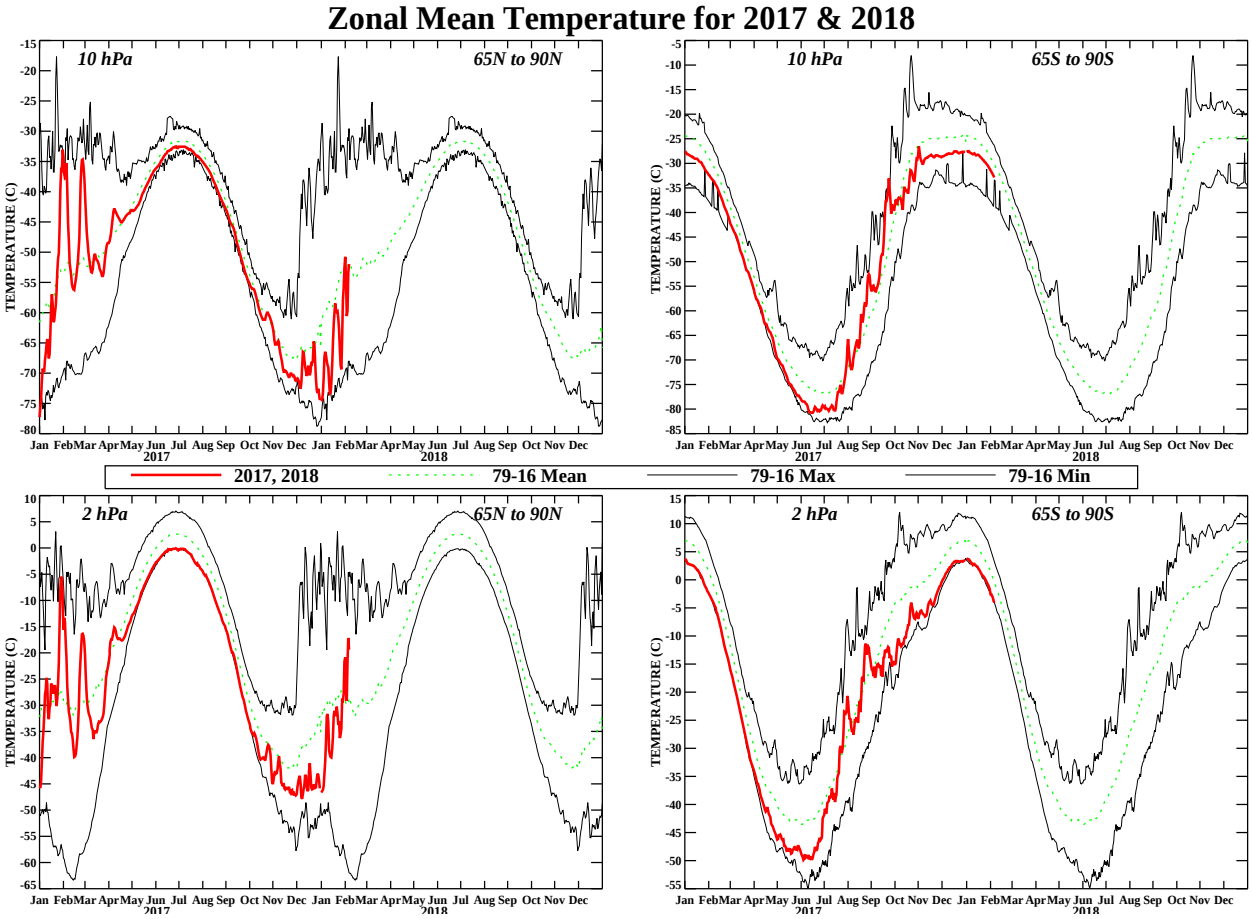

FIGURE S4. Daily mean temperatures at 10-hPa and 2-hPa (thick line) in the region 65°–90°N and 65°–90°S for the past two years. Dashed line depicts the 1981-2010 base period daily mean. Thin solid lines depict the daily extreme maximum and minimum temperatures.

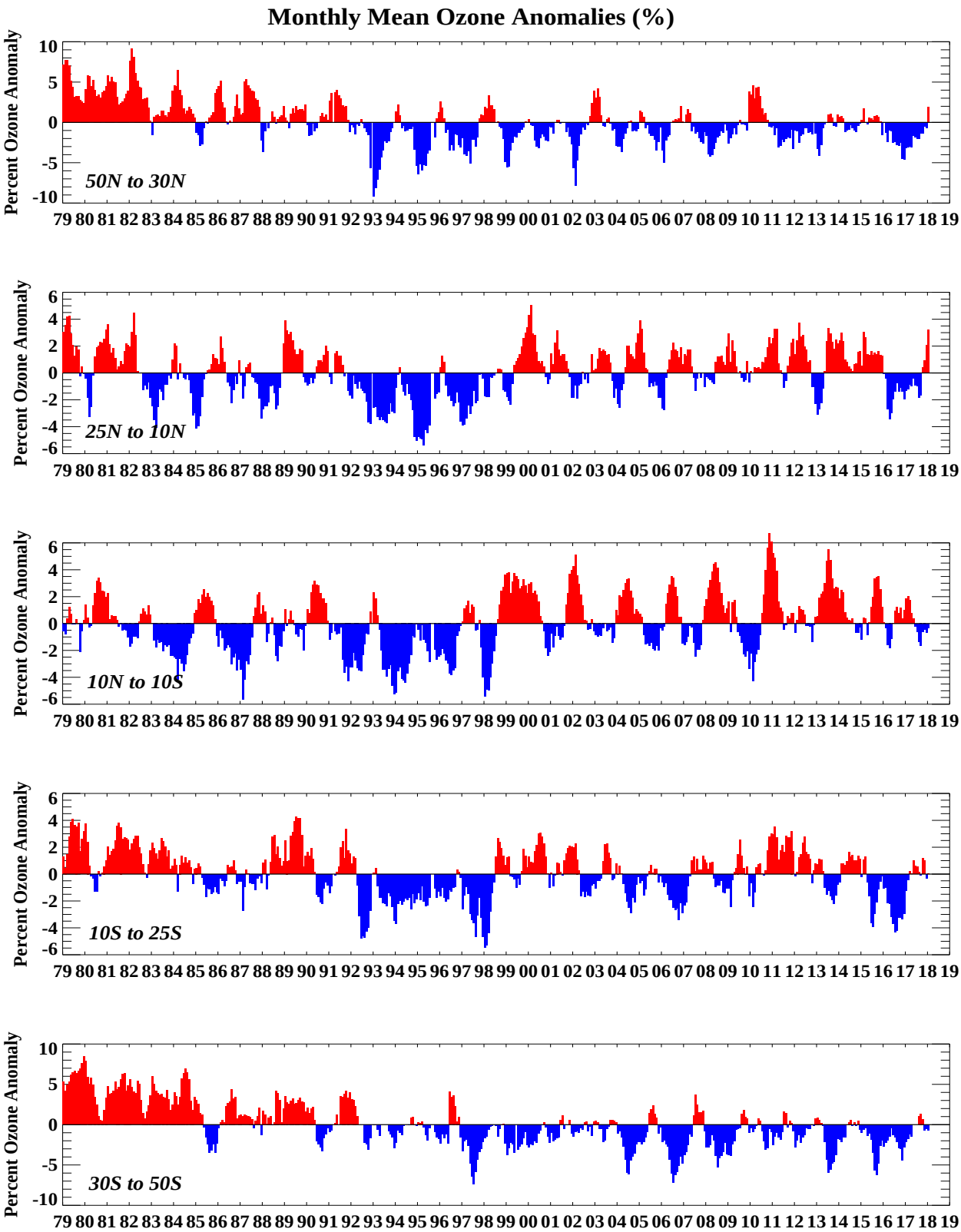

FIGURE S5. Monthly ozone anomalies (percent) from the long term monthly means for five zones: 50N-30N (NH mid-latitudes), 25N-10N (NH tropical surf zone), 10N-10S (Equatorial-QBO zone), 10S-25S (SH tropical surf zone), and 30S-50S (SH mid-latitudes). The long term monthly means are determined from the entire data set

JANUARY PERCENT DIFF (2018 - AVG[79-86])

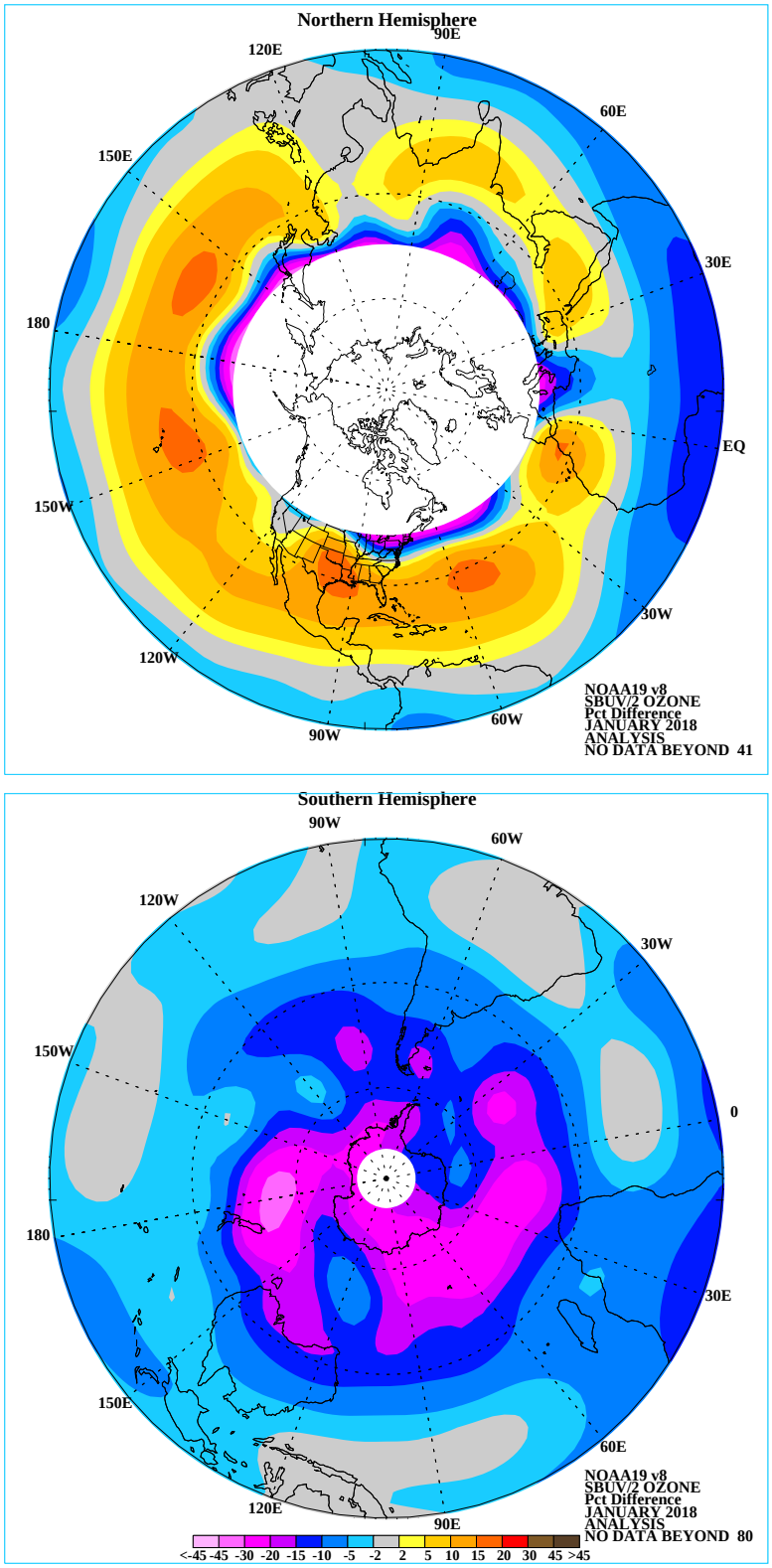

FIGURE S6. Northern (top) and Southern (bottom) Hemisphere total ozone anomaly (percent difference from monthly mean for the period 1979-1986). The region near the winter pole has no SBUV/2 data.

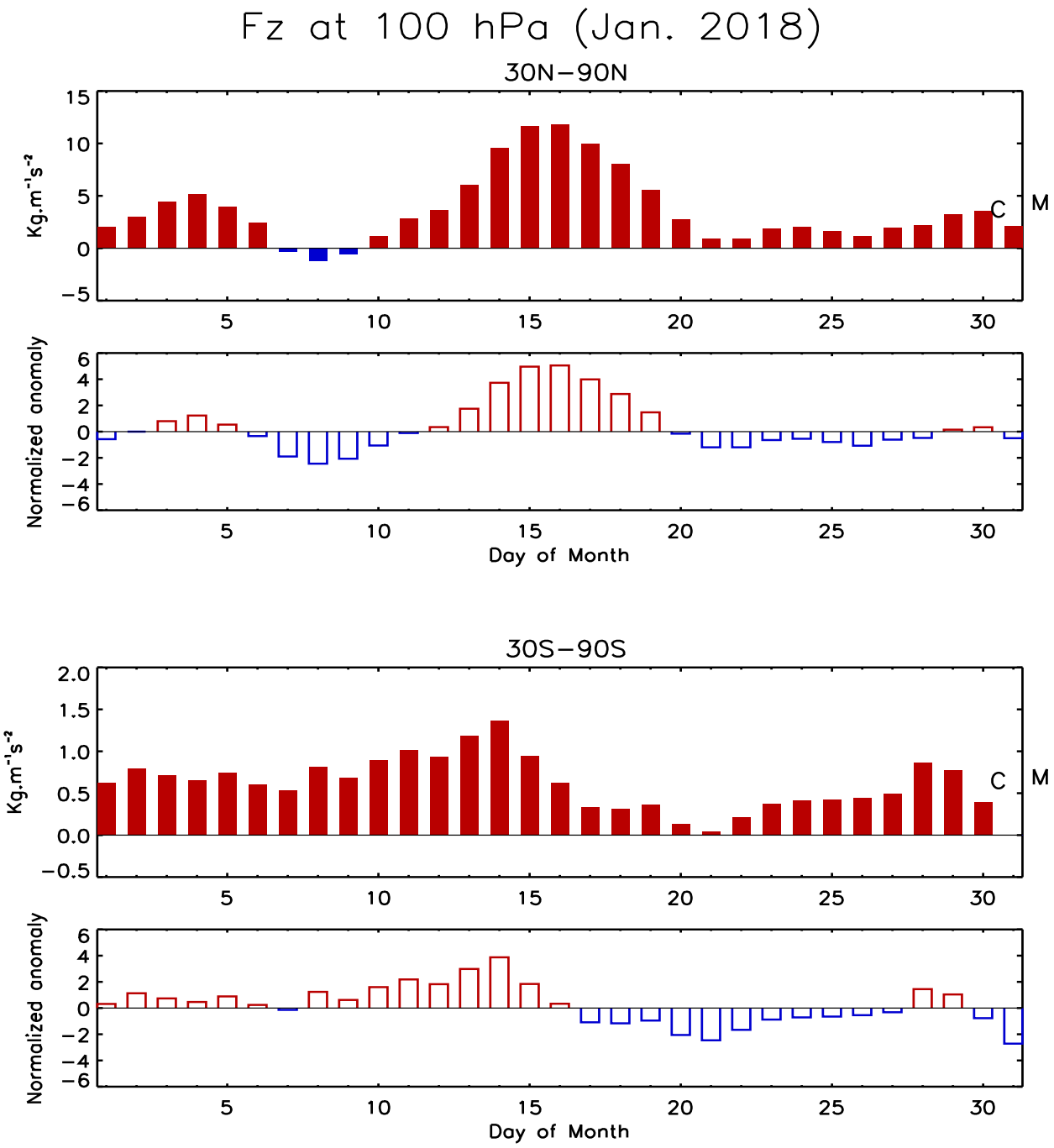

FIGURE S7. Daily vertical component of EP flux (which is proportional to the poleward transport of heat or upward transport of potential energy by planetary wave) at 100 hPa averaged over (top) 30°N–90°N and (bottom) 30°S–90°S for JAN 2018. The EP flux unit (kg m^{-1} s^{-2}) has been scaled by multiplying a factor of the Brunt Vaisala frequency divided by the Coriolis parameter and the radius of the earth. The letter 'M' indicates the current monthly mean value and the letter 'C' indicates the climatological mean value. Additionally, the normalized departures from the monthly climatological EP flux values are shown.

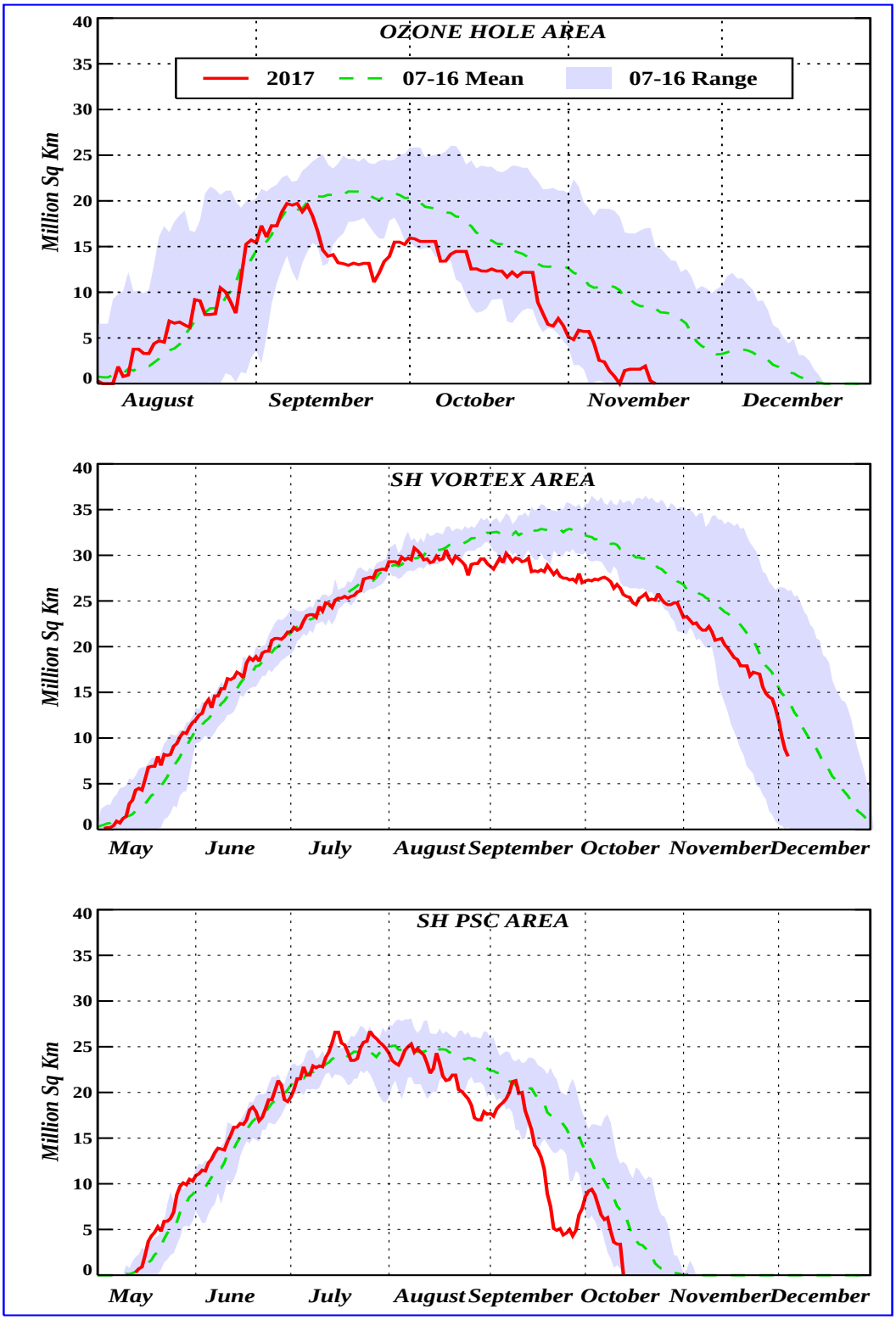

FIGURE S8. Daily time series showing the size of the SH polar vortex (representing the area enclosed by the 32 PVU contour on the 450K isentropic surface), and the areal coverage of temperatures < -78C on the 450K isentropic surface.

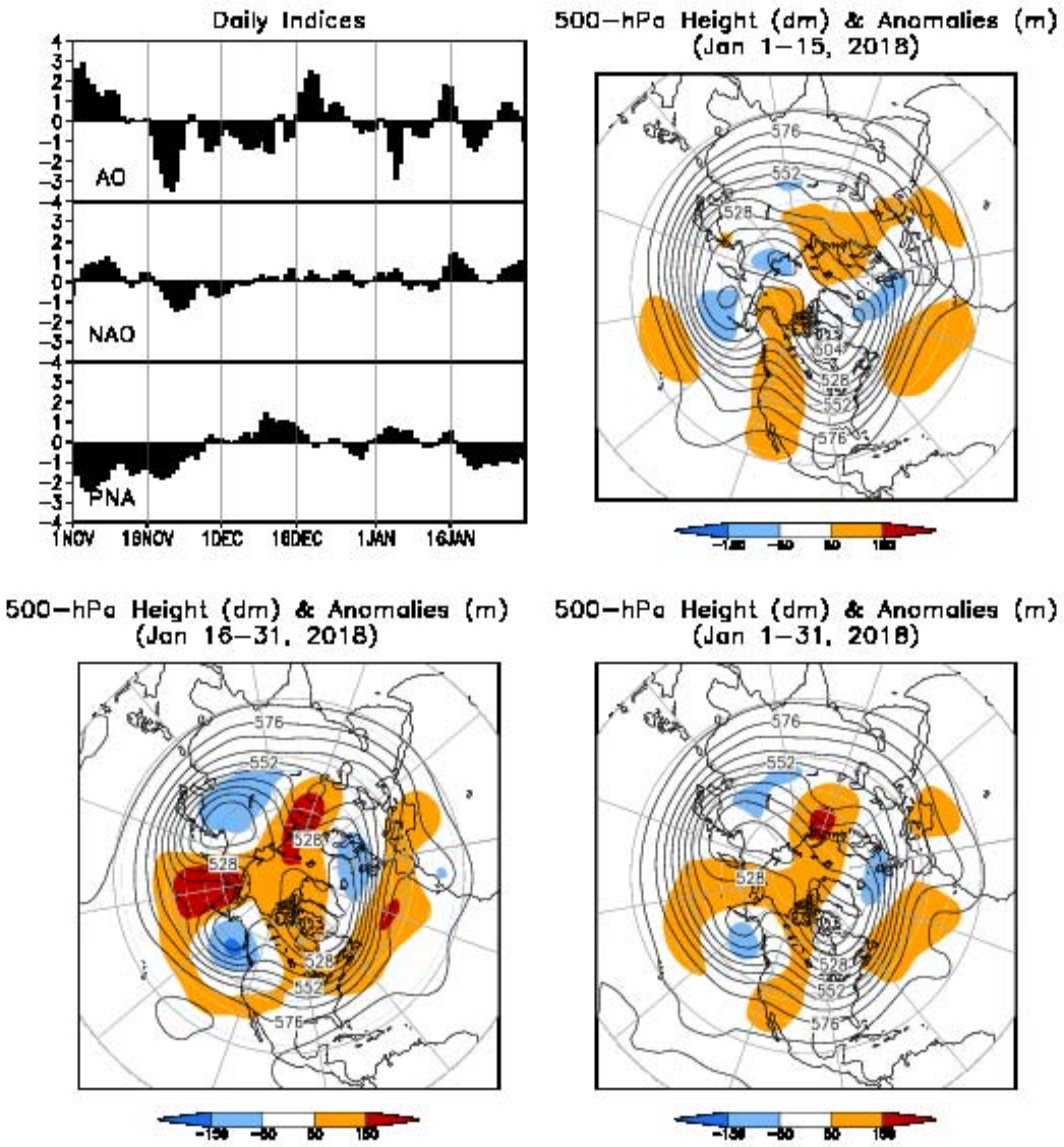

FIGURE A2.1. (a) Daily amplitudes of the Arctic Oscillation (AO) the North Atlantic Oscillation (NAO), and the Pacific-North American (PNA) pattern. The pattern amplitudes for the AO, (NAO, PNA) are calculated by projecting the daily 1000-hPa (500-hPa) height anomaly field onto the leading EOF obtained from standardized time- series of daily 1000-hPa (500-hPa) height for all months of the year. The base period is 1981–2010.

(b-d) Northern Hemisphere mean and anomalous 500-hPa geopotential height (CDAS/Reanalysis) for selected periods during JAN 2018 are shown in the remaining 3 panels. Mean heights are denoted by solid contours drawn at an interval of 8 dam. Dark (light) shading corresponds to anomalies greater than 50 m (less than -50 m). Anomalies are calculated as departures from the 1981-2010 base period daily means.

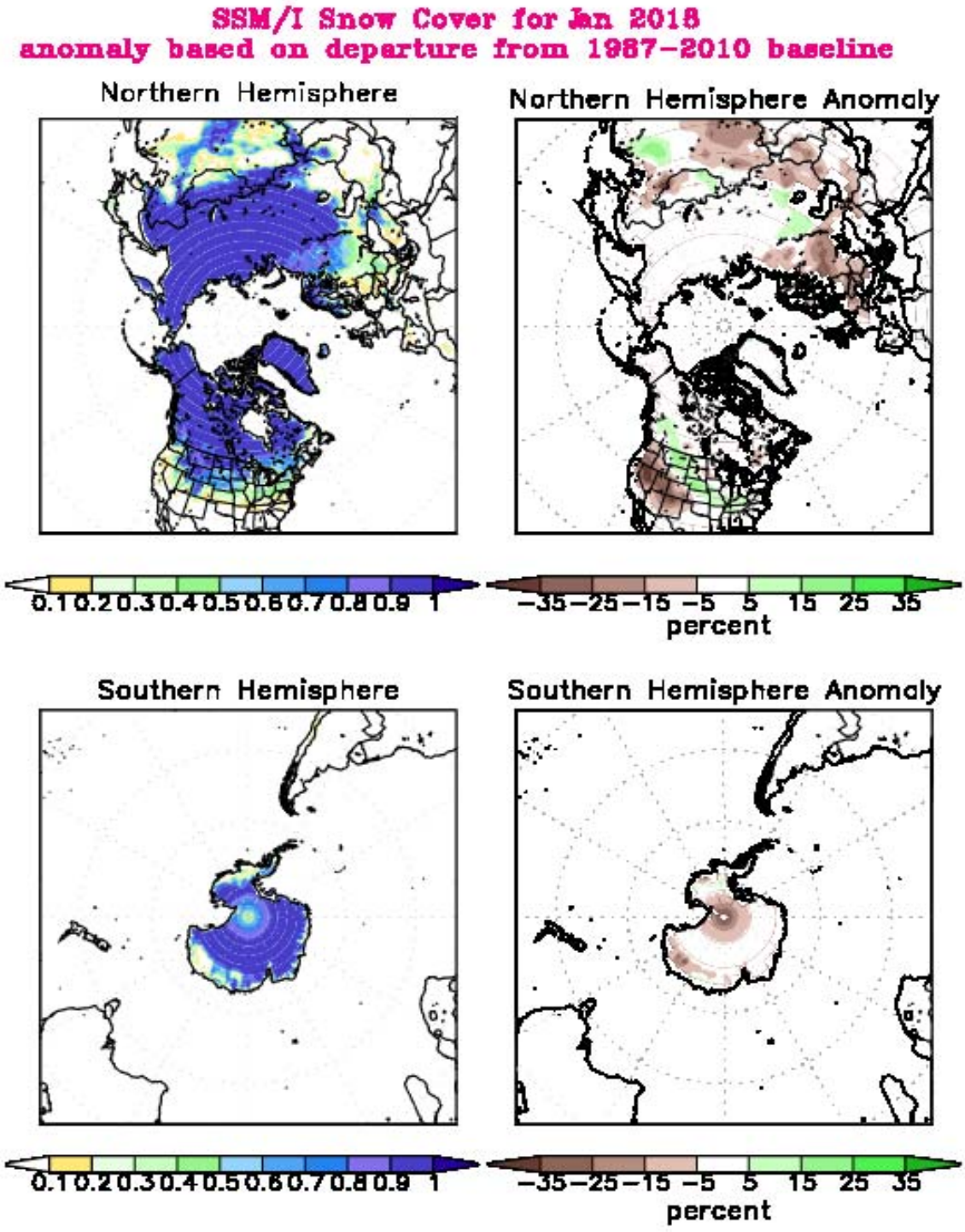

FIGURE A2.2. SSM/I derived snow cover frequency (%) (left) and snow cover anomaly (%) (right) for the month of JAN 2018 based on 1987 - 2010 base period for the Northern Hemisphere (top) and Southern Hemisphere (bottom). It is generated using the algorithm described by Ferraro et. al, 1996, Bull. Amer. Meteor. Soc., vol 77, 891-905.